University of Southern Queensland

Faculty of Health, Engineering & Sciences

Improved Cooling System for USQ's Small Scale Icing Wind Tunnel

A dissertation submitted by

Rhyan Wall

in fulfilment of the requirements of

Courses ENG4111 and ENG4112 Research Project

towards the degree of

Bachelor of Engineering (Mechanical)

Submitted: October, 2015

Abstract

Turbofan engine icing is a relatively new mode of icing attributed to solid phase ice accretion inside the engines. This occurs during flights at high altitudes through convective regions, where tiny ice crystals are ingested and make contact with the engine's warm internal surfaces. The University of Southern Queensland has a small scale icing wind tunnel dedicated to studying aspects of thermal and particle conditions characteristic of ice accretion initiation in turbofan engines.

This dissertation aimed to improve the operation of the facility's refrigeration system by investigating the feasibility of implementing a steady flow work extraction device to super cool pressurised air via expansion processes.

A DEPRAG rotary vane air motor was sourced to conduct the bulk of testing on, using K type thermocouples to measure a maximum temperature drop of 20.7^{o}C. After this preliminary testing, the air motor was disassembled to assist in development of a theoretical system model using equations based on geometry and fluid mechanics; tuned using recorded data as a reference. This went to show that the expansion process of air over short periods followed a roughly isentropic relationship. Further work was done to determine whether this relationship held over longer periods of expansion.

Secondary testing was conducted after redesigning the cylinder rotor housing to maximise temperature drop. Results from this test provided only minor improvement, producing a maximum temperature drop of 21.2^{o}C. The relative size of the cylinder bore, and the speed of the motor are believed to have nullified the adaptations made to initiate the expansion phase earlier (i.e. when the working chamber had a smaller initial volume). It

is posed that this resulted in the vanes reforming working chambers at a similar position to what they did in the original motor.

A customised rotary vane air motor was designed to overcome these issues in design and operation by being larger and slightly slower. Unfortunately time constraints prevented this from advancing into fabrication and testing phases.

The findings from this project suggest that small commercial air motors are not capable of conditioning air cold enough to be a feasible alternative to the current cooling system. It also suggests that small motors are difficult to modify when aiming to increase their maximum temperature drops. In the case of the DEPRAG air motor, its high speed and small cylinder bore are believed to interfere with the amount of expansion experienced by affecting vane (or working chamber) engagement.

Larger temperature drops may be possible using larger sized rotary vane air motors, such as the customised rotary vane air motor designed in this project. However a key assumption in this is that the isentropic behaviour of expanding air observed in the DEPRAG air motor carries over to larger motors, and there is no easy way to confirm this without additional testing on such an air motor.

University of Southern Queensland

Faculty of Health, Engineering & Sciences

ENG4111/2 *Research Project*

Limitations of Use

The Council of the University of Southern Queensland, its Faculty of Health, Engineering & Sciences, and the staff of the University of Southern Queensland, do not accept any responsibility for the truth, accuracy or completeness of material contained within or associated with this dissertation.

Persons using all or any part of this material do so at their own risk, and not at the risk of the Council of the University of Southern Queensland, its Faculty of Health, Engineering & Sciences or the staff of the University of Southern Queensland.

This dissertation reports an educational exercise and has no purpose or validity beyond this exercise. The sole purpose of the course pair entitled "Research Project" is to contribute to the overall education within the student's chosen degree program. This document, the associated hardware, software, drawings, and other material set out in the associated appendices should not be used for any other purpose: if they are so used, it is entirely at the risk of the user.

Dean

Faculty of Health, Engineering & Sciences

Certification of Dissertation

I certify that the ideas, designs and experimental work, results, analyses and conclusions set out in this dissertation are entirely my own effort, except where otherwise indicated and acknowledged.
I further certify that the work is original and has not been previously submitted for assessment in any other course or institution, except where specifically stated.

Rhyan Wall
0061032900

Acknowledgments

I've had a great deal of help in my thesis project and there are a few people I would like to thank for their assistance. First and foremost, I would like to acknowledge the contribution and support provided by the academic and technical staff of the University of Southern Queensland.

I would like especially to thank my supervisors, Dr. David Buttsworth and Dr. Khalid Hashim Saleh, and Dr. Ray Malpress for their valued guidance and continued assistance over the duration of my undergraduate dissertation project. I'd also like to thank Mr. Chris Galligan for his patience and insight regarding the fabrication of my test rig.

I really enjoyed this phase of my program and greatly appreciate the support you have all lent to me over the past year.

Lastly, I want to thank my family and friends for their overwhelming encouragement and support over the course of this degree. Additional acknowledgements go out to coffee, The Natural Confectionery Co. and Marvel Studios; for helping me to get to this point in my degree without having blown my brains out.

Rhyan Wall

Contents

List of Figures

List of Tables

Nomenclature

All values in SI units unless otherwise stated.

SYMBOLS		
A	Area	m^2
a, s	Gap Clearance	m
β,ϕ,θ	Angle	rad
c	Speed of Sound	m/s
c_p	Specific Heat Under Constant Pressure	J/kg.K
D	Diameter	m
η	Efficiency	
F, P	Force	N
f	Coefficient of Friction	
I	Second Moment of Inertia	m^4
k	Ratio of Specific Heats	
L	Depth	m
M	Mach Number	
$\dot{m}$	Mass Flow Rate	kg/s
n	Polytropic Index	
p	Pressure	Pa
Q	Volumetric Flow Rate	m^3/s
R	Universal Gas Constant	J/kg.K
r	Radius	m
rpm	Rotational Speed	rpm
T	Temperature	K

t	Thickness	m
τ	Torque	N.m
U	Velocity	m/s
w	Width of Vane	m
V	Volume	m^3
$\dot{W}$	Power	W
z	Number of Vanes	

SUBSCRIPTS

0	Under Stagnant Conditions
1	Initially / Leading
2	Finally / Lagging
act	Actuating
b	Base
beg	Beginning
c	Cylinder
cor	Coriolis Effect
ex	Exhaust
exp	Expansion
$fill$	Filling
i	Inner
∞	Under Free-Stream Conditions
L	Left
m	Centre of Mass
n	Normal
o	Outer
R	Right
r	Rotor
S	Shaft
s	Shear
rem	Remaining
t	Tangent

v	Vane
wc	Working Chamber

ACRONYMS

AIWT	Altitude Icing Wind Tunnel
AMR	Air Motor Rig
CIRA	Italian Aerospace Research Centre
IWT	Icing Wind Tunnel
IRT	Icing Research Tunnel
NASA	National Aeronautics and Space Administration
NRC	National Research Council
PIWT	Propulsion Icing Wind Tunnel
RVAM	Rotary Vane Type Air Motor
RVVP	Rotary Vane Type Vacuum Pump
USD	United States Dollar
USQ	University of Southern Queensland
VTT	Technical Research Centre Finland

Chapter 1

Introduction

1.1 Purpose

Given the continued role icing has in aircraft accidents, development of methods and technologies regarding the safe operation of aircraft under meteorological conditions promoting the occurrence of natural icing is of continued importance. The purpose of this project is to improve upon the current cooling system utilised by the small scale icing wind tunnel (IWT) at the University of Southern Queensland (USQ). As such, this project utilised the existing icing wind tunnel's setup, which is designed to simulate aspects of thermal and particle conditions characteristic of ice accretion initiation in turbofan engines.

This project aims to investigate the feasibility of improving the cooling system on USQ's small scale IWT through utilising steady flow work extraction based expansion in supercooling air; specifically by using a rotary vane type air motor (RVAM). Using expansion based cooling via work extraction as an alternative would eliminate several problems involving the current mode of cooling; particularly the large fluctuations in temperature and the introduction of vaporised liquid nitrogen in the air stream. This novel method of cooling also has a far lower running cost compared to typical refrigeration systems used in IWTs.

1.2 Background

The supercooling and freezing of water has been studied by a large number of workers for the better part of the last 300 years (Langham & Mason 1958). Significant breakthroughs having been made in the last 50 years by studies conducted on the effects of icing in a number of different sectors. An area of practical interest is the aerospace sector.

Although icing is not a new hazard to the aerospace sector, its capacity to cause major accidents even today remains considerable. For example ice accretion within turbofan engines during operation through or in the vicinity of highly convective regions is a reasonably new mode of icing where gaps in knowledge still remain. The continued need for ice accretion experimental studies forms this work's motivational precedence.

There are a multitude of testing techniques and facilities available for researchers to use today in simulating icing conditions, with one of the more popular facilities being icing wind tunnels (IWTs). Typical IWTs with refrigeration based cooling system are highly costly in operation; particularly so in simulating solid phase ice accretion. The development of USQ's small scale icing wind tunnel aimed to achieve the necessary operating characteristics required to gather meaningful data using a high efficiency, low cost mode of cooling. It was also aimed at allowing USQ to simulate the thermal and particle conditions characteristic of solid phase ice accretion initiation in turbofan engines (Saleh 2013).

1.3 Project Goals

This project seeks to improve the operational efficiency and realism of in flight icing simulation when using the small scale IWT at USQ. The primary goal of this project is to determine and investigate the validity of work extraction based cooling system in suitably conditioning an air stream for icing simulation and subsequent testing. The RVAM was specifically chosen as the expansion device. Secondary goals of the project were to integrate the system into the current IWT and optimise its operation.

Testing will be conducted on a commercially available RVAM to first determine if they

already have the capacity to provide the necessary expansion based cooling. Assuming performance in preliminary testing is acceptable, objectives of this project are as follows:

1. Research background information relating to icing wind tunnels, ice accretion particulate conditions, and devices capable of super cooling air; particularly through work extraction based expansion.
2. Analyse and model the predicted operating conditions of cooling system based on fluid and hardware properties using appropriate modelling techniques; based on excel, matlab and maybe ansys.
3. Source required hardware and performing preliminary testing.
4. Redesign and implement proposed alterations to the icing wind tunnel.
5. Perform testing and analyse results to improve efficacy, varying the initial pressure and work extraction.
6. Submit an academic dissertation on the research.

Should it be that performance does not meet the necessary criteria, the amended project objectives will be as follows:

1. Research background information relating to icing wind tunnels, ice accretion particulate conditions, and devices capable of super cooling air; particularly through work extraction based expansion.
2. Analyse and model the predicted operating conditions of cooling system based on fluid and hardware properties using appropriate modelling techniques; based on excel, matlab and maybe ansys.
3. Source required hardware and performing preliminary testing.
4. Redesign commercial air motor and perhaps design a purpose built air motor to optimise cooling capacity.
5. Perform additional testing on modified device and analyse results.
6. Submit an academic dissertation on the research.

1.4 Overview of the Dissertation

Chapter 2 This chapter is the literature review, which provides an adequate overview of modes of ice accretion (in particular engine icing conditions), the layout and operating characteristics of conventional icing wind tunnel systems, and the primary hardware of the proposed refrigeration system.

Chapter 3 This chapter is the case study of a Rotary Vane Vacuum Pump (RVVP), which provides insight to the feasibility of operating a redesigned vacuum pump in reverse to achieve similar expansion based cooling to that of an air motor (under steady flow conditions).

Chapter 4 This chapter is the methodology, which details the selection and design of hardware, and procedural considerations implemented in the physical testing and experimentation of the postured cooling system.

Chapter 5 This chapter is the results and discussion, which details the collected and secondary data from the preliminary experimental campaign, and analyses the results to determine the path to take in progressing.

Chapter 6 This chapter is the work conducted after the preliminary experimental campaign, and details a refined system model, the design for a modified rotor cylinder housing, and the design for a customised rotary vane air motor.

Chapter 2

Literature Review

2.1 Chapter Overview

This chapter summarises the present body of literature available in the scientific community pertaining to modes of ice accretion, the layout and operating characteristics of conventional icing wind tunnels, and the primary hardware of the proposed refrigeration system.

2.2 Introduction to Icing

Ice accretion is an environmental phenomenon that affects a wide range of systems; from wind turbines to sea vessels; and initiates critical situations in which proper operation of a system is impinged upon. From the perspective of the aerospace industry, icing is a serious hazard. It has played a significant role in a multitude of accidents occurring over the better part of the last century and continues to effect the operational capacity of aircraft today.

Icing is a cumulative hazard that conventionally reduces aircraft efficiency by accumulating on external surface, thereby increasing weight, reducing lift, increasing drag and

decreasing thrust. It also has the ability to impinge on engine performance, render flight instrumentation readings false, and cause loss of operation on secondary mechanisms (FAA 1975).

Ice formations are generally categorized into three main groups; in-cloud icing, precipitation and frost; though the context of icing in this thesis will mainly concentrate on in-cloud icing.

2.3 Structural Ice Accretion

Structural icing is a mode of ice accretion occurring on the aircraft's external structure (such as the wings and tail) when two necessary conditions are met (FAA 1975):

1. the aircraft must be flying through visible water such as a rain or cloud droplets.
2. the temperature at the point where the moisture strikes the aircraft must be 0^oC or colder.

These supercooled droplets are in an unstable liquid state and will partly freeze instantaneously on contact. However the latent heat of fusion they release raises the remaining portion to melting point. This remaining portion determines the type of icing exhibited.

2.3.1 Clear Ice

Clear ice forms when the remaining liquid portion of the supercooled droplet freezes gradually after initial impact as it flows over the contacting surface. This type of icing generally tends to form at combinations of high speeds or high cloud water concentration, and warm or "close to freezing" temperatures; between -15^{o}C and 0^{o}C (Saleh, Buttsworth & Yusaf 2010, FAA 1975, *Think Ice!* 2010). It is characteristically clear, hard, heavy and tenacious (FAA 1975).

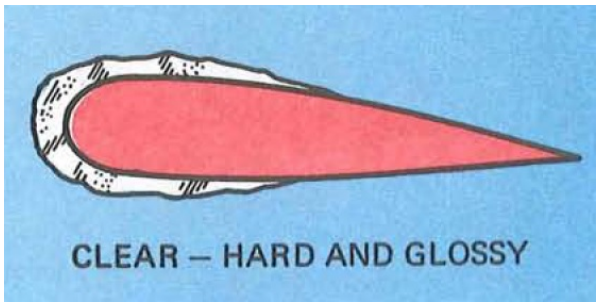

Figure 2.1: Clear icing on airfoil (FAA 1975)

2.3.2 Rime Ice

Rime ice forms when the remaining liquid portion of small supercooled droplet freezes rapidly after the initial impact, resulting in a white opaque accretion that is relatively streamlined. This type of icing generally tends to form at combinations of low speeds or low cloud water concentration, and low ambient temperatures; between -40^{o}C and -10^{o}C (Saleh et al. 2010, *Think Ice!* 2010, FAA 1975). It is characteristically clear, hard, heavy and tenacious (FAA 1975).

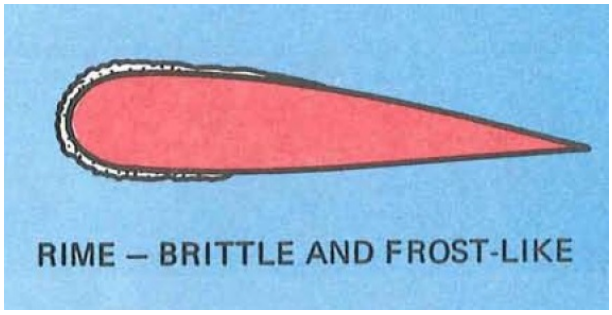

Figure 2.2: Rime icing on airfoil (FAA 1975)

2.4 Ice Crystal Engine Icing

Ice accretion initiation in turbofan engines is a mode of ice accretion that has only recently become a focal point of study, and is highly relevant to commuter and commercial aircraft engines; which is also known as ice crystal engine icing. Unlike aircraft failures due to

structural ice accretion, turbofan engine icing and power loss accidents can occur with no ice accretion on external surfaces of aircraft.

Failures of this kind have only been reported in the last thirty years during flights through highly convective flight regions (Saleh 2013). These regions are typically considered to be above altitudes associated with general icing conditions. However research has shown that high concentrations of moisture can be lifted to these high altitudes, where upon they almost instantly freeze and become tiny ice crystals in ambient temperatures generally less than -40^{o}C (Mason 2007).

The typical temperature of the first stage of an engine compressor's surface is above 0^{o}C (Saleh et al. 2010), so ingested ice particles will slightly melt on impact with internal warm surfaces. Here they form enough liquid friction to stick to surfaces and trap more ice particles in the air stream, which coalesce at certain locations within the turbofan compressor; such as stationary compressor blades. This ice formation has the potential to either (Buttsworth 2014):

1. cause flow blockages, degrading engine performance which has the potential to cause a sudden unwanted drop in engine power.
2. break off and be ingested into the combustion chamber, which could cause a flame-out or damage subsequent stages.

In late 2013, Turbofan engine icing was attributed to a number of Boeing's new 747-8 and 787 Dreamliner aircrafts losing power at high altitude. A new warning was subsequently posted to airlines to avoid flying aircraft with the affected engines within 50 nautical miles of thunderstorms that may contain ice crystals (BBC 2013). It is fair to say from this that icing maintains a clinch hold on the aviation industry today; in both health and safety, and financial respects. The continued study and investigation into ice accretion will help to combat icing on both these fronts by aiding in the development of new methods and technologies to mitigate related hazards.

The physics behind this type of ice accretion can be investigated with great assistance by analytical and computer modelling. Though despite their continued development, such

models have yet to progress to the point of completely replacing the physical performance and operation testing of aircraft and aircraft components. Traditional forms of testing are primarily comprised of in-flight testing (in both natural and simulated icing conditions) and ground testing.

In-flight testing under natural icing conditions is the most realistic means of studying the effects of icing on aircraft. It is often a necessary stage of testing in verifying the validity of artificial ice shapes for simulations and physically demonstrating a mitigation system's effectiveness. Unfortunately this method is costly and has a number of potential problems. These include difficulties involved in finding the ideal conditions to test equipment and demonstrate system adequacy, and in managing the related health safety issues (AGARD 1997). Time taken to find natural icing conditions can be reduced by conducting in-flight testing under simulated icing conditions using icing spray tankers, which fly in front of the test aircraft. Conducting in-flight tests in dry air using critical artificial ice shapes, determined using ground facilities (Bellucci 2007), is another approach to take in investigating the aircraft's degraded performance and handling characteristics.

In either case there are a number of health and safety issues associated with performing in-flight aircraft icing research. It is clear that a paradox exists: to gather accurate data on aircraft icing and new de-icing equipment under natural icing conditions safely requires an aircraft that is already invulnerable to the dangers of icing (Bugos 1998). In lieu of such an aircraft, ground based testing facilities are an attractive alternative for gathering the bulk of data on ice accretion.

2.5 Icing Wind Tunnel

Icing Wind Tunnels (IWTs) are the traditional ground facility used to simulate in-flight icing, and have existed in a functional capacity since the early 1950's. They are capable of producing reliable icing data in repeatable and controlled environments, and are valuable tools to use in analysis and generating critical artificial ice shapes. Limitations to their testing capabilities pertain to their size and their ability to recreate relevant environmental conditions accurately. For example, testing of full size aircraft cannot usu-

ally be accommodated, so aircraft components and scaled models are more commonly tested. An important benefit from using IWTs is that personnel and aircraft safety are not compromised by any damage to test equipment during icing tests (AGARD 1997).

The majority of facilities today utilise some form of refrigeration cycle operating device. These either operate independently or in tandem with local environmental conditions. Refrigeration systems or plants are a well tried and tested means to conditioning test air to temperatures well below freezing. However this method of cooling often goes hand in hand with significant facility operation costs and inefficiencies; given the number of processes involved. The novel idea of expansion based temperature reduction via steady flow work extraction forms the basis of the investigation conducted by this thesis, with an aim of reducing the operating costs and improving the efficiency of contemporary IWT refrigeration systems. Implementing such a device would also theoretically address the problems associated with the current cooling system on USQ's small scale IWT; i.e. temperature fluctuations and nitrogen entering the test air stream.

IWT systems are generally of a similar configuration to conventional dry air wind tunnels, however incorporate additional subsystems unique to their investigative purposes, primarily (Bellucci 2007):

- a refrigeration system, cooling the air to temperatures below freezing.
- a water spray system, injecting a fine mist of water droplets into the air stream to produce an icing cloud.

Despite their importance, there are very few places in the world that have large scale tunnels available for research/industrial activities (Bellucci 2007). This has led to the wider use of small scale icing facilities, in developing new instrumentation and for carrying out basic research on small and large supercooled droplets. At present, less than a dozen full sized icing facilities exist in the entire world; the largest and most advanced of these being the Italian Aerospace Research Centre (CIRA) IWT located in Capua, Italy.

CIRA IWT

The CIRA IWT is a closed loop, fan driven IWT that was officially inaugurated in September 2002. It is considered the world's most advanced facility to date and is capable of reproducing real flight conditions (i.e. altitude, temperature, humidity and velocity) on the ground in a totally secure, controlled and repeatable environment (CIRA 2015).

It is equipped with four different test sections configurations; each having synchronised turntables. The main test section is dimensioned at 2.35m x 2.25m x 7.00m and is capable of reaching temperatures as low as -32^{o}C, speeds up to 214m/s and simulating flight conditions at altitudes of 23,000ft (7km). The spray bar system is distanced at roughly 18m upstream of the test sections and produces droplet sizes with a mean volume diameter of 50μm to 300μm (Ferrigno et al. 2004).

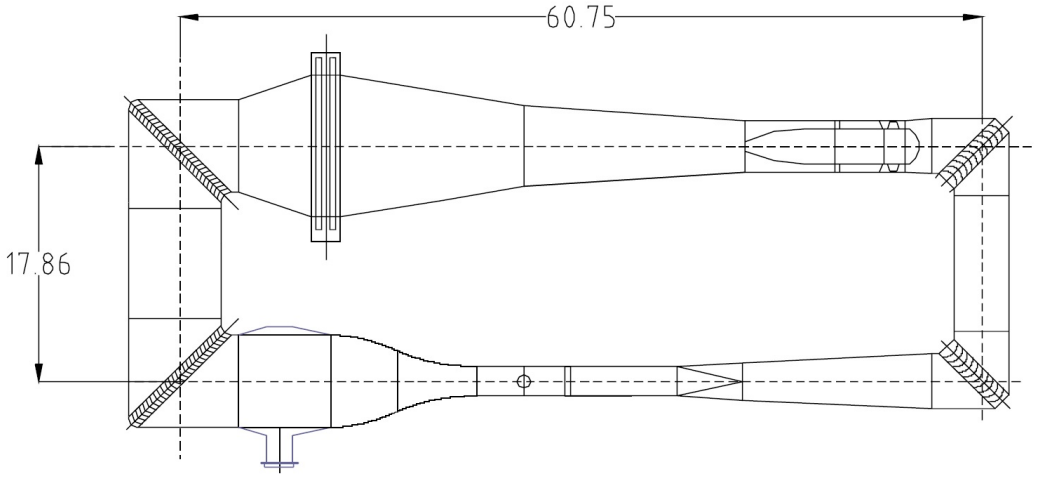

Figure 2.3: CIRA icing wind tunnel layout (Ferrigno et al. 2004)

NASA IRT

Another large refrigerated IWT system is the NASA Glenn Icing Research Tunnel (IRT) (NASA 2009). It was designed as an atmospheric tunnel, it owes its existence to the much larger and no longer used Altitude Wind Tunnel. The NASA Glenn IRT finished

construction in 1944 by the National Advisory Committee for Aeronautics (NACA) in Cleveland, Ohio. It was purposed with the task of investigating ways to prevent and mitigate catastrophic aircraft failures under icing conditions (Khalid) and has played a significant role in developing the anti icing technologies adopted by many aircraft today.

The IRT is a fan driven, closed loop, atmospheric IWT, which generates an icing cloud to simulate icing conditions using a 2,100 ton refrigeration plant and a spray bar system; producing droplet sizes of 15μm to 50μm with a liquid water content (LWC) between 0.2g/m^3 to 3.0g/m^3. As with the majority of closed loop IWTs, the heat exchanger used in the IRT is positioned in a corner section just downstream from the fan. Further downstream is the water injection system, positioned just before the settling chamber. The IRT's test section is dimensioned at 1.83m x 2.74m x 6.10m, and the facility operates at air speeds between 25.72m/s and 180.06m/s and temperatures between -40^{o}C and 5^{o}C (ASME 1987). The operation of this facility was costed by a recent journal article at roughly $34,000 USD a day, with scheduling required at least nine months in advance (Saleh 2013).

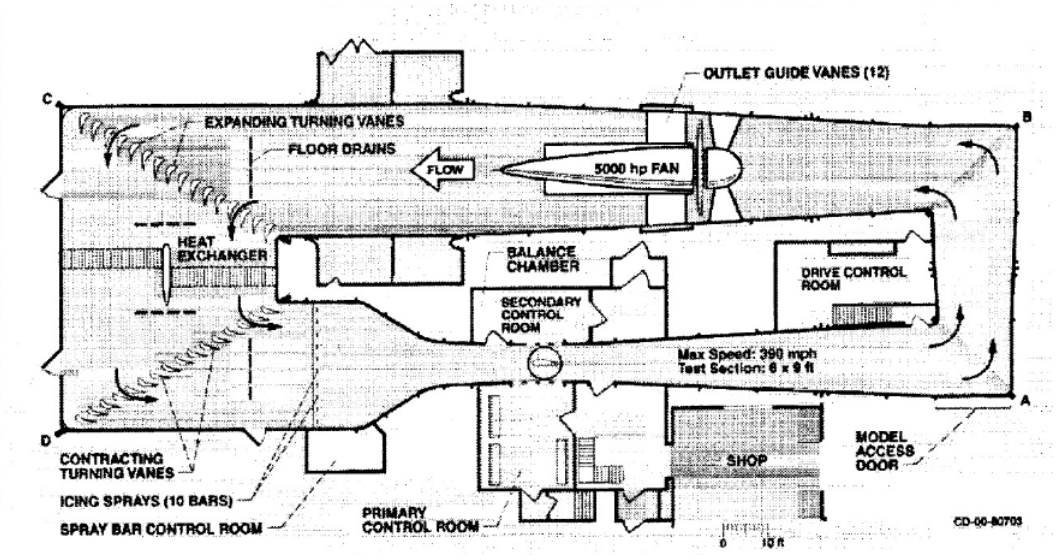

Figure 2.4: Loop configuration of the IRT after the 1999 modifications (Irvine et al. 2001)

NRC AIWT

The National Research Council's (NRC's) Altitude IWT, located in Ottawa (Ontario, Canada), is an IWT used to simulate in flight atmospheric icing; conditions reaching altitudes as high as 30,000ft (9.144km). The facility supports research organisations and commercial clients for a multitude of needs and produces test results that have been accepted by a number of high level certification authorities. The IWT has three test sections available (one standard and two reduced size sections), with its standard section dimensioned at 0.57m x 0.57m x 1.83m and reduced working sections dimensioned at 0.30m x 0.57m x 0.60m and 0.24m x 0.57m x 0.60m. This main test section operates at air speeds between 5m/s and 100m/s with the air temperature at maximum velocity reaching as low as -35^{o}C. The droplet sizes produced range between 8μm and 120μm with a LWC between 0.1g/m^3 and 3.5g/m^3 (NRC 2013*b*).

NRC PIWT

The NRC has another IWT located in Ottawa (Ontario, Canada) known as the Propulsion IWT. The facility has a single test section dimensioned at 3.1m x 6.1m x 12.2m and has an open circuit layout. This means a naturally cold test section is available during the Winter season (or when the local environmental and atmospheric conditions are suitable), which combined with the working section's height allows the facility to simulate larger water droplets than most other IWTs can support (NRC 2013*a*). Coupled with a 750kW electric fan at the entry point, the propulsion IWT is capable of simulating the effects of fluids and snow and ice pellets on a full sized tail test section under fully operational speeds in freezing conditions.

VTT IWT

Another open circuit IWT facility exists in Espoo Finland, which is operated by the Technical Research Centre of Finland (VTT). This particular IWT is fan driven and operates in a climate chamber with controlled air temperature and humidity conditions. The

IWT's test section is dimensioned at 0.70m x 0.70m x 1.00m, and the facility operates at speeds up to 45m/s and temperatures between -20^{o}C and 30^{o}C (TRCF 2010). The droplet sizes produced range between 20μm and 50μm with a LWC between 0.1g/m^3 and 1.0g/m^3.

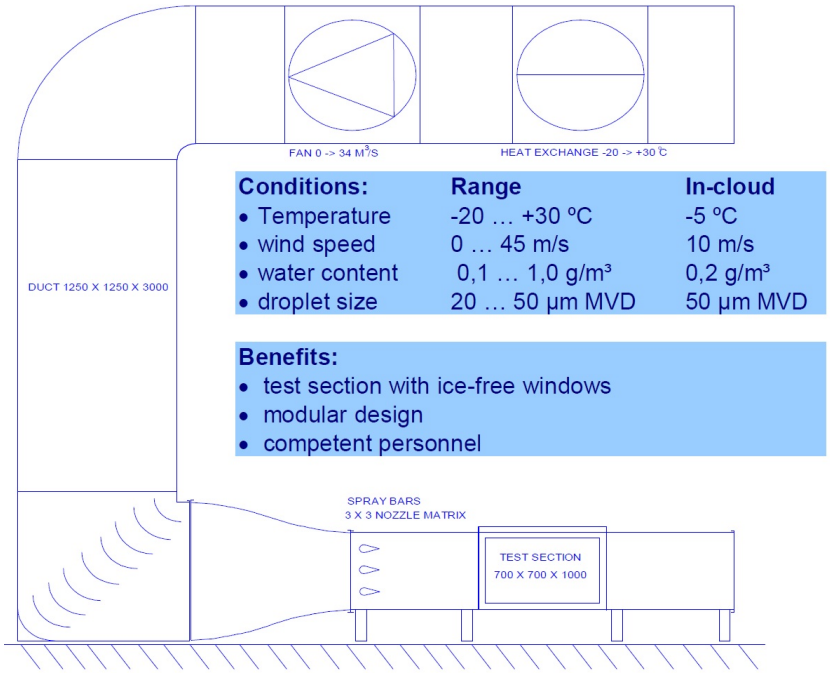

Figure 2.5: Configuration and specs of the VTT (TRCF 2010)

USQ Small Scale IWT

There is a small scale IWT that currently exists at USQ, which had been commissioned in 2013. It utilises a liquid nitrogen plenum based cooling system, which supplies liquid nitrogen from a 20L dewar fitted with a manual discharge device (Khalid), and has the capacity to simulate aspects of thermal and particle conditions characteristic of ice accretion initiation in turbofan engines. The droplet sizes produced are around 50μm with an ice water content of 0.42 $\pm$ 0.26g/m^3.

However, there are problems associated with the system's cold air conditions due to fluctuation in the mixed flow temperature at the exit of the plenum chamber; fluctuations varying between -80^{o}C and -150^{o}C (Saleh 2013). Additionally, the system's use of a liquid

nitrogen bath based heat exchanger introduces the likelihood of nitrogen being taken up with the air during the thermodynamic process, resulting in the icing simulation of a non characteristic air stream. To counter this, a new approach is being tested where a pressurised air stream is cooled by expanding while doing work through an air motor.

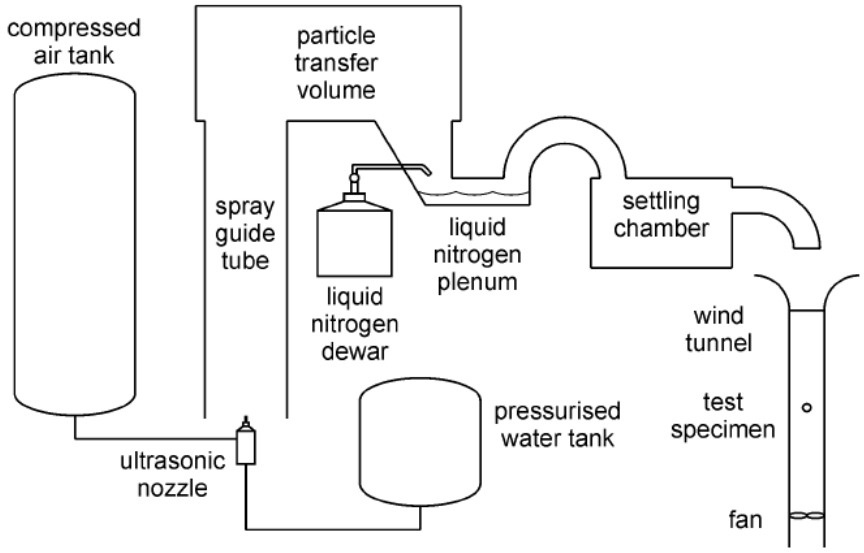

Figure 2.6: Current configuration of USQ's small scale IWT (Saleh 2013)

2.6 Expansion Based Cooling

Expansion based cooling occurs when a gas' average kinetic energy reduces after it does work on other molecules while expanding. As temperature is directly related to molecular kinetic energy, this drop correlates with a drop in gas temperature; the more work done through expansion, the greater the pressure drop and the lower the final temperature.

This principle is behind the idea to use a work extracting device to expand the working fluid or compressed air to achieve desired operating temperatures required for the homogeneous nucleation of water particles in solid phase icing tests.

The expansion of an ideal gas, such that the process is adiabatic and reversible, is known as isentropic expansion process. Assuming such a process occurs for the expansion of

air under steady flow conditions, and that air behaves like an ideal gas over the entire process (which is reasonable given its high composition of Nitrogen), allows for the use of a number of relevant thermodynamic and fluid mechanic equations (Cengel & Boles 2011):

$$\frac{\rho_0}{\rho_\infty} = \left(1 + \frac{k-1}{2}M^2\right)^{\frac{1}{k-1}} \tag{2.1}$$

$$\frac{p_0}{p_\infty} = \left(1 + \frac{k-1}{2}M^2\right)^{\frac{k}{k-1}} \tag{2.2}$$

$$\frac{T_0}{T_\infty} = 1 + \frac{k-1}{2}M^2 \tag{2.3}$$

$$\dot{m} = \rho U_\infty A \tag{2.4}$$

Where:	A	cross sectional area of pipe, in m^2
	k	ratio of specific heats
	$\dot{m}$	mass flow rate of fluid, in kg/s
	$M = \frac{U_\infty}{c}$	Mach number, where $c = \sqrt{kRT}$
	$\rho_{0/\infty}$	stagnant / free-stream fluid density, in kg/m^3
	$p_{0/\infty}$	stagnant / free-stream fluid pressure (abs), in Pa
	$T_{0/\infty}$	stagnant / free-stream fluid temperature, in degrees K
	U_∞	free-stream velocity of fluid, in m/s

2.7 Supercooling and Freezing of Small Water Droplets

The behaviour of supercooled water droplets has been an area of significant study over the last three centuries, with results that spread into a range of science and atmospheric based research fields. In clouds, supercooled water droplets are thought to sometimes freeze homogeneously through the organisation of water molecules into an ice lattice without the need for any external seeding agent (Wilson 2012). In the case of homogeneous nucleation, in which foreign particles are not involved, cloud physicists have found that supercooling of tiny water droplets a few microns in diameter may readily be supercooled to about

-39^{o}C. Bringing temperatures even slightly lower than this value rapidly transforms these droplets into ice crystals (Langham & Mason 1958, Kuhns & Mason 1968, Wilson 2012). The minimum temperature for heterogeneous nucleation as expected is slightly higher at -33^{o}C (Wilson 2012).

In order to replicate a similar performance to that of the current cooling system on USQ's small scale IWT, it will be necessary for the work extraction device to expand the air stream to temperatures as far below -40^{o}C as possible. The lower the air temperature is below -40^{o}C, the greater the heat transfer will be to drive the water particles' phase change. This may not impact significantly on the time necessary for full solidification if bringing the temperature slightly lower than -39^{o}C rapidly drives this change, so initial aims will be achieve temperatures close to this.

2.8 Air Motor

An air motor is a pneumatic system designed to produce continuous rotary power from the work done by expanding compressed air (using either linear or rotary motion). These motors have found great success in the hand held tool industry, and have uses in many other areas; including the automotive and manufacturing industries (*What is a Pneumatic Motor?* 2015). Some benefits to using air motors include the:

- ability to operate in volatile environments, as they do not require electrical power.
- ability to operate without auxiliary speed reducers.
- generally high power density.
- simple controls (e.g. speeds can be regulated with flow control valves in lieu of electronic speed controls).

Several different air motor designs exist, the most common ones include rotary vane, piston, turbine, and tooth-gear air motors. Tooth-gear or turbines variations are highly suitable for applications requiring continuous operation, while vane air motors are more suitable for regular operating cycles (*Air Motors: Customised Drive Solutions* 2012).

Piston Air Motor

Piston air motors are commonly used in applications that require high power, high starting torque and accurate speed control at low speeds; so they are well suited to loaded start applications (Korane 2012). They have a number of cylinders (usually two to six) arranged in a housing either radially or axially. The air pressure acting on the pistons then generates an output torque via reciprocating motion. The power developed by the motor largely depends on intake pressure, number of pistons, piston area, stroke and speed; with speed limited by the inertia of moving parts and the design of internal valves. A major limitation to these motors is the need for internal lubrication (*Air Motor Selection and Sizing* 2012).

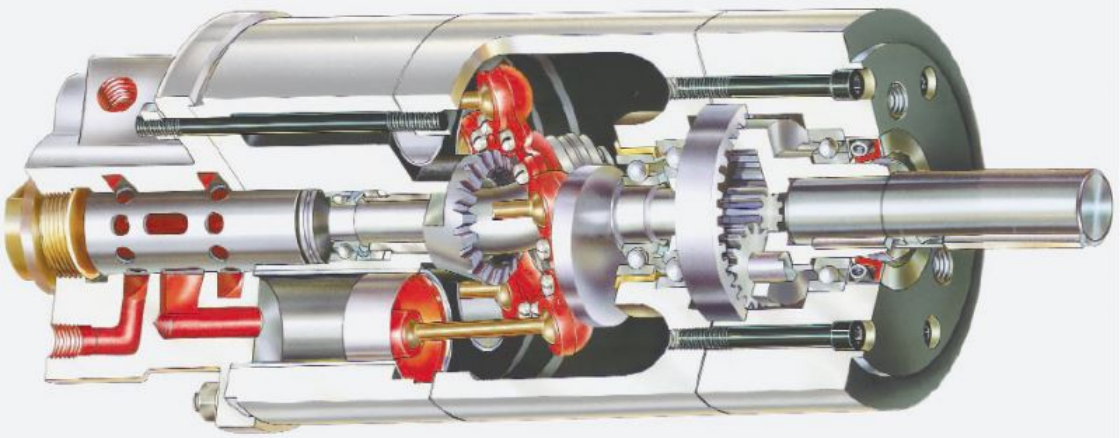

Figure 2.7: Cutaway view of an axial piston air motor (*Air Motor Selection and Sizing* 2012)

Rotary Vane Air Motor (RVAM)

Rotary vane air motors (RVAMs) are commonly used in applications involving low to medium level power requirements; particularly driving portable power tools. They have a number of axial vanes (usually three to ten vanes) fitted into radial slots that run the length of a rotor. These seal against the interior wall of the housing by some variable actuation mechanism (e.g. spring loading, thrust rings, CAM action, pressurised air etc.), which is bolstered during operation by the centrifugal forces that develop (*Air Motor Selection and Sizing* 2012).

The rotor is set to circulate in an eccentrically offset perforation of the air motor cylinder, which means vanes will form working chambers of variable volumes; which increase in the turning direction. So when the pressurised air passes through the entry port into one of the main motor chambers, it will start to expand and act against the exposed side of the longer (or "more protruding") vane. This expansion process causes an energy conversion from pressure energy to kinetic energy, resulting in rotation of the rotor and torque development. The cycle continues until the entry air is expanded to its exit pressure.

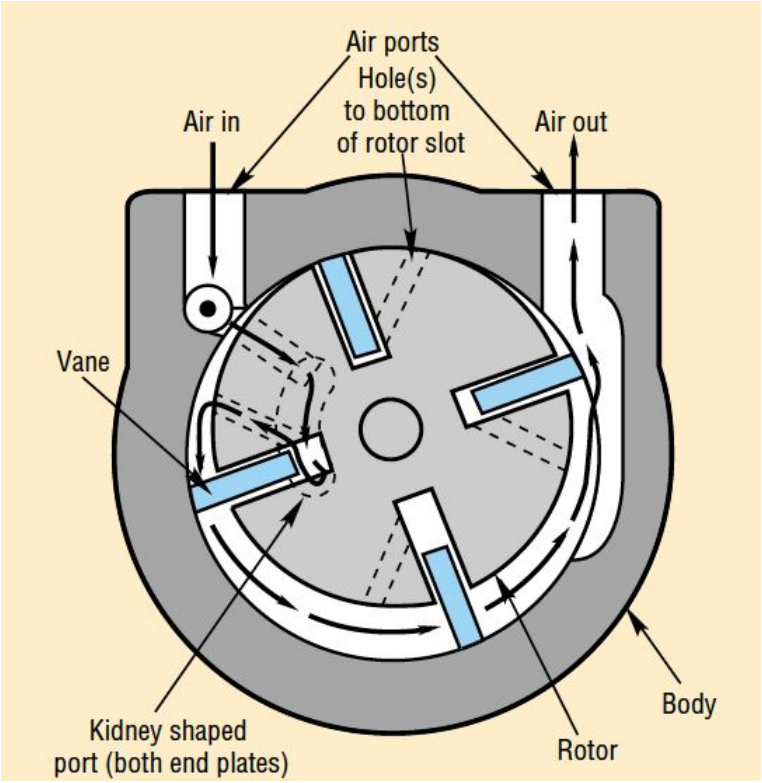

Figure 2.8: Cutaway view of a rotary vane air motor (*Air Motor Selection and Sizing* 2012)

The effects of expansion based cooling of air through air motors is not an area that has been heavily documented in its practical uses. However air motors are known to have their performances impinged upon due to icing, which can occur at temperatures below 5^{o}C (*Air Vane Motors* n.d.). This is understandable given that exhaust temperatures are often well below freezing due to extremely high relative decreases in pressure over short time periods (*Air Motor Icing* n.d., *Section 1: Air Motors Air Tool Manual* 1990).

A report produced by Mechanical Engineering undergraduate students from the Northeastern University (Al-Duwaisan, Sahaim, Roditi & Al-Husseini 1999) also demonstrates the air motor's capacity for supercooling compressed air. In the report, they detail the design setup of a lab to measure the efficiency of an air motor. One of the advantages to their laboratory design they made mention to was its ability to demonstrate how their air motor could extract work from the air at a temperature of 29.4^{o}C to reduce the exhaust air temperature to -71^{o}C. Part of this required calculating the theoretical temperature drop and extracted work through a RVAM assuming the process was steady and isentropic. Note that Al-Duwaisan et al. (1999) have effectively recommended taking 60% of the rated air motor's power in order to account for system losses when calculating expansion power. This is based on known operating conditions, measurements and design schematics; coupled with some knowledge of fluid mechanics theory.

Beater (2007) also recognises the capacity of an air motor to expel supercooled air given a high enough expansion ratio; noting that water in the air stream can freeze and finally block the air motor. Although all of this clearly demonstrates confidence in the air motor's capacity to expel very cold air, conducting testing is the only way to solidify these predictions.

2.9 Band Brake

A band brake will be employed to extract the desired power. This device generates its braking action by applying a flexible band of frictional material to a rotating drum via some actuating force. The drum is commonly made from steel and is lined with a band of woven friction material.

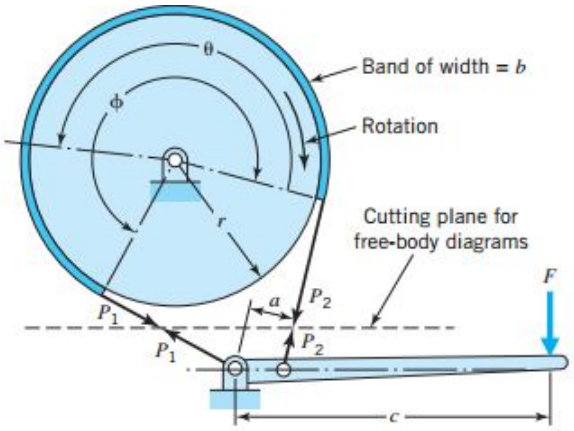

Figure 2.9: Band brake schematic (Juvinall & Marshek 2012)

Neglecting viscous effects of fluids, the following equations are associated with traditional band brake design:

$$\tau = (P_1 - P_2)r \tag{2.5}$$

$$\tau = \frac{60\dot{W}_{out}}{2\pi \times rpm} \tag{2.6}$$

$$\frac{P_1}{P_2} = e^{f\phi} \tag{2.7}$$

Where:	τ	torque developed by brake, in N.m
	P_2	actuating force, in N
	P_1	anchoring force, in N
	$\dot{W}_{out}$	power extracted by brake, in N.m
	rpm	rotational speed of drum, in rpm
	r	radius of drum, in m
	f	coefficient of friction
	ϕ	angle of contact, in rad

In this particular project, the drum and band will be supplemented with a v-pulley and v-section belt respectively. This is aimed at reducing the required actuating forces and improving bearing life. As such the equation relating the forces generated will be sightly different. Recall that v-belts grip the sides of the v-section and not the base. Considering

a v-pulley with a wedge angle of β, the force acting on an infinitely small element will be given by:

$$dP = \frac{Pf\mu d\theta}{\sin\beta}$$

This can be used to derive a relationship for P_1 and P_2 by integrating over θ:

$$\int_{P_2}^{P_1} \frac{dP}{P} = \int_0^{\phi} \frac{f d\theta}{\sin\beta}$$

$$\frac{P_1}{P_2} = e^{\frac{f\phi}{\sin\beta}} \tag{2.8}$$

2.10 Chapter Summary

The study of ice accretion in turbofan engines is of great importance in the aerospace sector. Unlike structural icing, ice crystal engine icing can cause degraded performance and power loss events without ice adhering to external surfaces. It generally occurs in highly convective regions while aircraft are travelling at high altitudes, where ambient temperatures are generally -40^{o}C or less.

IWTs are a practical and economical means of accomplishing this study safely in a controllable and repeatable environment. These facilities are generally capable of reaching temperatures of -40^{o}C, and speeds of 100m/s while producing droplet sizes of 50μm and a liquid water content of 3.0g/m^3.

USQ's small scale IWT currently utilises a liquid nitrogen based cooling system, however there are problems in its operation pertaining to large temperature fluctuations. The novel approach taken by this thesis is to replicate the cooling conditions required for solid phase ice accretion of small water droplets by extracting work from pressurised air. The particular mode of work extraction investigated in this project is the RVAM.

The rotary vane air motor is a pneumatic system that converts work done by expanding compressed air to rotational power. It operates with an eccentrically offset rotor fitted with several vanes in the air motor's cylinder, which create working chambers that increase

in volume with the turning direction. Given the documentation present on air motor icing, it is postured that an air motor with a large enough expansion ratio will be able to provide the required cooling conditions needed to be a viable alternative to the current cooling system.

A band brake will act as the powered device. As opposed to the traditional drum and band design, this project will supplement these components with a v-pulley and v-section belt.

Chapter 3

Vacuum Pump Case Study

3.1 Chapter Overview

This section covers the case study analysis conducted on USQ's rotary vane vacuum pump (RVVP). This was based on its geometry and theoretical performance characteristics in reverse operation.

3.2 Introduction

RVVPs are positive displacement pumps that are setup similarly to RVAMs, in that they consist of an eccentrically offset rotor inserted with vanes to form working chambers. During the filling cycle, working chambers increase in volume; creating a vacuum at the intake port. They then transition to the discharge phase of the cycle; where the chamber's volume decreases, and creates pressure at the exhaust port (*Rotary Vane Compressors and Vacuum Pumps: February 2012 GAST Catalog* 2012).

As noted by Beater (2007), an air motor operating with a high enough expansion ratio is capable of freezing the water entrained in an air stream. Given their geometric similarity, it is postured that a similar result from the expansion of compressed air to that

experienced in an air motor may be achieved by reversing the processes carried out by a RVVP to produce a net power output. USQ currently has a RVVP in their inventory, which looks to have the potential to be redesigned and operated in reverse as an RVAM equivalent. The current design of this vacuum pump does not lend itself to an expansion ratio capable of reducing air to a suitably cold temperature necessary for recreating icing conditions. A case study will be conducted to determine its theoretical cooling capability (based on isentropic relationships) using simple, non-intrusive design adaptations. These mainly constitute:

- relocating the intake and exhaust air ports.
- increasing the number of spring loaded vanes in the rotor

3.3 Analysis

Geometric

The area swept by a working chamber (as a function of the leading rotor vane's angle of rotation) can be calculated by applying trigonometry to the simple geometry relating the rotor and the cylinder to one another (refer to figure 3.1):

$$\begin{aligned} A(\theta_1) &= A_{\theta_2} - A_{scalene} - A_{\theta_1} \\ &= \frac{r_o^2\theta_2}{2} - \frac{r\sin\theta_1(r_o - s - r_i)}{2} - \frac{r_i^2\theta_1}{2} \end{aligned} \tag{3.1}$$

Where:
- A cross sectional area of vacuum pump's working chamber, in m^2
- θ_1 the leading rotor vane's angle of rotation, in rad
- θ_2 the internal vacuum pump case's angle as a function of θ_1, in rad
- s the shortest space between the rotor and cylinder surfaces, taken as 10^{-4}m
- r_o internal radius of vacuum pump casing, taken as 0.12690m
- r_i outer radius of rotor, taken as 0.10334m
- r polar arm of the internal casing surface relative to centre of rotor, in m

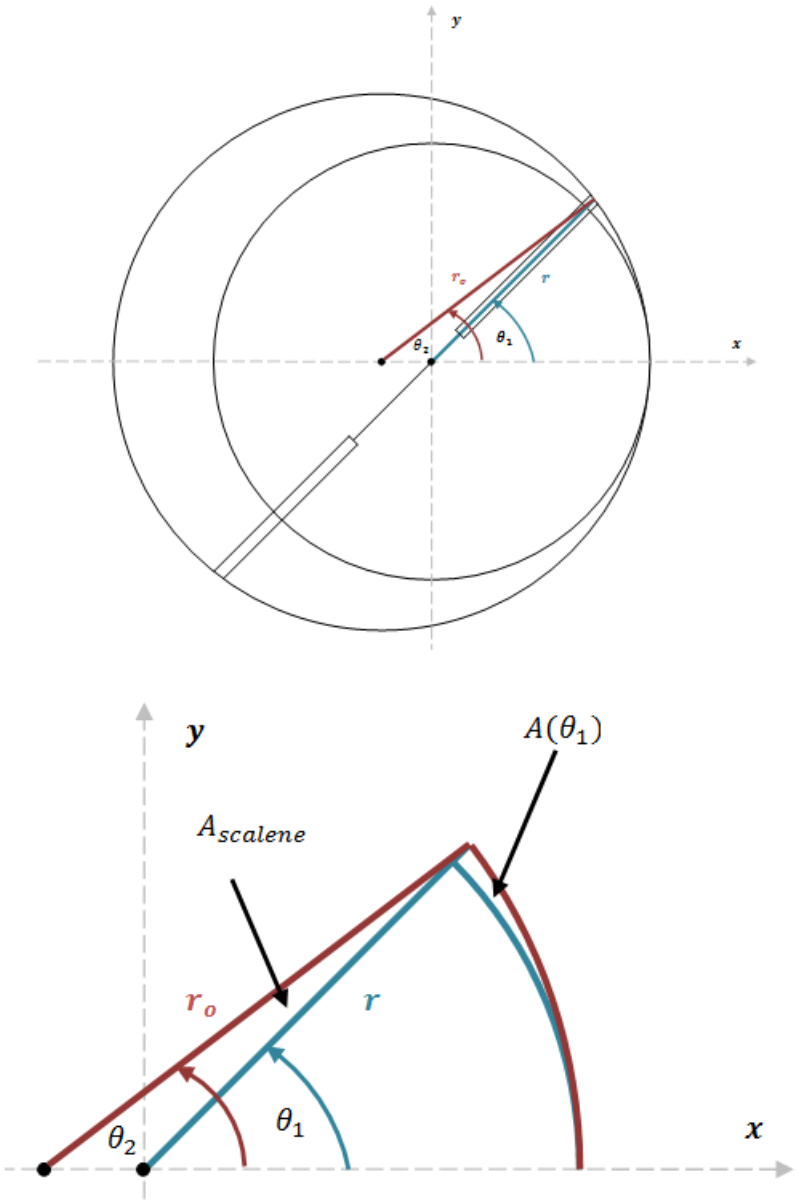

Figure 3.1: Cross section of vacuum pump

θ_2 can be evaluated as a function of θ_1 by the following:

$$\theta_2 = \begin{cases} \arccos\left(\frac{r_o - s - r_i + r\cos\theta_1}{r_o}\right) & 0 < \theta_1 \leq \pi \\ 2\pi - \arccos\left(\frac{r_o - s - r_i + r\cos\theta_1}{r_o}\right) & \pi < \theta_1 \leq 2\pi \end{cases} \tag{3.2}$$

and so can r, using the polar form of an offset circle:

$$r_o^2 = (x + [r_o - s - r_i])^2 + y^2$$

$$0 = r^2 + r\left(2\cos\theta_1[r_o - s - r_i]\right) + \left([r_o - s - r_i]^2 - r_o^2\right)$$

Rearranging into quadratic form and taking its positive root:

$$r = \frac{-b + \sqrt{b^2 - 4ac}}{2a} \tag{3.3}$$

Where: $a = 1$

$b = 2\cos\theta_1(r_o - s - r_i)$

$c = (r_o - s - r_i)^2 - r_o^2$

Volume was determined simply by multiplying this function by the length or internal depth of the casing:

$$V(\theta_1) = \frac{L}{2}\left(r_o^2\theta_2 - r\sin\theta_1(r_o - s - r_i) - r_i^2\theta_1\right) \tag{3.4}$$

Where: V volume of vacuum pump's working chamber, in m^3

L internal depth of the vacuum pump casing, taken as 0.19970m

From this, the volume of the working chamber can be evaluated as a function of θ_1 for a full rotation:

$$V_{wc}(\theta_1) = \begin{cases} V(\theta_1) & 0 < \theta_1 \leq \frac{2\pi}{z} \\ V(\theta_1) - V\left(\theta_1 - \frac{2\pi}{z}\right) & \frac{2\pi}{z} < \theta_1 \leq 2\pi \\ V(2\pi) - V\left(\theta_1 - \frac{2\pi}{z}\right) & 2\pi < \theta_1 \leq 2\pi + \frac{2\pi}{z} \end{cases} \tag{3.5}$$

Where z is the number of rotor vanes. It is assumed that there will not be a control valve at the intake port to regulate the volume of each working chamber. Therefore filling will cease and expansion will begin in the working chamber once the lagging vane passes beyond the intake port. Likewise, expansion will cease and emptying will begin once the leading vane passes beyond the exhaust port. Based on this, the expansion ratio can be expressed by:

$$\varepsilon_{exp} = \frac{V\left(\theta_{out} + \frac{2\pi}{z}\right)}{V(\theta_{in})} \tag{3.6}$$

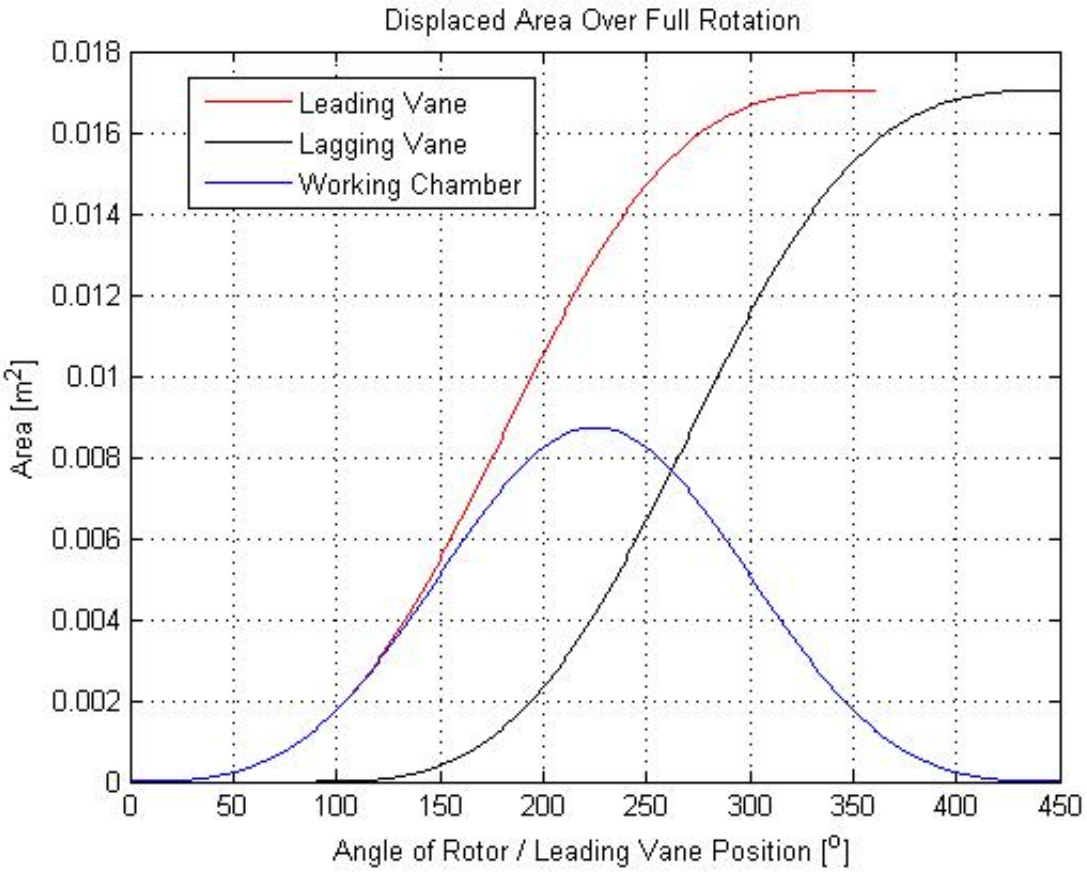

Figure 3.2: Displaced area of 4 vane vacuum pump arrangement

Figure 3.2 illustrates the changing area displaced by the leading vane, the lagging vane and the working chamber of a 4-vane variation of the vacuum pump.

Fluid

Assuming air acts like an ideal gas and follows a steady flow, isentropic expansion process and polytropic compression process, with no leakage and negligible frictional generation, the maximum pressure and temperature drops can be predicted with the following equations (Cengel & Boles 2011):

$$\left(\frac{V_{exp}}{V_1}\right)^{-k} = \frac{p_{exp}}{p_1} = \left(\frac{T_{exp}}{T_1}\right)^{\frac{k}{k-1}} \tag{3.7}$$

$$\left(\frac{V_2}{V_{exp}}\right)^{-n} = \frac{p_2}{p_{exp}} = \left(\frac{T_2}{T_{exp}}\right)^{\frac{n}{n-1}} \tag{3.8}$$

Where k and n are the ratio of specific heats for air and an arbitrarily chosen polytropic index, taken as 1.4 and 1.25 respectively. Any drop in air temperature during the filling and exhaust processes were neglected.

Ignoring the effects of kinetic and potential energies, an equation for the maximum possible amount of power generated by the isentropic expansion and polytropic compression processes can be approximated by the following derivation:

$$\begin{aligned}\frac{\dot{W}_{exp}}{\dot{m}} &= -\int_1^2 v dp \\ &= c_p(T_1 - T_{exp}) + \eta c_p(T_{exp} - T_2)\end{aligned} \tag{3.9}$$

Where c_p is the specific heat capacity of air at constant pressure, taken as 1.005kJ/kg.K, η is the isentropic compression efficiency, taken as 85%, and $\dot{m}$ is the maximum possible mass flow rate of air (i.e. flow under sonic conditions). This can be found by determining critical properties at the valve's throat, based on assumed initial stagnant conditions:

$$\rho_0 = \frac{p_0}{RT_0} \tag{3.10}$$

$$T^* = T_0\left(1 + \frac{k-1}{2}M_1^2\right) \tag{3.11}$$

$$\rho^* = \rho_1\left(1 + \frac{k-1}{2}M_1^2\right)^{\frac{1}{k-1}} \tag{3.12}$$

Where: M Mach number under sonic conditions, taken as 1
T_0 stagnant air temperature, taken as 293K
p_0 stagnant air pressure (abs), taken as 600kPa
R universal gas constant of air, taken as 287J/kg.K

Mass flow rate can then be determined by inputting the relevant values into equation (2.4). Note that the critical area considered in this case is the control valve's throat; with an arbitrarily chosen diameter of 3mm. Recall that (Al-Duwaisan et al. 1999) recommended

using only 60% of the operating mass flow rate in power calculations to account for losses in the system.

If the cold air exhausts before any compression begins, equation (3.8) should be ignored and the net power generated by expansion in the motor will be simplified to:

$$\frac{\dot{W}_{exp}}{\dot{m}} = c_p(T_1 - T_2) \tag{3.13}$$

3.4 Results

Simulations for different RVVP arrangements were run based on the previous equations. Each of these simulations ran on the assumption that the intake gauge pressure and static air temperature were 600kPa (or 6 bar) and 20^{o}C respectively.

Table 3.1: MATLAB Vacuum Pump Simulation Results

vanes	*Port (^{o})		ε_{exp}		**Min. Exit	ΔT (^{o}C)		$\dot{W}_{exp}$ (kW)	
	In	Exit	Max	60%	Press. (kPa)	Max	60%	Max	60%
2	40	270	1.17	1.10	461.38	17.87	10.72	0.210	0.126
	10	270	1.51	1.27	292.03	44.62	26.77	0.525	0.315
4	40	270	2.14	1.47	158.49	76.83	41.93	0.916	0.550
	40	225	2.41	1.63	103.49	86.87	52.12	1.021	0.613
	10	270	4.39	2.02	-6.30	130.82	71.85	1.548	0.929
	10	225	4.94	2.30	-26.41	138.36	83.01	1.627	0.976
6	40	270	2.91	1.69	78.64	102.00	55.50	1.220	0.732
	40	210	3.66	2.01	12.50	118.71	71.23	1.396	0.838
	10	270	7.82	2.51	-56.16	164.33	90.17	1.947	1.168
	10	210	9.84	3.05	-72.76	175.59	105.35	2.065	1.239

*port's angular position using figure 3.1's convention

**gauge pressure

The exhaust air temperature will need to be well below -40^{o}C in order to be assured of solidification of water particles in a reasonable time frame. As seen by the simulation

results from a small sample of arrangements, reducing the exhaust air's temperature is most effectively accomplished by assemblies with a larger number of vanes and a smaller intake port position. An outlet port position closer to its optimal position (i.e. at $\frac{\pi(z+1)}{z}$ rad) also improves the temperature.

As minimal effort in redesign is desired, the best theoretical performance based assemblies to consider implementing would be those that have more than 2 vanes and intake ports repositioned at a lesser angle to the rotor's horizontal line of symmetry. Some of these arrangements have a minimum output pressure well below standard atmospheric pressures. If such an arrangement is adopted, a fan or pump will likely need to be employed downstream of the vacuum pump's exhaust port to ensure positive flow.

Assuming that the expansion process occurs very quickly is a crucial assumption when viewing the isentropic expansion simulation results for the different arrangements. If the shaft speed is not fast enough then these performance characteristics are not likely to hold.

3.5 Chapter Summary

USQ are in possession of a RVVP. Given their similar geometry and assembly, it is predicted that these types of pumps can operate similarly to a RVAM when the processes are reversed. One significant advantage gained through utilising a redesigned RVVP over conventional RVAMs is the theoretically larger expansion ratios, particularly when the number of vanes employed are increased and the ports are repositioned optimally. This will see a larger portion of work extracted from the air stream, thereby reducing the exhaust air temperature.

The performance characteristics of these different arrangements however hinge on the assumption that shaft speed will be high enough to validate an assumption of isentropic expansion. However the overall size of the device would likely prove to be contrary to this assumption operating under low intake pressures. The weight of components would also be likely to affect its performance in practical application of these findings.

Chapter 4

Methodology

4.1 Chapter Overview

This section details the methodology used in the testing of a commercially available air motor, including the design and sizing of necessary experimental hardware, the experimental set up, procedure and post processing analysis conducted. Hardware sizing and design was all based on known operating parameters and available base equipment at USQ's P10 laboratory.

4.2 Experimental Design and Materials

The experimental campaign was purposed toward testing the cooling capacity of commercially available air motors while operating under steady flow conditions. This was aimed at both:

- determining whether or not readily available equipment was suitable to use in providing a viable alternative to the cooling system currently in use.
- setting a point of reference to use in theoretical modelling to simulate pressurised air expanding in an air motor during operation.

Simplifying the experimental processes, compressed air from a large vessel at ambient temperatures steadily flows through a pressure regulator toward an open control valve upstream of the air motor. Work is then extracted from the air by the air motor before being discharged at it's exhaust pressure and temperature. Several hardware components were required to facilitate this set of experimentation conducted on the air motor rig (AMR); most notably the air motor and work extraction device.

Note that the early rounds of preliminary testing used two thermometers for temperature readings (see figure 4.1), however they were replaced by a single dual thermometer when it became available.

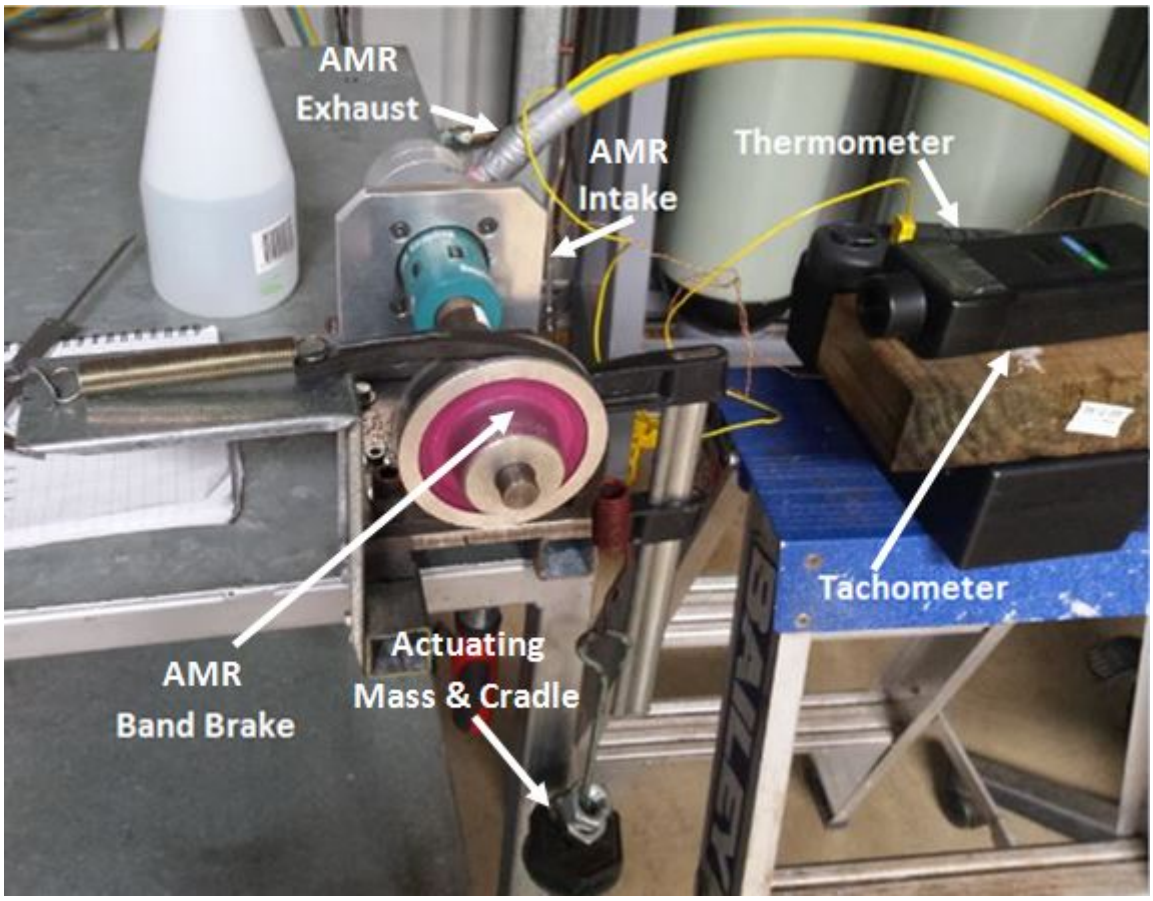

Figure 4.1: AMR Experimental Set-up for Initial Testing. The yellow exhaust hose leads to a volumetric reader while the black intake tube leads under the table to the acting control valve; positioned off screen.

4.2.1 Theoretical Model of Fully Expanded Air

Air motor distributors openly provide their motors' operating specifications on websites. Although cooling is not considered their primary function, predicted drops in temperature can be approximated knowing an air motor's power specifications (Al-Duwaisan et al. 1999).

A rudimentary model of an air motor was developed from ideal fluid mechanics equations, and assumed the work extraction processes would fully expand the pressurised air.

A large majority of the performance data readily available online is related to an intake air pressure (gauge) of roughly 6 bar. This value was set as the initial pressure in the simulation conducted (refer to Appendix B). As it was assumed that the theoretical air motor would be able to fully expand air to atmospheric pressure at its exhaust (with no compression occurring at all), the final pressure (abs) will be taken as 101.325kPa. An entering air temperature of 20^oC was chosen.

Table 4.1: MATLAB Air Motor Simulation Results

Quantity	Value
Temperature Drop (^oC)	124.42
Maximum flow speed in pipe (m/s)	0.71
Maximum mass flow rate through system (g/s)	11.71
Maximum volumetric flow rate through system (m^3/min)	0.58
Max air motor expansion power (W)	1462.96

Looking at table 4.3, it can be seen that quite a significant temperature drop can be expected from fully expanding the compressed air isentropically.

It again assumed that air acts like an ideal gas and follows a steady flow, isentropic expansion process, with no leakage and negligible frictional generation. The maximum possible mass flow rate of air (i.e. flow under sonic conditions) expected was determined from critical quantities, and inputted into equation (3.13) to provide an upper limit for expansion power. This was based on an equivalent throat diameter of 3mm; simulating an

open floating ball valve's diameter. The values obtained in this simulation were used to compare against a number of specification sheets provided by air motor distributors. The maximum volumetric flow rate through the system was the particular quantity chosen in matching to the air consumption of a suitable candidate air motor.

4.2.2 Air Motor Sizing

Given that power is a function of both temperature drop and flow, higher sized air motors typically offset their lacking expansion ratios with a greater air consumption. Therefore it is desirable for the chosen air motor to maximise power generation through expansion. It is also desirable to have high nominal speed to ensure expansion processes are occurring quickly.

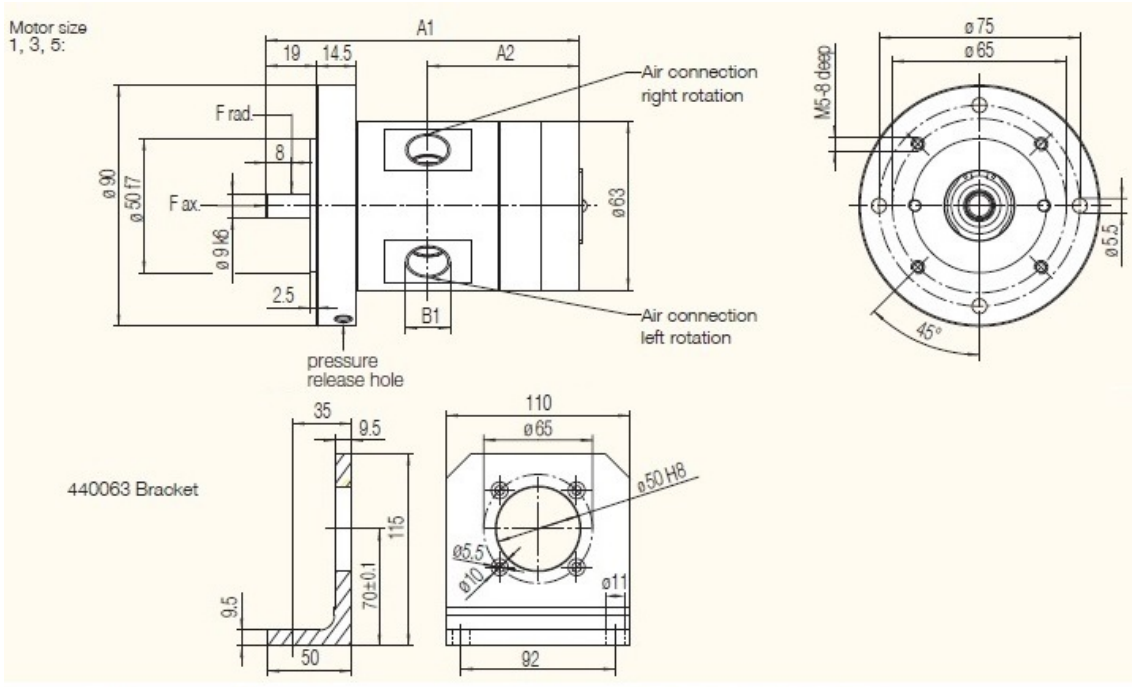

Motor size	Type	Dimensions of Air motor (mm)		
		A1	A2	B1
1	63-001F01	82	39	1/8
3	63-001F03	102	49	3/8
5	63-001F05	117	56.5	3/8
7	63-001F07	116.3	54.8	1/2
8	63-001F08	136.3	64.3	1/2

Figure 4.2: DEPRAG air motor catalogue extract (*Basic Line: Air Motors from 200W to 1.2kW* 2015)

Knowing this, the highest rated air motor operating near 6 bar with an air consumption of approximately 0.6m^3/min was a 400W reversible model (without gearing) sourced from DEPRAG. The particular model purchased was the 63-001F03 DEPRAG air motor (*Basic Line: Air Motors from 200W to 1.2kW* 2015). A supporting bracket was also added to the purchase order.

The operating specifications of this air motor were used in conjunction with equations (3.7) and (3.9) to determine expected cooling performance characteristics. 60% of the air motor's power output was taken as the motor's effective expansion power (Al-Duwaisan et al. 1999). This provided an expected temperature drop of 20.41^{o}C, with the expansion power being 240W. Note that the entering air's gauge pressure and temperature were again assumed to be 6 bar and 20^{o}C.

Table 4.2: Preliminary MATLAB DEPRAG Air Motor Simulation Results

Expansion Power	Quantity	Value
100% of rated power	Expansion Power (W)	400.00
	Minimum exhaust pressure (kPa)	354.00
	Minimum exhaust flow temperature (^{o}C)	-14.02
	Temperature Drop (^{o}C)	34.02
	Effective Expansion Ratio	1.36
60% of rated power	Expansion Power (W)	240.00
	Minimum exhaust pressure (kPa)	443.38
	Minimum exhaust flow temperature (^{o}C)	-0.41
	Temperature Drop (^{o}C)	20.41
	Effective Expansion Ratio	1.20

It would have been preferable to have determined these performance characteristics using equations based on both fluid mechanics and the air motor's geometry (similar to the model developed in Chapter 3), however this would have required deconstructing the air motor before any physical testing had even begun.

These values can be supported by "Pneumatic Drives: System Design, Modelling and

Control" (Beater 2007), in which Beater refers to another study having measured volumetric expansion ratios up to 1.43 in non-reversible RVAMs. Substituting this value into equation 3.7 (assuming only expansion is experienced) and using an initial temperature of 20^oC, the expected temperature drop is approximately 39^oC. Note that the particular air motor model being tested in this thesis is a reversible motor, so it can be expected that the magnitude of temperature drop will be less than this.

4.2.3 Dynamometer for DEPRAG Air Motor

The 400W of theoretical power available from the air motor has to be extracted by a secondary device. The amount of power drawn will need to be measured. As a working dynamometer was not available, a mechanical braking system was designed; specifically a band brake due to the ease of analysis, design and construction.

Band Brake

An Aluminium 1A v-pulley with a $3\frac{1}{4}$" pitch diameter and a $\frac{5}{8}$" bore was adopted (*Blackwoods Catalogue* 2014). Note that the imperial pulley happened to be more easily sourced at the time, which is the only reason it was chosen over a metric pulley. A readily available spring and a length of rubber v-section belting were also utilised in the construction of the band brake.

Figure 4.3: Stenco Aluminium 1A v-pulley (*Blackwoods Catalogue* 2014)

Equations (2.5) to (2.8) were arranged to determine the required actuating force, and resulting anchoring and friction force after defining certain parameters (see `am.m` code in Appendix B).

$\dot{W}_{out}$	work output by air motor, taken as 400W
rpm	nominal rotational speed of air motor, taken as 5000rpm
r	radius of v-pulley, taken as 0.034m
f	coefficient of friction, taken as 0.5
β	half of the v-pulley's wedge angle, taken as $\frac{\pi}{9}$ rad (or 20^o)

The length of friction material in contact with the pulley is one easily changeable parameter that significantly affects the amount of mass required. Reasonable values for the angle of contact between the v-section belt and v-pulley would be taken as π and $\frac{\pi}{2}$ rad:

Table 4.3: MATLAB DEPRAG Band Brake Simulation Results

Angle of contact, ϕ (^{o})	Quantity	Value
180	Anchoring Force (N)	22.70
	Actuating Mass (g)	23.43
	Friction Force (N)	22.47
90	Anchoring Force (N)	24.98
	Actuating Mass (g)	256.26
	Friction Force (N)	22.47

Given that the actuating force required by a band with 180^o degrees of contact is such a small figure, a fully characterised set-up will be best served with around 90^o of contact.

Several secondary components were required in order to connect the air motor to the band brake. The more important of these were a transmission shaft, a bearing and housing, power transmission coupling, an anchoring mechanism, and mounting plate. These were either sourced or fabricated in house; refer to the appendices for detailed design drawings.

Radial Ball Bearing and Housing

To minimise the moment arm experienced by the shaft, the bearing and bearing housing were placed as close as possible to the v-pulley. As there are no thrust loadings involved in the band brake, a radial ball bearing was an appropriate choice of bearing to utilise. The maximum radial force acting on the radial ball bearing will be approximated as 70N (i.e. the maximum force acting on the v-pulley with a factor of safety of 3). Assuming no thrust loading and 90% reliability, the following are parameters to be used based on Juvinall & Marshek (2012):

L_r life corresponding to rated capacity, taken as 90×10^6 revolutions (table 14.2)

K_a application factor, taken as 1.0 (table 14.3)

K_r life adjustment reliability factor, taken as 1.0 (figure 14.13)

L life corresponding to radial load (F_r), taken as 12000 hours (table 14.4)

For radial ball bearings with zero thrust forces, $F_e = F_r$ (equation 14.3). Therefore the required value of rated capacity for this application can be determined using equation 14.5b (Juvinall & Marshek 2012):

$$\begin{aligned} C_{req} &= F_e K_a \left(\frac{L}{K_r L_R}\right)^{0.3} \\ &= 70 \times 10 \left(\frac{12000hr \times 5000rpm \times 60mins/hr}{1 \times 90 \times 10^6}\right)^{0.3} \\ &\approx 211.7N \end{aligned} \tag{4.1}$$

Comparing these values against those listed in table 14.2, the required rated capacity for this application is well below those listed (even in the extra light series). Given that the bore of the v-pulley is $\frac{5}{8}$", the chosen ball bearing will need a bore of at least 17mm. Based on the information above, an open design extra light deep groove ball bearing (10mm in width, with a 17mm bore and a 35mm outer diameter) was chosen (*Blackwoods Catalogue* 2014). Although no speed rating is provided in the catalogue, a very similar SKF model is rated for 45000rpm; well over the air motor's maximum rated speed of 10000rpm (*Deep groove ball bearings, single row* 2015). This model corresponds roughly to the L03 basic bearing number specified in table 14.1, so the bearing housing's shoulder bore will be taken as 32mm in diameter.

Coupling

A jaw type coupling was chosen, given its cost effectiveness and ability to perform at speeds over 10000rpm. It is also relatively forgiving for minor misalignment of coupling shafts. Hubs were selected based on the diameters of the coupling shafts.

Figure 4.4: Fenner SX jaw coupling (*Blackwoods Catalogue* 2014)

Shaft

Given the low forces and moments involved in the operation of the AMR, neither a stress or fatigue analysis was conducted on the shaft; suffice it to say that the stainless steel shaft will be more than capable of withstanding the relatively small radial forces acting on it for a prolonged period of time. As such, the shaft design primarily accounted for the seating and mating needs of components.

Mounting Plate and Spring Anchoring

The 10mm thick mounting plate was made from stainless steel and served as a structural mount for the air motor bracket and the bearing housing. A small length of wire was attached to a length of thin sheet metal to form the spring's anchoring device. This sheet was positioned with screws into the AMR's base supports. Given the low forces and moments involved in operation, no in depth material, stress or fatigue analyses were conducted prior to the design of these.

4.2.4 AMR Assembly

The assembly of the AMR proceeded in accordance with the drawings provided in Appendix D. The anchoring mechanism was sourced from scrap sheet metal, so has not been included in this collection.

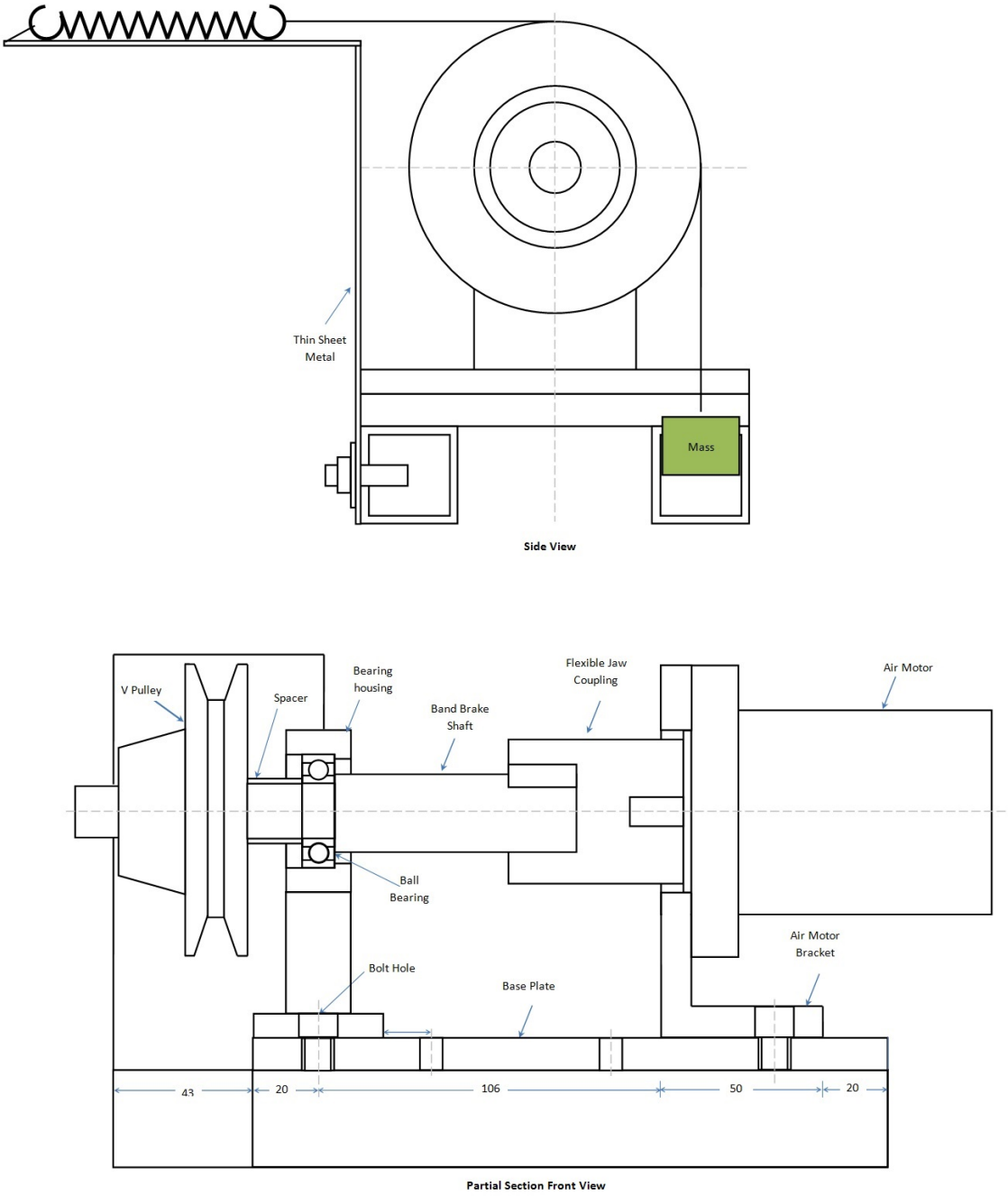

Figure 4.5: Air Motor Rig Assembly (initial design drawing)

4.3 Experimental Set-up and Procedure

This section aims to enable the reproduction of the project's experimental campaign, including necessary measurements to enable proper interpretation of the results. Each round of experimental testing was conducted by a student undergoing supervision from an appropriately qualified and inducted staff member. Note that more reliable measuring equipment would have been used if it were available.

4.3.1 Materials and Equipment

The primary experimental facility used in testing was an air compressor and its receiver tank (capable of maintaining pressures close to 6 bar during discharge). Assuming negligible head losses between the high pressure air reservoir and the air motor's intake port, the air pressure regulator will provide the intake air's gauge pressure. A ball valve push fitted into the air pressure regulator served as a switch to start and stop motor operation.

The static temperature of the incoming pressurised air was measured by a Type K thermocouple. This was positioned further downstream of the ball valve and just upstream of the air motor's intake port, where it was fitted within an acrylic sleeve bonded to the inside a t-type tubing junction with "super glue" (see figure 6.1).

Figure 4.6: High Pressure K-type thermocouple arrangement

Another thermocouple was positioned as close to the air motor's exhaust port as possible to measure the "cooled" air's temperature prior to secondary expansion occurring. Both K-type themocouples were connected to an EXTECH Instruments "EasyView 10 Dual K Thermometer".

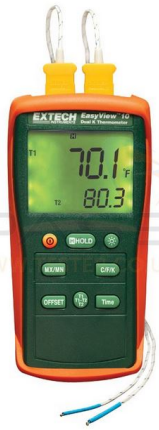

Figure 4.7: EasyView 10 Dual K Thermometer

Note that the initial testing/trial period used two separate thermometers, one of which is seen in figure 4.1. However as soon as the EasyView 10 Dual K Thermometer was made available, subsequent testing used only this single thermometer. The torque generated by the air motor was measured through a spring based arrangement, where the actuating force A Lutron DT-2236 photo-tachometer was positioned near the AMR (perpendicular to the reflective tape adhered to the AMR's shaft) to measure the output shaft speed.

Figure 4.8: Lutron DT-2236 photo-tachometer

Further downstream was a volumetric reader, which in tandem with a stopwatch acted to measure the average mass flow rate of air travelling through the system. All of the components were connected using appropriately chosen fittings and tubing, given the predicted operating pressures.

It would have been more preferable to have implemented a mass flow reader and a proper dynamometer, however there were not any available that could be sourced in time. It also would have been preferable to have had a quick response pressure transducer within the air motor itself to measure the chamber pressure before and after the exhaust port however including one inside the commercial air motor would have been too difficult and intrusive.

4.3.2 Testing of AMR

Experimentation was conducted in accordance with the approved risk management plan. Over the several test rounds conducted, the AMR was operated at 6 bar (gauge) under varying loads via increases in brake actuating mass. It was ensured that all other variables affecting motor performance were constrained as well as reasonably possible.

Prior to each round of testing, the initial length of the spring (under tension from the actuating mass' weight) was measured and the intake pressure was reset to 6 bar. Tests on average lasted a minute in length, so as to allow the system to reach a steady state of operation; after which point readings were recorded. These were the measurement of rotational speed, actuating mass, spring length (final) and temperature (inlet and outlet). Test air volume and test time were measured just prior to ceasing operation.

The time between tests was set at a minimum of 5 minutes to allow pressure in the air receiver tank to build up again. In the mean time, the band brake was cooled with water to maintain a reasonably uniform braking friction coefficient. This was done to maintain uniform increases in power extracted with increases in actuating mass. It would have been preferable to have allowed more time between tests, however time constraints wouldn't allow this.

4.4 Chapter Summary

The experimental design and methodology adopted in this work was first and foremost focussed on testing the proposed cooling system separate to the wind tunnel. If testing of the commercial air motor proved to possess the necessary cooling capacity required, then integrated testing would be considered.

Chapter 5

Results and Discussion

5.1 Chapter Overview

This chapter defines and evaluates the performance data recorded from the several test runs of the AMR. Decisions regarding the direction of this thesis will be dependent on these results.

5.2 Experimental Results

Recall from the previous chapter that the AMR was operated in experimental testing by connecting the system's intake up to a pressurised air source. Temperature, intake pressure, speed and volumetric flow rate were measured respectively by thermocouples, a pressure regulator, an optical tachometer, a volumetric reader and stopwatch.

Table 5.1 provides a summary of the raw data gathered from the last set of testing conducted. Recall that it would have been preferable to determine what pressure the working air was expanded to just prior to the exhaust stage, however this would have required intrusive tinkering of the air motor. As such, this measure was excluded from the testing regime.

Table 5.1: Recorded Data From Round 4 of AMR Testing

Run No.	M_{act} (g)	L_{spring} (mm)		Temp (^{o}C)		rpm	t (sec)	V (L)
		Initial	Final	In	Exit			
1	542	87.0	169.1	14.6	-5.8	2403	61	472
2	-	-	-	12.6	-3.8	8221	57	548
3	463	85.3	150.0	13.8	-10.1	3645	77	660
4	395	83.3	121.8	14.0	-8.0	4459	68	580
5	327	78.6	118.9	14.1	-10.1	4730	66	596
6	272	77.4	115.9	14.2	-9.1	4545	78	657
7	204	76.5	116.8	14.6	-10.1	5003	72	617
8	136	75.9	108.6	14.5	-8.4	5225	74	623
9	68	75.0	91.6	14.4	-6.2	6536	70	623
10	542	87.9	152.1	15.5	-5.0	2850	63	464
11	610	92.7	165.2	15.9	-6.2	2715	81	450

Table 5.2: Secondary Results From Round 4 of AMR Testing

Run No.	$\dot{m}$ (kg/s)	τ_{brake} (Nm)	ΔT(^{o}C)	Power (W)	
				Brake	Expansion
1	0.0102	1.267	20.4	318.88	209.61
2	0.0126	0	16.4	0	207.81
3	0.0115	0.999	23.9	381.18	276.48
4	0.0114	0.594	22.0	277.48	251.25
5	0.0121	0.622	24.2	308.102	294.94
6	0.0113	0.594	23.3	282.83	263.87
7	0.0115	0.622	24.7	325.89	285.67
8	0.0112	0.505	22.9	276.16	258.53
9	0.0118	0.256	20.6	175.37	243.82
10	0.0097	0.991	20.5	295.74	199.89
11	0.0074	1.119	22.1	318.15	163.28

The recorded data was inputted into an excel sheet and then manipulated in MATLAB to provide secondary data for brake torque and equivalent expansion power, flow power, temperature drop, and mass flow rate (see Appendix B). Note that equivalent expansion power is calculated assuming temperature drop was achieved purely through isentropic expansion under steady flow conditions.

Due to the methods used in measuring volumetric flow rate, there will be a degree of inaccuracy present in the calculations used to derive the following predicted quantities according to the 1st law of thermodynamics:

- Measuring the volume of test air caught and time elapsed during testing would only serve to provide an average flow rate rather than an instantaneous quantity.
- the capacity of the compressed air source was a problem as the compressor would regularly start up toward the end of the testing round.

5.3 Discussion of Results

Comparing the torque curves from figures 5.1 and 5.2 (i.e. measured brake torque versus rotational speed and the manufacturer's performance data for 6 bar operating pressure) shows that there is a reasonable level of accuracy between them. It can be implied from this that the other experimental measurements were also recorded with a reasonable level of accuracy.

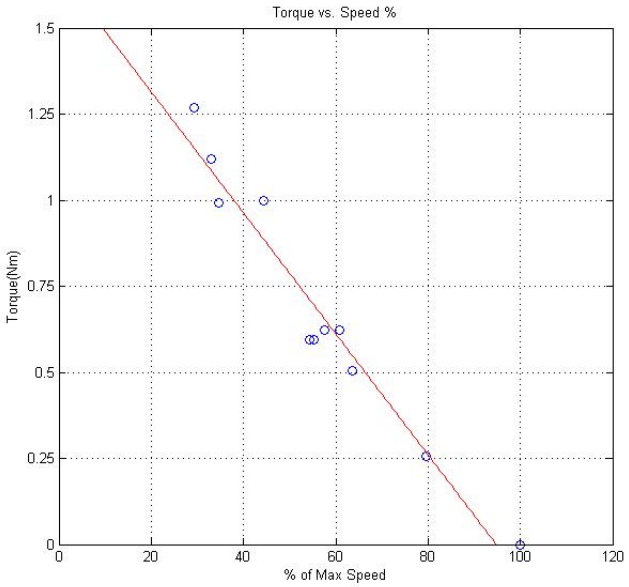

Figure 5.1: MATLAB Plot of Torque versus Rotational Speed

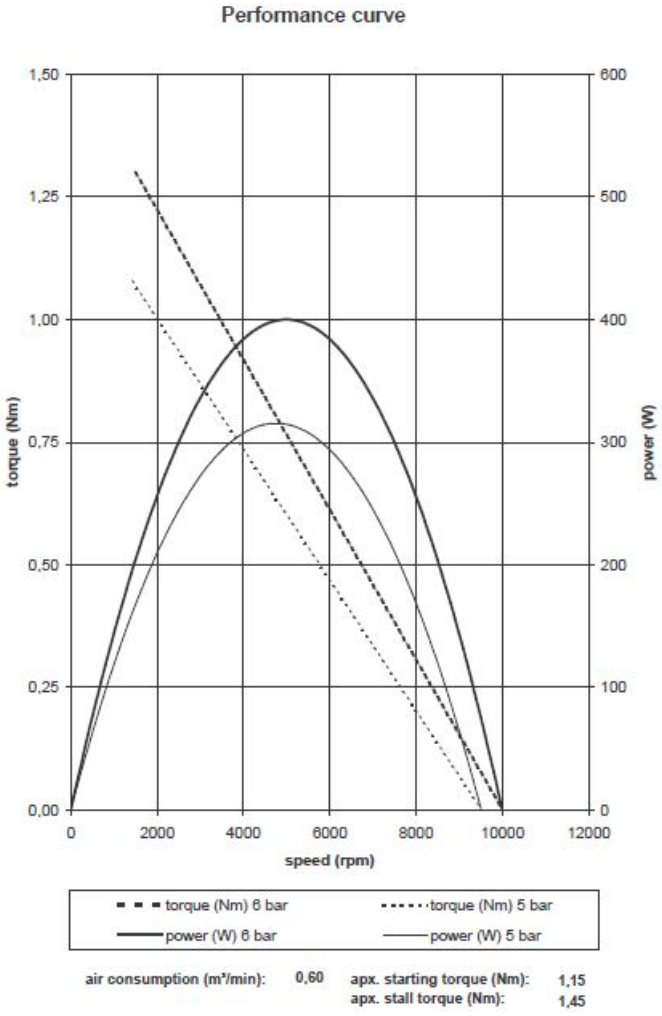

Figure 5.2: DEPRAG 63-001F03 Performance Curve

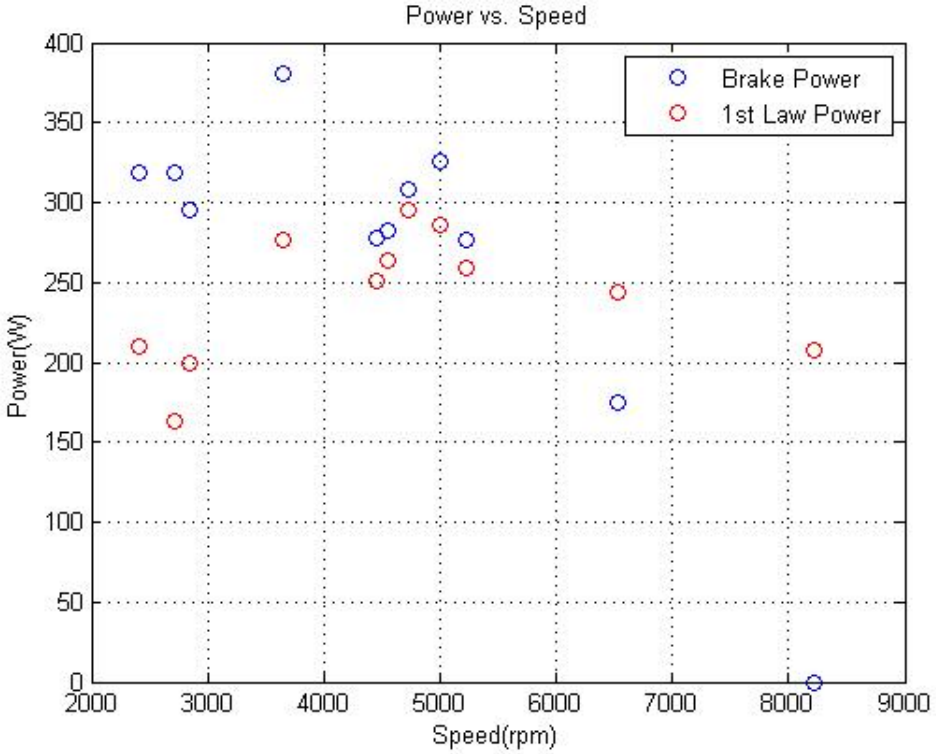

Figure 5.3: MATLAB Plot of Power versus Rotational Speed

The above plot of power versus rotational speed shows that brake power values corresponding to rotational speeds between 2000 and 4000 rpm are below the expansion power values predicted by the 1st law of thermodynamics. This means that at speeds below nominal speeds the air motor expands air at low isentropic efficiencies (given that brake power is recorded to be lesser than flow power according to the 1st law of thermodynamics).

The power values corresponding to rotational speeds between 6000 and 9000 rpm seemingly suggest that the air must still be doing a fair amount of work while expanding inside the device, despite the low amount of brake power extracted. This is particularly so in the case of non-loaded operation, where there is obviously still a significant drop in temperature despite there being no brake power extracted.

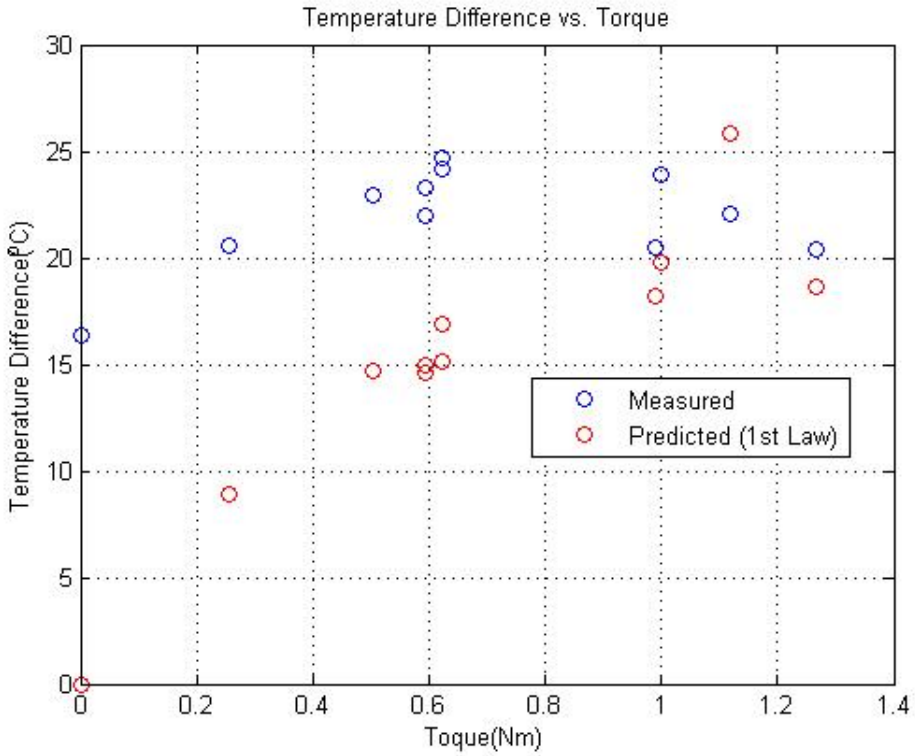

Figure 5.4: MATLAB Plot of Temperature Difference versus Brake Torque. Note that predicted temperature was calculated using equation 3.13, assuming 60% of calculated power is used.

The predicted and measured values shown in figure 5.4 follow a similar relationship to those in figure 5.3. As the applied torque increases, the temperature difference is generally expected to also increase. This is true up until a point, where maximum power is being extracted. After this point, increasing torque will only decrease the air motor's rotational speed, thereby the mass flow rate of exhaust air and the amount of brake power being extracted.

The greatest drop in recorded temperature is approximately 25^{o}C. Unfortunately this means that a commercial rotary vane air motor's performance is not sufficient to provide the temperature drop necessary to support its use as a viable alternative cooling system; when operating at ambient conditions. However this was the expected outcome given the results of early simulation models, which only returned a maximum possible temperature drop of approximately 20^{o}C. For the sake of future work, the behaviour of the expanding

air is of greater interest.

As seen by both of the above figures, the predicted values generated by the preliminary system model (presented in table 4.2) and recorded data (at speeds and torques in the proximity of the nominal values specified in figure 5.2, i.e. 5000rpm and 0.75Nm) present a high level of similarity. This means that expanding air can be modelled as an isentropic process with reasonable accuracy when in a rotary vane air motor operating at nominal speeds and torques; a useful relationship to replicate. Therefore improving the cooling capacity of air motors

To confirm this relationship, a more refined system model can be generated that incorporates both fluid and geometric characteristics. This model will then be used to assist in a possible redesign of the DEPRAG air motor's rotor cylinder housing.

A customised air motor can also be designed in an attempt to fully expand air; and maximise potential temperature reduction. This move would be further supported should retesting of the adapted DEPRAG air motor prove to align with the refined system model predictions.

5.4 Chapter Summary

The experimental and secondary results recorded during the testing regime were defined and discussed in this section. It was found that expanding air in a commercial rotary vane air motor does not exhaust air that is cold enough to be justify its use as a viable alternative cooling system to that of the current nitrogen plenum system. The results of these tests did support that the expansion of air in the motor follows an approximately isentropic process. This hypothesis will be confirmed in the next chapter by firstly developing a refined system model of the expansion processes in a motor and assist in the redesign of the DEPRAG air motor's rotor cylinder housing.

Chapter 6

Post Experimental Design Work

6.1 Chapter Overview

This section details the collection of work on air motor design after conducting the AMR experimental testing. The chapter will detail a refined system model, a modified cylinder rotor housing design for the DEPRAG air motor and a customised RVAM.

6.2 Refined System Model

The preliminary model provided a reasonable prediction for temperature drop, however it was based on literature rather than analysis. As such a more refined system model (combining both fluid and geometric quantities) was developed in conjunction with the experimental results, aimed at assisting in design work and improving performance predictions. This model's development was instead based on geometric and fluid analytical methods; similar to those detailed in chapter 3, with a few additions.

A steady mass flow rate defined by choked flow through the equivalent of a 3mm diameter throat will be assumed in the simulation. Intake and exhaust channels were taken into consideration in this latest system model iteration. This means that the working cham-

ber's pressure will remain constant for longer over the intake and exhaust processes (at average intake and exhaust pressures); thus reducing the possible amount of expansion and compression over a cycle.

The power generated and used in displacing air during the intake and exhaust processes was also included in the system model to approximate a figure for total flow power:

$$\begin{aligned}\frac{\dot{W}_{total}}{\dot{m}} &= c_p(T_1 - T_{exp}) + \eta c_p(T_{exp} - T_2) + \frac{p_1}{m}(V_{fill(2)} - V_{beg}) \\ &\quad -\frac{p_2}{m}(V_{ex(1)} - V_{rem}) \end{aligned} \tag{6.1}$$

Where:

η	isentropic compression efficiency, taken as 85%
m	mass of air in expanding working chamber, in kg
p_2	average exhaust pressure (abs), taken as the mean of the air motor's expanded pressure and ambient pressure in Pa
$V_{fill(2)}$	Working chamber volume as lagging vane passes beyond intake channel, in m^3
V_{beg}	Volume between the x-axis and leading vane (i.e. see figure 6.1), in m^3
$V_{ex(1)}$	Working chamber volume as leading vane passes into exhaust channel, in m^3
V_{rem}	Volume between the lagging vane and x-axis (i.e. see figure 6.1), in m^3

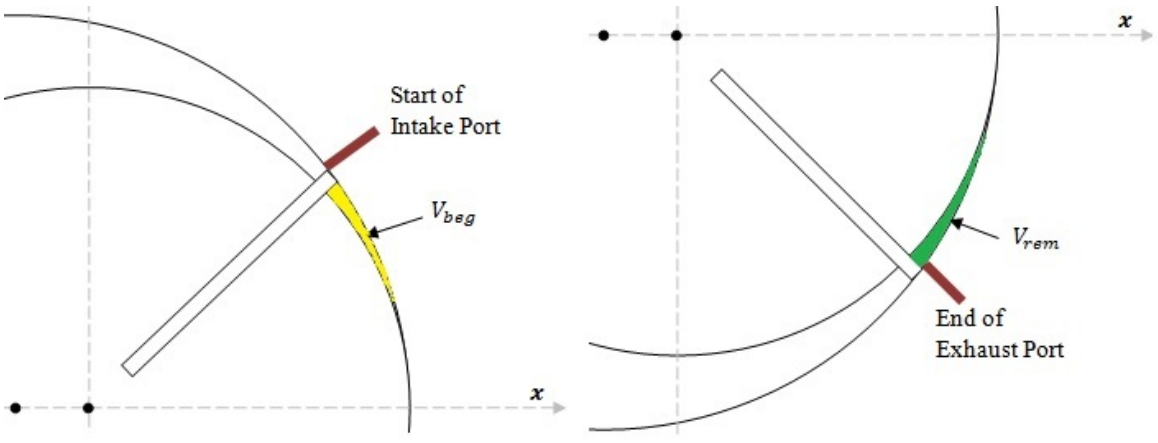

Figure 6.1: Convention for volumes in refined model geometric calculations.

Shaft rotational speed can be determined by using the following equation:

$$rpm = \frac{60\dot{m}}{z\left(\frac{p_1 V_{fill(2)}}{RT_1} - \frac{p_2 V_{rem}}{RT_2}\right)} \tag{6.2}$$

Where: R universal gas constant, in J/kg.K

z number of vanes

Blow-by is another factor considered, as V_{rem} and V_{beg} in equation 6.1 depend on little to no blow-by occurring during operation (i.e. rely on there being a sufficiently small gap between the small space between the rotor and the cylinder surface). The worst case scenario will be when only the rotor separates the intake and exhaust ports, so blow-by must be small enough to determine what percentage of air flows backward through the gap. Blow-by estimates were calculated using the following equation (Fox, McDonald & Pritchard 2012):

$$Q = l\left(\frac{Ua}{2} - \frac{1}{12\mu}\left(\frac{dp}{dx}\right)a^3\right) \tag{6.3}$$

Where: Q volumetric flow rate, in m^3/s

l transverse width of gap, in m

U relative linear speed of rotor to cylinder housing, in m/s

a gap clearance, in m

μ air viscosity, taken as 1.5×10^{-5} N.s/m^2

$\frac{dp}{dx}$ rate of change of pressure over distance (assumed to be a linear relationship), in Pa/m

This calculation is valid for flow between two infinite plates, which is a reasonable assumption over finite radial segments.

The system model was tuned by adjusting the polytropic indices used during the expansion and compression processes. After conducting additional testing and retesting (as defined in the next section), values of 1.35 and 1.03 respectively were found to best fit the recorded data; justified by the small dimensions of the device.

Refer to Appendix B for the refined MATLAB system model code in full. The following

table details the results of the refined analysis on the DEPRAG air motor. The intake air's temperature and pressure (gauge) was taken as 15^{o}C and 6bar.

Table 6.1: Refined MATLAB DEPRAG Air Motor Simulation Results

Quantity	Value
Minimum exhaust flow temperature (^{o}C)	-6.30
Temperature Drop (^{o}C)	21.30
Net Expansion/Compression Power (W)	256.00
Predicted Flow Power (W)	708.79
Maximum mass flow rate (kg/s)	11.81
Nominal shaft rotational speed (rpm)	4204
Blow-by (% of Q_{max})	0.23
Effective Expansion Ratio	1.21

In viewing the results from running this adapted simulation, there is a great deal of similarity between them and the air motor's known operating parameters and AMR's adapted experimental results (see table 6.4 and 6.5); in particular the predicted temperature drop, shaft speed and net expansion/compression power. The net expansion/compression power is slightly larger than the expansion power from the previous model, however the previous iteration didn't account for any recompression occurring. Therefore it can be concluded that the air does approximately follow processes within the air motor that are aligned with this refined model. However in the original rotor cylinder housing, expansion only occurs over a small portion of each rotation. Therefore further investigation will need to be conducted to determine whether this relationship holds over extended periods of expansion.

6.3 Redesigned Rotor Cylinder Housing

The most effective way to increase the cooling experienced by expanding air is to increase the expansion ratio. It was decided that the most effective way to accomplish this was by redesigning the DEPRAG air motor's rotor cylinder housing. Redesigns considered were

limited by the need to retain several key features of the original component. As such, the only changes made were a reduction in size of the intake port, removal of the intake channel and increase in length of the exhaust channel.

The internal dimensions of the component were not specified in any detailed drawings provided by DEPRAG, so appropriate metrology equipment and techniques were used to find unknown dimensions. A model and detailed drawing of the proposed redesign (see Appendix D) was submitted to the University's metal fabrication workshop. The internal surface finish of the fabricated component was slightly less than that specified in the detailed drawing due to equipment limitations, however the surface finish achieved was considered to be suitable.

6.3.1 Testing Results and Discussion

Table 6.2 provides a summary of the raw data gathered from the redesigned AMR testing conducted. It was desired in this redesign to allow the measurement of the working chamber's air pressure immediately prior to the exhaust stage, however time constraints did not allow for this. Testing followed the same methodology described in Chapter 4.

Table 6.2: Recorded Data From Redesigned AMR Testing

Run No.	M_{act} (g)	L_{spring} (mm)		Temp (^{o}C)		rpm	t (sec)	V (L)
		Initial	Final	In	Exit			
1	-	-	-	21.7	8.4	6313	47	386
2	34	75.0	81.7	21.9	5.8	5046	67	538
3	68	75.0	88.6	22.2	5.2	4720	55	435
4	136	75.0	104.0	21.9	4.6	4523	64	506
5	170	75.2	108.0	21.5	3.5	3858	79	607
6	238	75.8	112.2	21.6	2.5	3509	74	572
7	327	78.4	117.4	21.7	2.7	3329	96	737
8	395	82.1	124.1	21.9	2.0	3098	79	596
9	497	85.1	145.2	22.7	5.2	2094	55	411
10	395	82.1	125.7	22.7	1.5	3068	79	575

Table 6.3: Secondary Results From Redesigned AMR Testing

Run No.	$\dot{m}$ (kg/s)	τ_{brake} (Nm)	ΔT(^{o}C)	Power (W)	
				Brake	Expansion
1	0.0103	0	13.3	0	137.73
2	0.0102	0.103	16.1	54.65	164.53
3	0.0100	0.210	17.0	103.76	171.48
4	0.0101	0.448	17.3	212.01	174.82
5	0.0098	0.506	18.0	204.53	177.48
6	0.0099	0.562	19.1	206.45	190.14
7	0.0098	0.602	19.0	209.85	187.72
8	0.0097	0.648	19.9	210.31	193.71
9	0.0095	0.928	17.5	203.41	166.79
10	0.0094	0.673	21.2	216.21	199.45

Again the recorded data was inputted into an excel sheet and then manipulated in MATLAB to provide secondary data (see Appendix B).

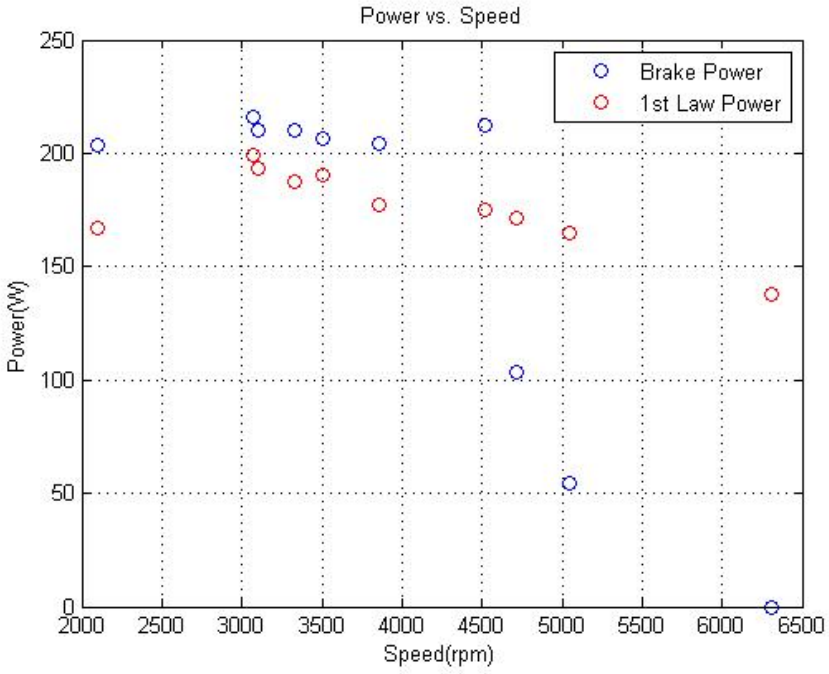

Figure 6.2: MATLAB Plot of Power versus Rotational Speed

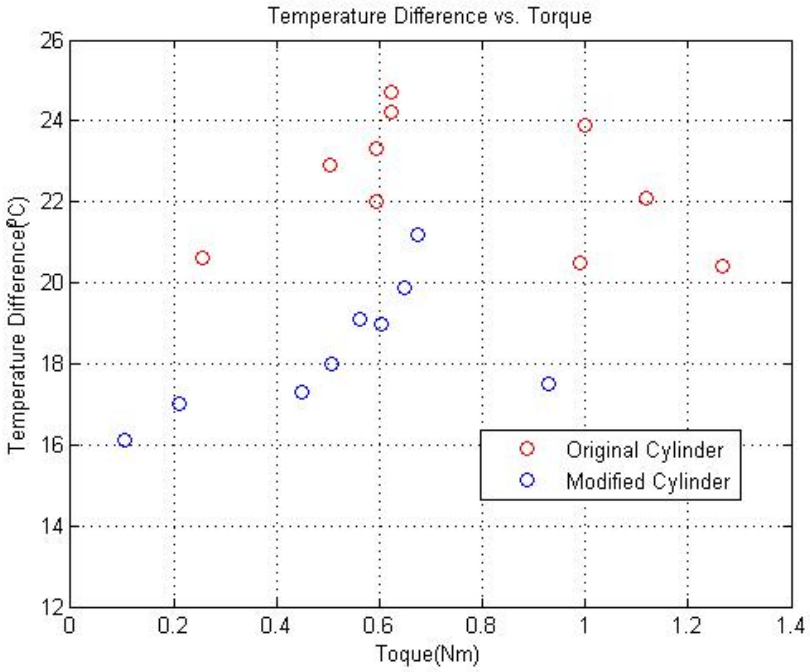

Figure 6.3: MATLAB Plot of Temperature Difference versus Brake Torque.

The results of the modified AMR testing show cooling performance didn't really vary from previous testing. In fact, these results were actually worse than those recorded during preliminary testing; producing a maximum temperature drop of 21.2^{o}C compared to 24.7^{o}C. Several potential causes have been considered responsible for limiting expansion, however chief among them is the DEPRAG air motor's open pressure relief bore (see figure 6.4). Secondary expansion is likely to have occurred, creating an additional temperature drop that was not accounted for by the system model.

Although testing of the modified motor accounted for this secondary expansion cooling by sealing the bore, testing of the original motor did not. This means that the results in Chapter 5 did not give a proper representation to the amount of expansion occurring inside the motor, so the original DEPRAG motor was reassembled and retested with this bore closed.

A shorter round of testing was conducted to redetermine the maximum temperature drop achievable under primary expansion using the original DEPRAG motor assembly.

Table 6.4: Recorded Data From AMR Re-Testing

Run No.	M_{act} (g)	L_{spring} (mm)		Temp (^{o}C)		rpm	t (sec)	V (L)
		Initial	Final	In	Exit			
1	204	75.2	115.6	24.9	4.2	4000	52	425
2	136	75.2	106.4	24.1	5.1	4350	64	513
3	102	75.2	106.4	23.3	3.7	5000	60	498
4	327	79.7	122.1	23.3	4.6	3300	71	553

Table 6.5: Secondary Results From AMR Re-Testing

Run No.	$\dot{m}$ (kg/s)	τ_{brake} (Nm)	ΔT(^{o}C)	Power (W)	
				Brake	Expansion
1	0.0104	0.624	20.7	261.20	216.55
2	0.0102	0.482	19.0	219.37	194.31
3	0.0106	0.482	19.6	252.15	208.61
4	0.0099	0.654	18.7	226.16	186.16

Figure 6.4: DEPRAG Exhaust Port

As seen above, these results showed that the maximum temperature drop was 20.7^{o}C. The refined model was retuned accordingly.

Given similar temperature drops from primary expansion were achieved in both arrange-

ments, it was predicted that the size and speed of the air motor prevented additional expansion from occurring. Complete removal of the intake channel and reduction of the intake port in the modified component likely compounded the problem.

It is further predicted that vanes passing over the intake port were forced out of contact with the cylinder wall and did not reform their working chambers until they reached a position similar to what they did in the original. This would explain why little difference in temperature drop was observed between the original and adapted DEPRAG motor in operation. However, all of this is difficult to confirm without testing different RVAMs and arrangements.

6.3.2 Conclusions

Temperature drops larger than those exhibited by the original and adapted DEPRAG air motor are possible to achieve in RVAMs. According to the Ingersoll-Rand Company (*Section 1: Air Motors Air Tool Manual* 1990), typical RVAMs only expand air about 25% before it is exhausted; to prevent any moisture in the motor freezing from supercooled air. Observations during testing found this claim to be reasonable.

Unfortunately the results from testing the DEPRAG adaptation will not be suitable to further refine the system model. Tuning will have to be conducted in future work. In hindsight, it is apparent some existing features might have been overlooked during the design process when redesigning the cylinder rotor housing for increased expansion. It also would have been preferable to have fabricated a customised air motor to address this problem, however time constraints were ultimately a deciding factor.

6.4 Customised Rotary Vane Air Motor (RVAM)

When considering its cooling applications, a major drawback of commercial RVAMs is the purposeful expansion limitations integrated into their design. This was evident during experimentation of the DEPRAG motor (both before and after design modifications). A

customised RVAM was developed to overcome this.

The customised air motor's major components were back-engineered from the desired expansion ratio (i.e. full expansion of air at 6 bar to ambient pressures) based on the assumption of isentropic expansion. This provided a starting point to determining major dimensions on these key components.

Several iterations of calculations were conducted after adapting initially chosen dimensions to optimise for high expansion, low blow-by and reduced stresses. This concluded that a cylinder bore and rotor diameter of 95mm and 76mm respectively, and a cylinder depth of 100mm would be suitable dimensions to work with. Five vanes, 28mm in length, were also chosen as this is a commonly used configuration, therefore stress levels in the rotor should be manageable. A fine tolerance of 0.025mm was considered to be realistic and achievable in fabrication; were it to get to that stage.

Detailed design drawings were drawn up in CREO 3.0 (see Appendix D). Note that an intake channel was reintroduced in the hopes of preventing the expansion problem experienced operating the modified DEPRAG motor from reoccurring.

6.4.1 Material Selection

Main factors considered in the material selection were wear (given intended dry running), corrosion and fatigue failure. This process was conducted in conjunction with an air motor design manual (*Section 1: Air Motors Air Tool Manual* 1990) and ASM Handbooks Online. Table 6.6 shows the materials selected:

Table 6.6: Material Selection Summary

Component	Material
Cylinder Housing	Stainless Steel (4140)
End Plate	Acrylic (Low Flow Grade)
Shaft/Rotor	Aluminium (2014-T3)
Footing	Mild Steel
Vane	PTFE (Teflon)

6.4.2 Performance Simulation Results

The refined system model simulation assumed an initial temperature and pressure of 15^oC and 6 bar respectively, and a steady maximum mass flow rate (based on choked flow through an equivalent throat diameter of 3mm).

Table 6.7: Refined MATLAB Customised Air Motor Simulation Results

Quantity	Value
Minimum exhaust flow temperature (^oC)	-71.75
Temperature Drop (^oC)	86.75
Net Expansion/Compression Power (W)	1028.85
Predicted Flow Power (W)	1466.81
Maximum mass flow rate (kg/s)	11.81
Nominal shaft rotational speed (rpm)	430.45
Blow-by (% of Q_{max})	4.43
Effective Expansion Ratio	2.45

6.4.3 Stress Analysis

The stress analysis undertaken only involved the assembly's main moving components (i.e. the rotor/shaft, bearings and vanes). Component mass was neglected in these calculations, given the light mass of materials chosen and size of components.

Assuming constant rotational speed (i.e. zero net tangential force), a static force analysis was conducted on a vane using basic force and moment summations. See figure 6.5 for the related conventions.

$$\begin{aligned} \sum F_t &= F_f + F_2 - F_1 - F_{cor} + F_L - F_R \\ F_L - F_R + F_f &= F_1 - F_2 + F_{cor} \end{aligned} \tag{6.4}$$

Where:
- F_t force acting tangent to vane, in N
- F_1 force acting on lagging side of vane, in N
- F_2 force acting on leading side of vane, in N
- F_{cor} force due to Coriolis effect, in N
- F_f force due to friction, in N
- F_L rotor reactive force on left side of vane, in N
- F_R rotor reactive force on right side of vane, in N

$$\begin{aligned} \sum F_n &= F_b + F_m - F_n - F_L\mu_r - F_R\mu_r \\ 0 &= F_b + F_m - \frac{F_f}{\mu c} - F_L\mu_r - F_R\mu_r \\ F_L + F_R + F_f\left(\frac{1}{\mu c \mu r}\right) &= \frac{1}{\mu r}\left(F_m + F_b\right) \end{aligned} \tag{6.5}$$

Where:
- F_n force acting normal to the vane, in N
- F_b force acting on the vane's base, in N
- $F_n = \frac{F_f}{\mu c}$ force acting normal to top of vane, in N
- μ_c dynamic friction coefficient of cylinder
- μ_r dynamic friction coefficient of rotor

$$\begin{aligned} \sum M_b &= c(F_1 - F_2) - F_f w - eF_L \\ &\quad + \frac{t_v \mu r}{2}\left(F_L - F_R\right) + \frac{w}{2}F_{cor} \\ F_L\left(\frac{2e}{\mu r t_v} - 1\right) + F_R + F_f\left(\frac{2w}{\mu r t_v}\right) &= \frac{2c}{\mu r t_v}(F_1 - F_2) + \frac{w}{\mu r t_v}F_{cor} \end{aligned} \tag{6.6}$$

Where:
- M_b moment about base of vane (+ve clockwise), in N.m
- c pressure forces' moment arm, in m
- w width of the vane, in m
- e F_L's moment arm, in m
- t_v thickness of the vane, in m

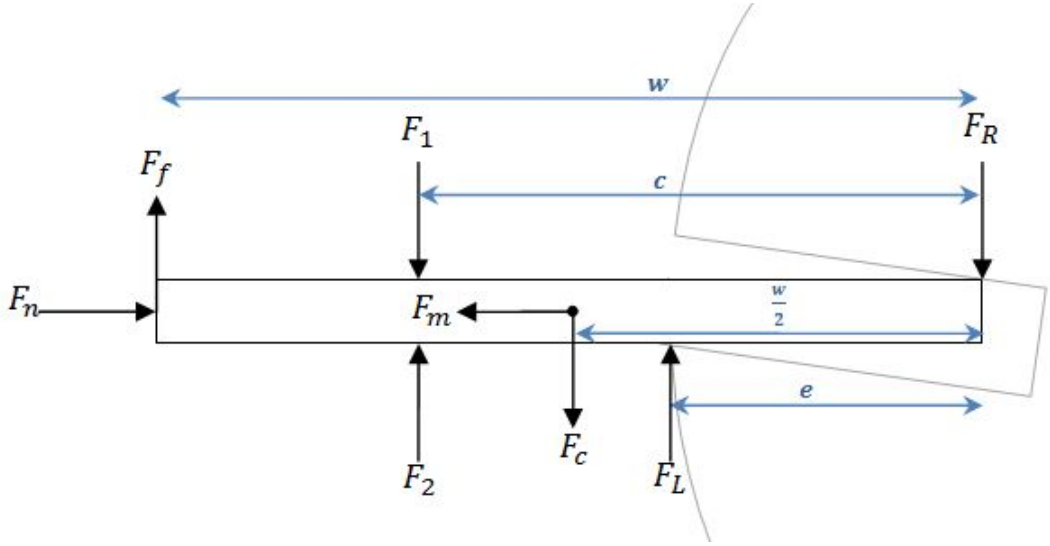

Figure 6.5: Vane Force Analysis Conventions

Given the design of vane slots in rotors, the maximum stress will occur at the base of the slot (i.e. the point of minimum material in each rotor section). The left and right reaction forces were then used to determine the stresses acting at this point. Consideration was given to which forces would be acting on a section (i.e. if certain F_R and F_L are positive or negative, see figure 6.6):

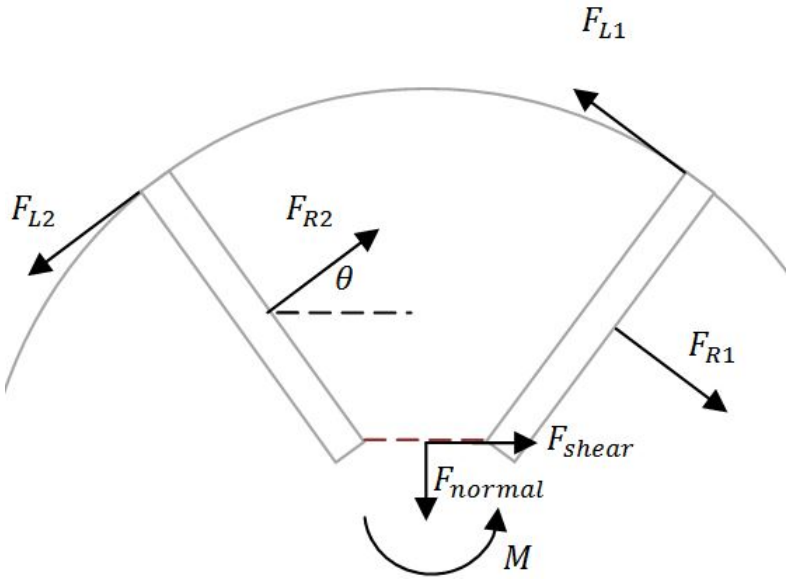

Figure 6.6: Rotor Force/Moment Convention, *If F_{R1} or F_{L2} are positive, and F_{R2} or F_{L1} are negative, then equate them to 0.*

Assuming little gap exists between the vane and its slot, it can be assumed that the reaction forces act perpendicular to the vane slot surface. The section's internal forces and moment were calculated using the following equations:

$$F_s = \cos\theta(F_{R1} + F_{L1} - F_{R2} - F_{L2}) \tag{6.7}$$

$$F_n = \sin\theta(F_{R2} + F_{L2} + F_{R1} + F_{L1}) \tag{6.8}$$

$$M = -\left(\sin^2\theta + \cos^2\theta\right)[F_{R1}(r_1 - w - r_S) - F_{R2}(r_2 - w - r_S) + F_{L1}(r_i - r_S) - F_{L2}(r_i - r_S)] \tag{6.9}$$

Where:

F_s	internal shear stress at rotor section, in Pa
F_n	internal normal stress at rotor section, in Pa
$\theta = \frac{\pi}{z}$	half of rotor section angle, in rad
M	internal moment about rotor section of maximum stress, in N.m
r_1	polar radius at lagging vane position, in m
r_2	polar radius at leading vane position, in m
r_S	shaft radius (OR radius to vane slot base), taken as 0.01m
r_i	radius of rotor, taken as 0.038m

From here, shear stress and total normal stress can be calculated:

$$\sigma_s = \frac{1.5Fs}{A} \tag{6.10}$$

$$\sigma_{n,total} = -\frac{M \times r_S \sin\theta}{I} + \frac{F_n}{A} \tag{6.11}$$

Where:

A	area of rotor segment, taken as $L(2r_S \sin\theta - t\cos\theta)$ in m^2
$I = \frac{bh^3}{12}$	second moment of inertia, in m^4
$\theta = \frac{\pi}{z}$	half of rotor section angle, in rad
M	internal moment about section of maximum stress, in N.m

Further analysis was conducted on the rotor's shaft section given it has the smallest area. This summed the forces (i.e. their components) acting on each rotor section (based on each chamber's pressure) over a full revolution before then determining the shear and bending stresses acting at this point using equation 6.11.

The maximum force predicted to be acting on the bearing was also determined from a similar process:

$$F_{bearing} = \frac{\sqrt{F_x^2 + F_y^2}}{2\pi {r_S}^2} \tag{6.12}$$

Where: F_x x component of net force acting on shaft section

F_y y component of net force acting on shaft section

See further details in the stress analysis code section in Appendix B.

6.4.4 Vane Displacement Analysis

The displacement of a vane during operation was also looked into, adopting the stiffness displacement method described by Hibbeler (Hibbeler 2012). The member stiffness matrices are given:

$$\begin{bmatrix} q_{Ny'} \\ q_{Nz'} \\ q_{Fy'} \\ q_{Fz'} \end{bmatrix} = \begin{bmatrix} \frac{12EI}{L^3} & \frac{6EI}{L^2} & -\frac{12EI}{L^3} & \frac{6EI}{L^2} \\ \frac{6EI}{L^2} & \frac{4EI}{L} & -\frac{6EI}{L^2} & \frac{2EI}{L} \\ -\frac{12EI}{L^3} & -\frac{6EI}{L^2} & \frac{12EI}{L^3} & -\frac{6EI}{L^2} \\ \frac{6EI}{L^2} & \frac{2EI}{L} & -\frac{6EI}{L^2} & \frac{4EI}{L} \end{bmatrix} \begin{bmatrix} d_{Ny'} \\ d_{Nz'} \\ d_{Fy'} \\ d_{Fz'} \end{bmatrix}$$

Figure 6.7: Stiffness matrix calculation (Hibbeler 2012)

Assuming the displacement corresponding to F_L and F_R is 0, the matrix equation simplifies down to 4 simultaneous equations:

$$\begin{bmatrix} Q_1 \\ Q_2 \\ Q_4 \\ Q_6 \end{bmatrix} = EI \begin{bmatrix} \frac{12}{L_1^3} & \frac{6}{L_1^2} & \frac{6}{L_1^2} & 0 \\ \frac{6}{L_1^2} & \frac{4}{L_1} & \frac{2}{L_1} & 0 \\ \frac{6}{L_1^2} & \frac{2}{L_1} & \frac{4}{L_1} + \frac{4}{L_2} & \frac{2}{L_2} \\ 0 & 0 & \frac{2}{L_2} & \frac{4}{L_2} \end{bmatrix} \begin{bmatrix} D_1 \\ D_2 \\ D_4 \\ D_6 \end{bmatrix} \tag{6.13}$$

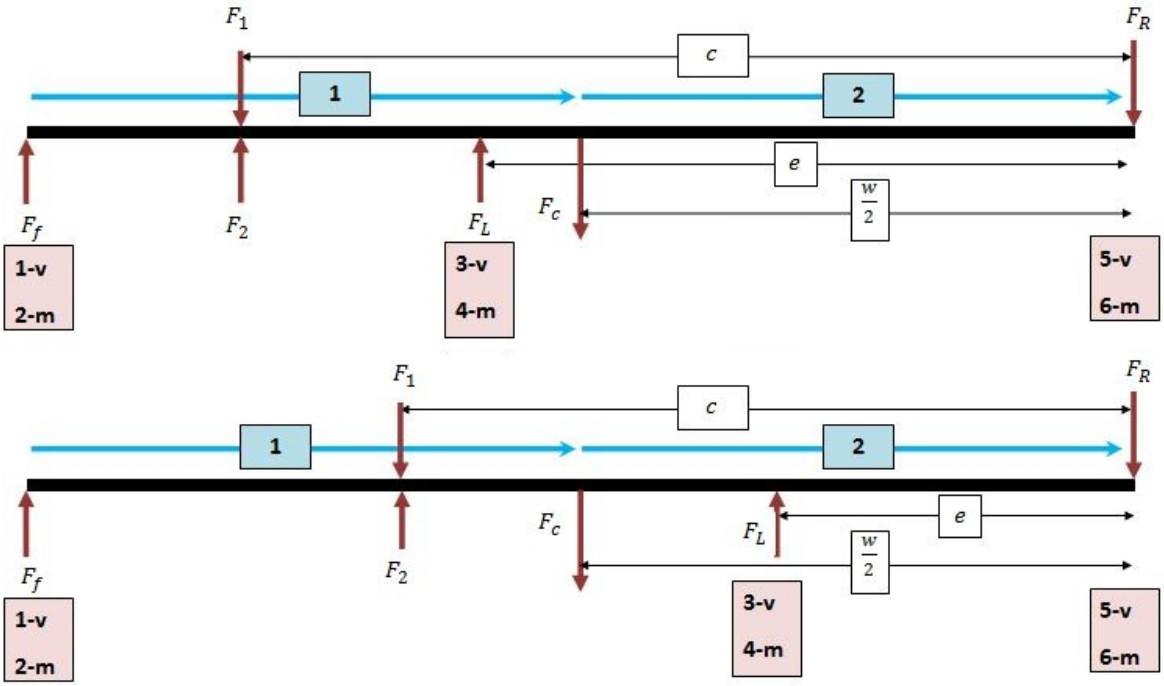

Figure 6.8: Stiffness Analysis Convention: (above) F_L acting before centre of gravity, (below) F_L beyond centre of gravity

During one revolution there will be two possible scenarios for the force matrix when combining both section's stiffness matrices.

When $\frac{w}{2} < e$, the loading matrix is given by:

$$\begin{bmatrix} Q_1 \\ Q_2 \\ Q_4 \\ Q_6 \end{bmatrix} = \begin{bmatrix} F_f + \frac{F_2 - F_1}{2} \\ -\frac{(F_1 - F_2)(w-e)}{8} \\ \frac{(F_1 - F_2)(w-e)}{8} - \frac{F_c(w/2)(e-w/2)^2}{e^2} \\ \frac{F_c(e-w/2)(w/2)^2}{e^2} \end{bmatrix} \tag{6.14}$$

When $\frac{w}{2} > e$, the loading matrix is given by:

$$\begin{bmatrix} Q_1 \\ Q_2 \\ Q_4 \\ Q_6 \end{bmatrix} = \begin{bmatrix} F_f + \frac{F_2 - F_1}{2} - F_c\frac{w/2 - e}{w-e} \\ -\frac{(F_1 - F_2)(w-e)}{8} - \frac{F_c(w/2)^2(w/2-e)}{(w-e)^2} \\ \frac{(F_1 - F_2)(w-e)}{8} + \frac{F_c(w/2)(w/2-e)^2}{(w-e)^2} \\ 0 \end{bmatrix} \tag{6.15}$$

Where:	E	stiffness modulus of vane material, in MPa
	$I = \frac{Lt^3}{12}$	second moment of inertia of vane, in m^4
	L_1	length of first section, in m
	L_2	length of second section, in m

6.4.5 Fatigue Analysis

A fatigue analysis was also conducted based on the maximum and minimum total normal stresses involved in an operational revolution. This involved calculating mean stress, cyclic stress and 10^6 life stress, and determining whether or not the point lies within the area defined by the 10^6 life (i.e. infinite life, S_n) and yield strength lines. The following parameters associated with bending loading were used based on Juvinall & Marshek (Juvinall & Marshek 2012):

$S'_n = 0.5S_u$	R.R. Moore endurance limit (table 8.1)
C_L	loading factor, taken as 1.0 (table 8.1)
C_G	gradient factor, taken as 1.0 (table 8.1)
C_S	surface factor, taken as 0.8 (figure 8.13)
C_T	temperature factor, taken as 1.0 (table 8.1)
C_R	reliability factor, taken as 0.814 for 99% reliability (table 8.1)

$$\sigma_m = \frac{\sigma_{max} + \sigma_{min}}{2} \tag{6.16}$$

$$\sigma_a = \frac{\sigma_{max} - \sigma_{min}}{2} \tag{6.17}$$

$$S_n = S'_n C_L C_G C_S C_T C_R \tag{6.18}$$

6.4.6 Simulation Results

These equations were solved simultaneously in a MATLAB code (see Appendix B) at every degree of rotation over one full cycle. These are displayed graphically in the following figures.

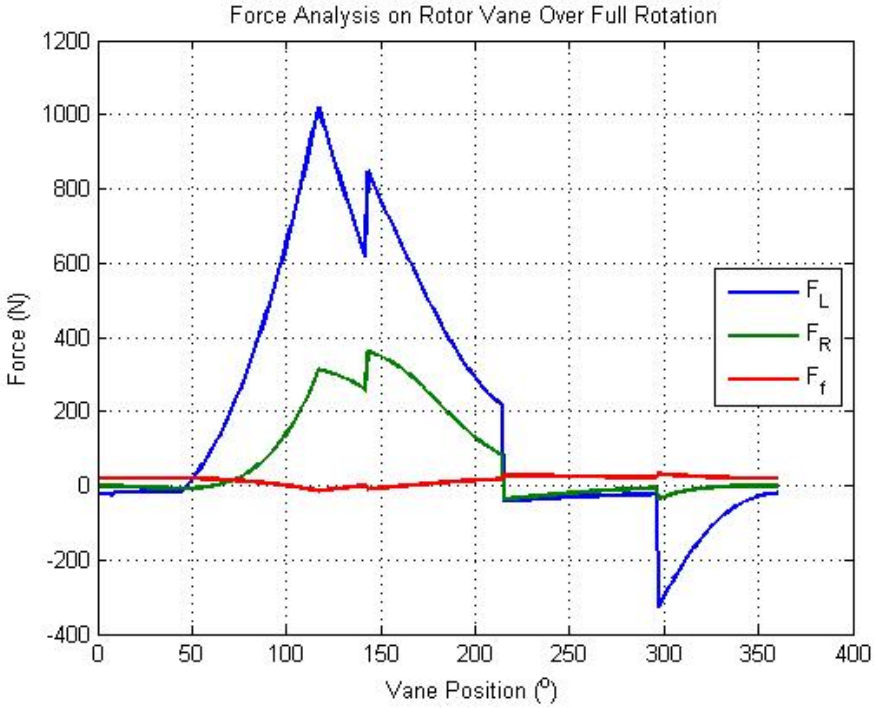

Figure 6.9: Vane Force Simulation

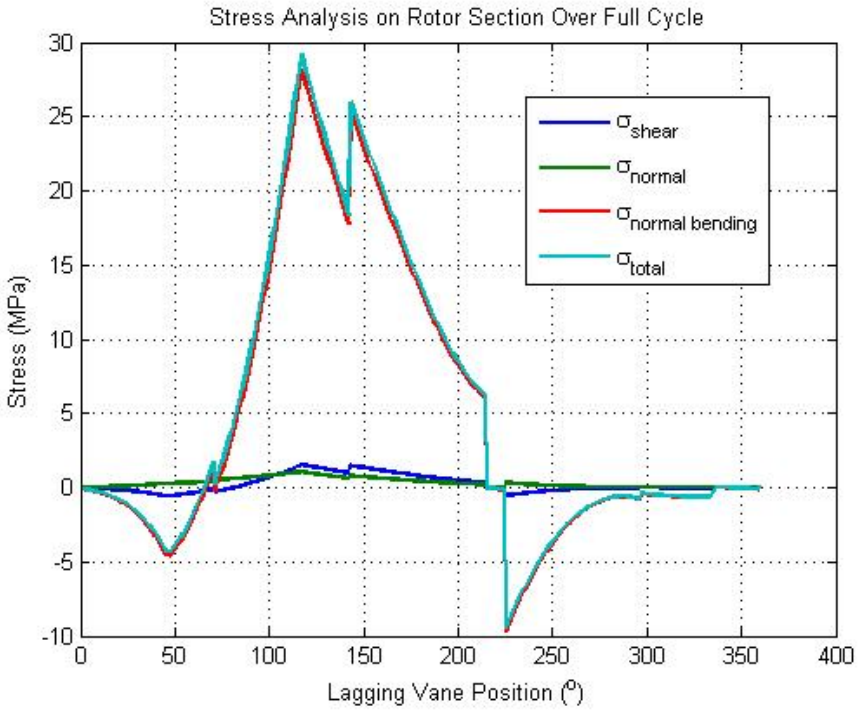

Figure 6.10: Rotor Stress Simulation

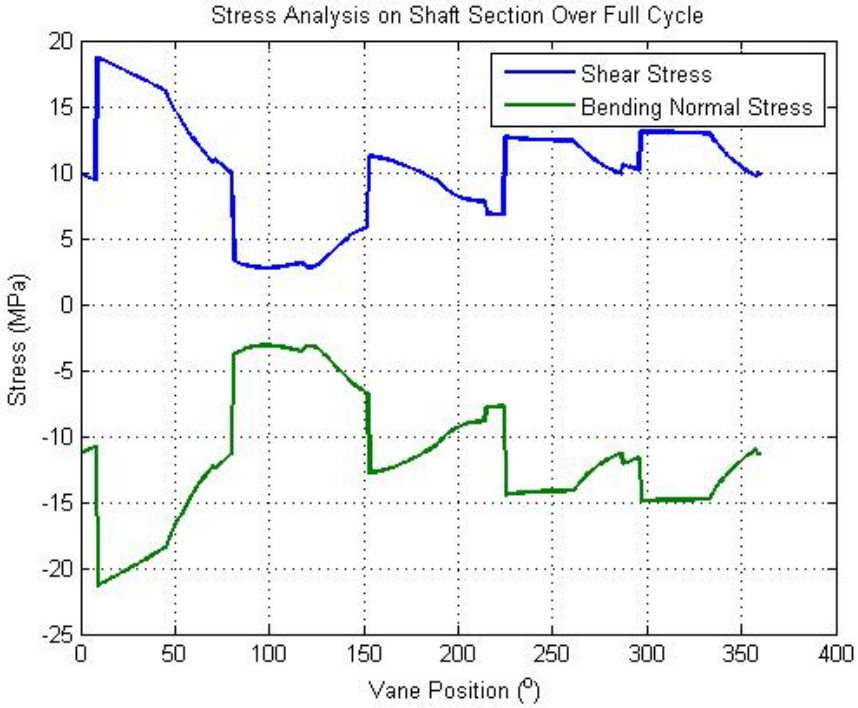

Figure 6.11: Shaft Stress Simulation

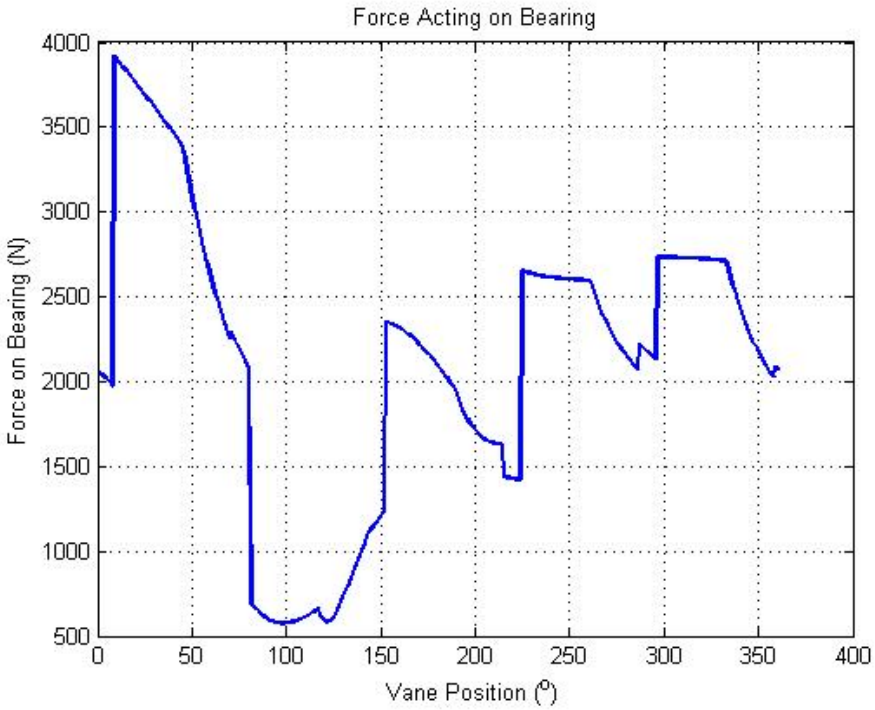

Figure 6.12: Bearing Force Simulation

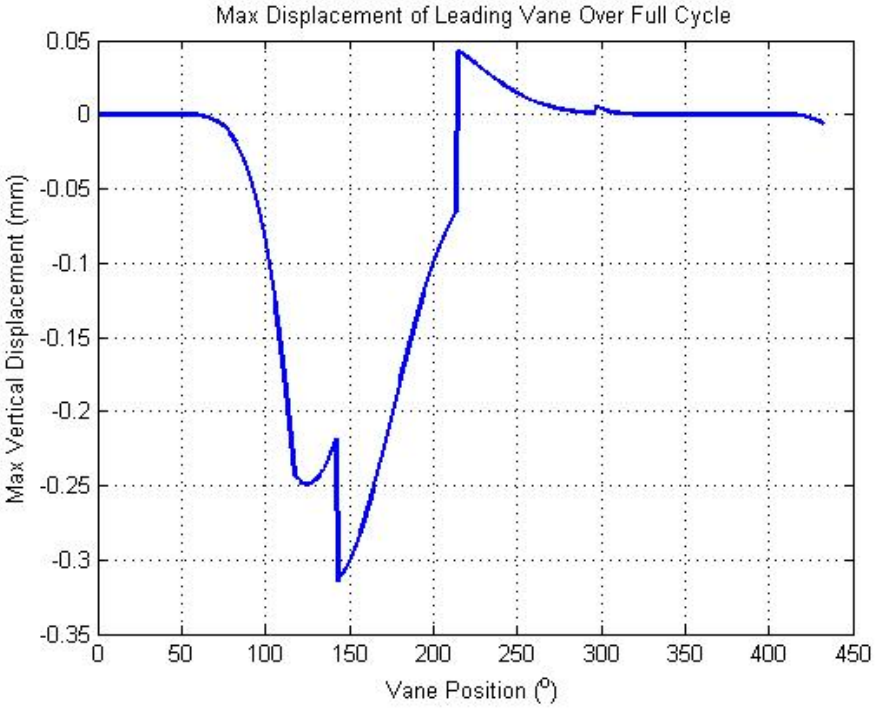

Figure 6.13: Maximum Vane Displacement Simulation

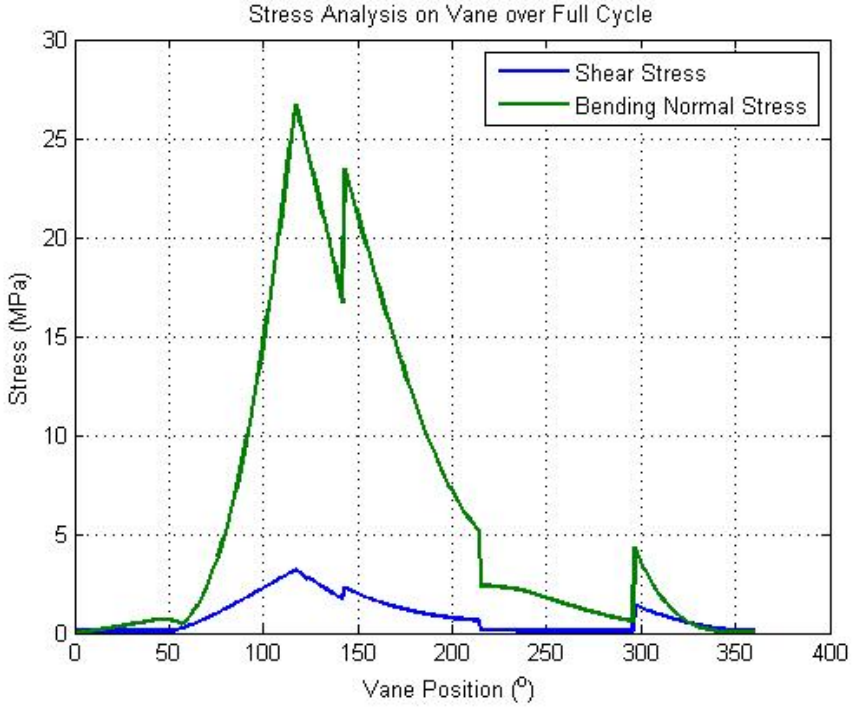

Figure 6.14: Vane Stress Simulation

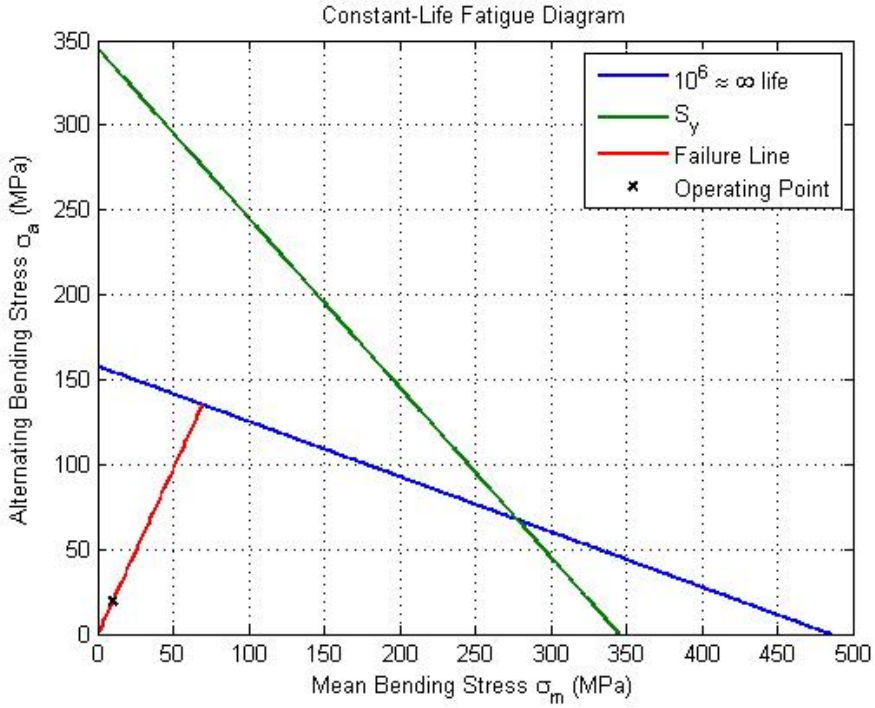

Figure 6.15: Rotor Section Constant Life Fatigue Diagram

As a measure of accuracy, one of the rotor sections was statically analysed in CREO (under the most demanding load combination).

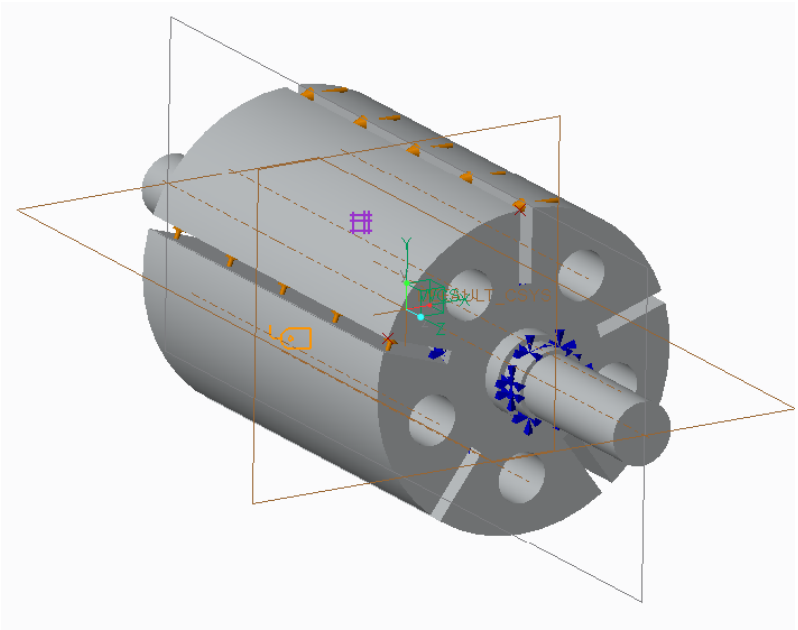

Figure 6.16: CREO model constraints and forces setup

A fine 8mm mesh was placed around the volume of interest. The component was constrained at the rotor section base, with the maximum loads (F_{L1} = 1020N and F_{R2} = 179N, see figure 6.6) applied to both sides of the rotor along their respective lines of action. The results produced were comparable to those calculated in the MATLAB code.

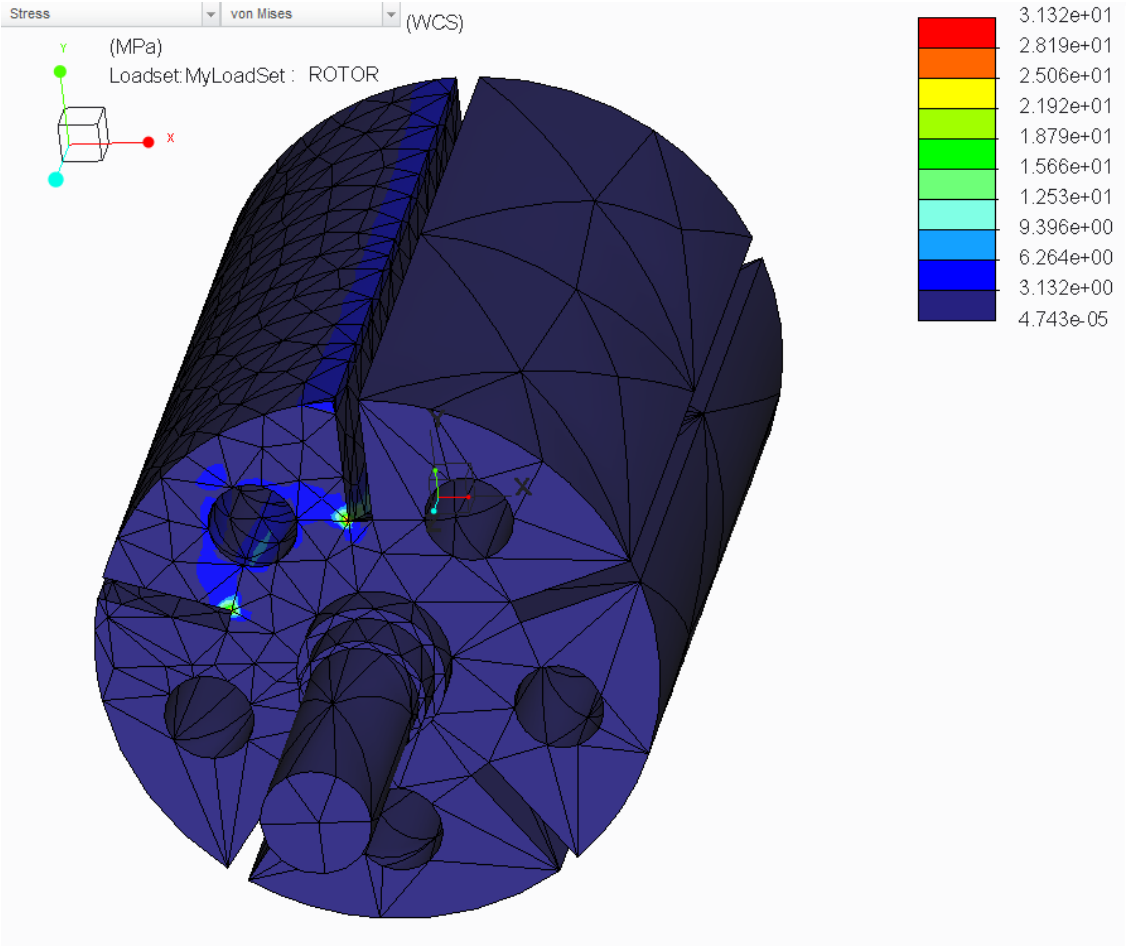

Figure 6.17: CREO rotor model's von Mises stress results from static analysis

6.4.7 Conclusions

The analysis conducted suggests the customised RVAM design and material selection is suitable. Assuming that performance follows the trends described by the refined system model, much colder air should be exhausted from this motor than the smaller DEPRAG motor. This relies on having a greater throughput, thereby a high RPM, to ensure expansion processes occur quickly; maintaining the assumption of isentropic expansion.

6.5 Chapter Summary

The work done after completing preliminary testing was presented in this section. A refined system model was developed after disassembling the DEPRAG air motor.

It was found that a refined DEPRAG cylinder did not help to improve the cooling performance of the air motor as significantly as predicted by the refined system model. This is believed to have been caused by a combination of the motor's high rotational speed and the small cylinder bore.

Vanes passing over the reduced intake port are predicted to have been forced out of contact with the cylinder wall, and weren't able to reform their working chambers (thereby begin their expansion phase) until they reached a position similar to what they did in the original.

This would explain why little difference in temperature drop was observed between the original and adapted DEPRAG motor in operation. However, all of this is difficult to confirm without testing different motors and arrangements.

Additionally, other inbuilt expansion-suppressing features were not considered during the redesign process of the DEPRAG cylinder. A customised RVAM was designed to avoid these issues. However due to time constraints, fabrication will not be covered in the scope of this project.

Chapter 7

Conclusion

7.1 Review of Dissertation

This project was aimed at determining whether or not steady flow work extraction is a viable mode of supercooling air to temperatures necessary for icing wind tunnel operation. The mode of work extraction specifically investigated in this dissertation is a rotary vane air motor. Aims and goals of this project were presented in Chapter 1, as well as the relevance and purpose this work in the context of icing research.

Background knowledge and information necessary for understanding the path taken in this project was covered Chapter 2. This mainly focussed on defining existing methods of cooling, the necessary temperatures required for homogeneous nucleation to occur and the principle of isentropic expansion. The function of air motors and band brakes was also described.

A case study into redesigning a rotary vane vacuum pump was described in Chapter 3. This was mainly aimed at forming the beginnings of the geometric and thermodynamic analysis to be conducted on these types of devices. The study concluded that the most effective way to reduce the exhaust temperature would be to reposition the intake port further backwards and to increase the number of vanes used.

Chapter 4 detailed the adopted methodology used in all physical experiments conducted. It featured the hardware design and set-up used in the testing rig, and the experimental set-up used in testing.

The results gathered from testing the DEPRAG 63-001F03 commercial rotary vane air motor were recorded and discussed in Chapter 5. Although the commercial device was not capable of cooling air to the desired temperatures, it was found that the expansion cooling experienced could be approximated as an isentropic process.

Additional work on air motor design and analysis was detailed in Chapter 6. A refined system model was described, and the design and analysis of both a modified DEPRAG motor and a customised rotary vane air motor was presented. Additional testing on the modified DEPRAG motor presented less than favourable performance, which was largely attributed to unforeseen design problems/constraints. A customised motor was subsequently designed to overcome these problems.

7.2 Conclusions

The results from this study have demonstrated that commercially available rotary vane air motors are not capable of supercooling air to temperatures necessary for the study of solid phase ice accretion. In fact, most aim to avoid these temperatures to prevent moisture inside the motor from freezing and impinging on performance; meaning that air is only expanded a fraction of what is possible. This was also the case with the DEPRAG rotary vane air motor purchased.

Findings from physical testing have supported the hypothesis that the quick expansion process occurring in rotary vane air motors can be considered to be isentropic in nature. However this relationship was only confirmed for a small amount of expansion in a small motor. The redesign of the DEPRAG air motor aimed to increase the experienced expansion ratio by reducing the intake port and removing the intake channel, however temperature drop was only minimally improved. It is presumed that these changes forced vanes passing over the intake port back into their slots, and that the vanes were not able

to regain contact with the cylinder bore surface until they reached a position similar to what they did in the original. However this is difficult to confirm without testing different arrangements.

A customised air motor was designed to overcome the issues of the DEPRAG air motor and its adaptation to produce the necessary cold temperatures. It features a short intake channel, larger working chambers and no expansion limiting design features. Assuming that the developed system model relationships hold over a longer expansion process in slightly larger air motors, this air motor should be capable of producing a larger temperature drop than experienced in both the original and adapted DEPRAG motor. It would have been preferable to have organised its fabrication and testing to increase the amount of data gathered, however time restrictions prevented this.

The importance of this finding could be helpful for further work in this area if a motor with an increased expansion ratio is fabricated or redesigned.

7.3 Limitations and Further Work

The data presented in this thesis is sufficient to draw some positive conclusions about generating cold air using small scale rotary vane air motors. Experimental design limitations of this campaign may have affected the accuracy of these results and thereby the theoretical system model developed, however the main measure of temperature drop was most accurately recorded. So any errors induced by less than desirable methods of measurement are not considered to be of significant influence.

The major limitation of this experimental design was the lack of a proper dynamometer. This would have enabled more sensitive and incremental changes to the amount of power extracted from the motor, thereby improving the reliability of the maximum temperature drop recorded is the one the motor is fully capable of.

Another limiting factor in this project is considered to be the lack of multiple testing rigs. Studying their operation and generalising relationships would have been greatly assisted

were there several different rigs – differing in size, arrangement, geometry etc. – to test. Having the customised rotary vane air motor fabricated and tested would also have been of great benefit.

Other significant limitations during testing and in additional work conducted (particularly model development) were not being able to track temperature and pressure changes during the expansion process.

There have been several areas identified throughout the project that hold further work, whether time did not allow for them to be fully looked into or if they are outside of this project's scope:

Investigate temperature drop using variable intake pressures: The intake pressure through the entirety of this thesis has been taken as 6 bar. There may lie some promise in investigating temperature drops using variable intake pressures.

Tune system model: The results from testing the adapted DEPRAG air motor were not suitable to use in further refinement of the system model generated. Tuning will be best accomplished by testing an air motor which has a larger expansion ratio and using the results accordingly.

Investigate another work extraction device: Rotary vane air motors are only a single type of work extraction device with the ability to super-cool air. Others considered to be of interest include a turbo-expander and a reciprocating piston air motor; the latter of which can theoretically have an infinite expansion ratio.

Fabricate rotary vane air motor: Time did not allow for fabrication of the customised air motor, so looking into whether or not expansion can be increased upon in relatively small motors is still open to investigation.

References

AGARD (1997), AGARD AR-344: Ice Accretion Simulation, Advisory report, Advisory Group for Aerospace Research & Development (AGARD), Fluid Dynamics Panel (FDP) Working Group 20.

Air Motor Icing (n.d.), GRACO: Technical Support. `http://graco.custhelp.com/app/answers/detail/a_id/109/~/air-motor-icing`, [accessed March-2015].

Air Motors: Customised Drive Solutions (2012), DEPRAG. `http://www.deprag.com/fileadmin/bilder_content/emedia/broschueren_pics/emedia_druckluftmotoren/D6000/D6000en.pdf`, [accessed March-2015].

Air Motor Selection and Sizing (2012), Hydraulics & Pneumatics. `http://hydraulicspneumatics.com/200/TechZone/FluidPowerAcces/Article/False/6422/TechZone-FluidPowerAcces`, [accessed March-2015].

Air Vane Motors (n.d.), SELLTECH: Sommer Automatic catalogue. `http://selltech.com.pl/admin/Editor/assets/sommer/14.Silniki_pneumatyczne.pdf`, [accessed March-2015].

Al-Duwaisan, A., Sahaim, H., Roditi, A. I. & Al-Husseini, A. (1999), Design of a lab setup for the measurement of an air motor efficiency, Thesis, Northeastern University.

ASME (1987), *An International Historic Mechanical Engineering Landmark: Icing Research Tunnel*, American Society of Mechanical Engineers. `https://www.asme.org/getmedia/f9fb127c-7ba2-4b73-ba34-75fca7265485/117-Icing-Research-Tunnel-NASA-Lewis-Research-Ce.aspx`, [Online; accessed February-2015].

Basic Line: Air Motors from 200W to 1.2kW (2015), DEPRAG. http://www.depragusa.com/files/catalogs/D6200en.pdf, [accessed March-2015].

BBC (2013), *Boeing: 15 airlines warned over high-altitude ice*, British Broadcasting Corporation (BBC). http://www.bbc.com/news/business-25068222, [Online; accessed March-2015].

Beater, P. (2007), *Pneumatic Drives: System Design, Modelling and Control*, Springer Science+Business Media. "https://books.google.com.au/books?id=JIAw0SIfa4IC&printsec=frontcover#v=onepage&q&f=false, [accessed April-2015]".

Bellucci, M. (2007), Cloud Characterization in CIRA Icing Wind Tunnel, Thesis, University of Naples Federico II.

Blackwoods Catalogue (2014), 20th edn, Blackwoods. http://content-au.secure-zone.net/wesfarmers/BlackwoodsCatalogue2014/, [accessed March-2015].

Bugos, G. E. (1998), *Lew Rodert, Epistemological Liaison, and Thermal De-Icing at Ames*. http://history.nasa.gov/SP-4219/Chapter2.html, [Online; accessed March-2015].

Buttsworth, D. (2014), 'Project Offer: Turbofan Engine Icing', University of Southern Queensland.

Cengel, Y. & Boles, M. (2011), *Thermodynamics: An Engineering Approach*, 7th edn, McGraw-Hill, New York, USA.

CIRA (2015), *IWT - Icing Wind Tunnel*, Italian Aerospace Research Centre (CIRA). http://www.cira.it/en/impianti-en/iwt-icing-wind-tunnel, [Online; accessed February-2015].

Deep groove ball bearings, single row (2015), SKF. http://www.skf.com/au/products/bearings-units-housings/ball-bearings/deep-groove-ball-bearings/single-row-deep-groove-ball-bearings/single-row/index.html?prodid=1050010003&imperial=false, [accessed March-2015].

FAA (1975), *Aviation Weather: AC 00-6A (For Pilots and Flight Operations Personnel)*, Federal Aviation Administration (FAA) Flight Standards Service, National Weather Service (NWS), Washington D.C.

Ferrigno, F., Esposito, B., Esposito, G., Vernillo, P., Ragni, A., Caserta, G., Bellucci, M., Marrazzo, M., Dinardo, M., De Gregorio, F., Auletta, A. & Albano, F. (2004), *CIRA Icing Wind Tunnel User Manual*, Italian Aerospace Research Centre (CIRA).

Fox, R., McDonald, A. & Pritchard, P. (2012), *Fluid Mechanics*, 8th edn, John Wiley & Sons.

Hibbeler, R. (2012), *Structural Analysis*, 8th edn, Pearson, New Jersey, USA.

Irvine, T. B., Kevdzija, S. L. & Sheldon, D. W. (2001), *Overview of the Icing and Flow Quality Improvements Program for the NASA Glenn Icing Research Tunnel*, National Aeronautics and Space Administration.

Juvinall, R. & Marshek, K. (2012), *The Fundamentals of Machine Component Design*, 5th edn, Wiley.

Korane, K. (2012), *Sorting Out Air Motors*, Hydraulics & Pneumatics. `http://hydraulicspneumatics.com/cylinders-amp-actuators/sorting-out-air-motors`, [accessed March-2015].

Kuhns, I. & Mason, B. (1968), *The Supercooling and Freezing of Small Water Droplets Falling In Air and Other Gases*, The Royal Society. [accessed February-2015].

Langham, E. & Mason, B. (1958), *The Heterogeneous and Homogeneous Nucleation of Supercooled Water*, The Royal Society. [accessed February-2015].

Mason, J. (2007), 'Engine Power Loss in Ice Crystal Conditions', *Boeing: AERO Magazine* . `http://www.boeing.com/commercial/aeromagazine/articles/qtr_4_07/AERO_Q407.pdf`, [Online; accessed February-2015].

NASA (2009), *NASA's Aeronautics Test Program: Icing Research Tunnel*, National Aeronautics and Space Administration. `https://facilities.grc.nasa.gov/documents/TOPS/TopIRT.pdf`, [Online; accessed February-2015].

NRC (2013*a*), *3m x 6m Icing Wind Tunnel*, National Research Council of Canada (NRC). `http://www.nrc-cnrc.gc.ca/eng/solutions/facilities/wind_tunnel/3x6_metre.html`, [Online; accessed February-2015].

NRC (2013*b*), *Altitude Icing Wind Tunnel*, National Research Council of Canada (NRC). http://www.nrc-cnrc.gc.ca/eng/solutions/facilities/wind_tunnel/altitude_icing.html, [Online; accessed February-2015].

Rotary Vane Compressors and Vacuum Pumps: February 2012 GAST Catalog (2012), GAST. http://www.gastmfg.com/catalogs/F-5_Rotary_Vane_Feb17-2012_lores.pdf, [accessed March-2015].

Saleh, K. H. (2013), Initial Development of Ice Crystal Ice Accretion at Conditions Related to Turbofan Operation at High Altitude, PhD thesis, University of Southern Queensland.

Saleh, K. H., Buttsworth, D. & Yusaf, T. (2010), 'Development of a Small Icing Wind Tunnel for Simulating the Initial Stages of Solid Phase Ice Accretion, University of Southern Queensland'.

Section 1: Air Motors Air Tool Manual (1990), Ingersoll-Rand Company.

Think Ice! (2010), Icing Awareness for BAE Systems Regional Aircraft Operators, BAE SYSTEMS.

TRCF (2010), *Icing Wind Tunnel*, Technical Research Centre of Finland (TRCF). http://www3.vtt.fi/img/research/ene/energysystems/icing_wind_tunnel.pdf, [Online; accessed February-2015].

What is a Pneumatic Motor? (2015), wiseGEEK. http://www.wisegeek.com/what-is-a-pneumatic-motor.htm, [accessed February-2015].

Wilson, P. (2012), *Supercooling of Water*, Tsukuba University. www.intechopen.com/download/pdf/31428, [Online; accessed February-2015].

Appendix A

Project Specification

University of Southern Queensland

FACULTY OF HEALTH, ENGINEERING & SCIENCES

ENG 4111/2 Research Project

Project Specification

For:	**Rhyan Fai-Yin Wall**
Topic:	Improved Cooling System for USQ's Small Scale Icing Wind Tunnel
Supervisors:	David Buttsworth Khalid Hashim Saleh
Project Aim:	To investigate the effectiveness of using steady flow work extraction based expansion in supercooling air as a viable alternative to conventional methods of extracting heat from air streams
Program:	Issue A, 18 March 2015

1. Research background information relating to icing wind tunnels, ice accretion particulate conditions, and devices capable of super cooling air; particularly through steady flow work extraction based expansion
2. Analyse and model the predicted operating conditions of cooling system based on fluid and hardware properties using appropriate modelling techniques; based on Excel, Matlab and maybe Ansys
3. Source required hardware and perform preliminary testing
4. Redesign and implement proposed alterations to the icing wind tunnel
5. Perform testing and analyse results to improve efficacy, varying the initial pressure and work extraction
6. Submit an academic dissertation on the research

As time and resources permit:

1. Optimise the wind tunnel design
2. Confirm performance

Note that these specifications may change depending on performance and outcomes.

Additional Information

Project Timeline

January 11 - March 20:	Complete preliminary work on project (i.e. background research on topic, required ice accretion conditions)
March 1 - May 20:	Complete preliminary report on project
February 11 - April 1:	Hardware preparation (i.e. design, sourcing and fabrication) and testing
April 1 - April 30:	Conduct appropriate analysis and modelling based on Matlab, Excel (and perhaps Ansys)
May 1 - June 15:	Complete the icing wind tunnel reconstruction process, be this at P block or in the Z-Block refrigerated room (decision pending completion of hardware testing)
June 15 - July 31:	Complete integration testing of the icing wind tunnel system
May 1 - September 16:	Complete final dissertation on project

Required Resources

1. Air motor of appropriate size and rating (or redesigned rotary vane vacuum pump, pending completion of feasibility study) and compressed air source
2. Loading device (i.e. compressor, pump or brake) and secondary components (i.e. power transmission / coupling, shaft etc.)
3. Thermocouple, tachometer, video camera, mass flow reader
4. Current small scale icing wind tunnel system

Project Timeline

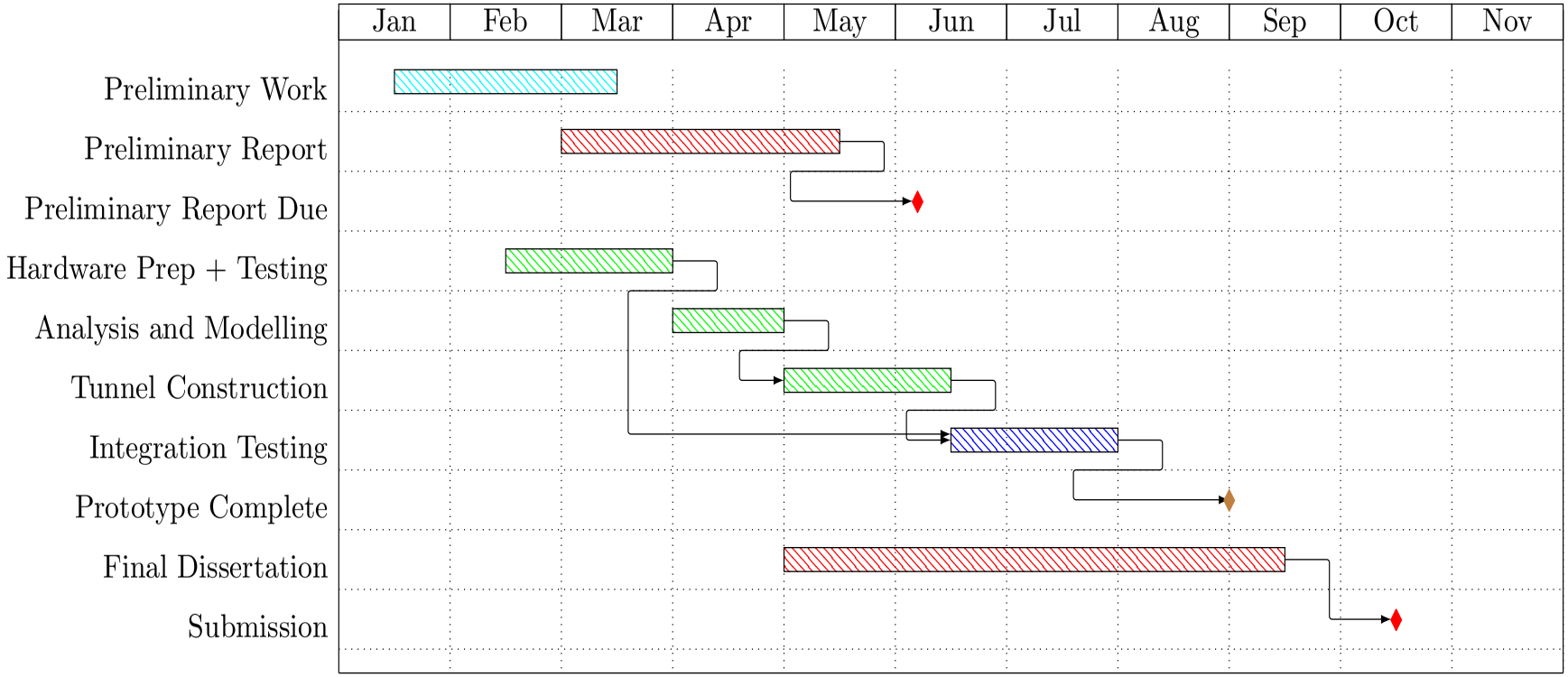

Appendix B

MATLAB Code

B.1 AMR Simulation - am.m

```
%% ------------------ ENG4111 - FINAL YR PROJECT (2015) ------------------
% This code will simulate the operating characteristics of an air motor
% capable of fully expanding compressed air to ambient pressures. This will
% assist in sizing of the required air motor.
% This code also predicts the exhaust temperature, expansion ratio and
% exhaust pressure of air undergoing work extraction via expansion in the
% DEPRAG 63-001F03 400W rotary vane air motor.

% INPUTS
% Power (P) in W, rated work output by selected motor
% Rotational speed (n) in rpm, nominal speed of air motor at max power
% Radius (r) in m, radius of V-belt pulley (based on common sizes)
% Angle (phi) in rad, v-section belt's angle of contact with v-pulley

% NOTE: air consumption needs to be as close as possible to the theoretical
% value calculated.

% WRITTEN: Rhyan Wall
% DATE MODIFIED: 29/05/15

% NOTE: air consumption needs to be as close as possible to the theoretical
% value calculated.


% WRITTEN: Rhyan Wall
% DATE MODIFIED: 29/05/15
function [] = am(P,n,r,phi)
disp 'ENG4111'
disp ' '
disp 'Rhyan Wall'
disp '0061032900'
disp ' '

% DEPRAG AIR MOTOR ------------------------------------------------------
% P = 400; %W, output power of air motor
% n = 5000; %rpm, nominal speed of air motor
```

```
% r = 0.038; %m, band brake v-pulley radius
% phi = pi/2; %rad, v-belt's angular contact with v-pulley

%% Theoretical Air Motor Exhaust Temperature and Power Predictions
% Air properties ------------------------------------------------------
R_g = 287; %universal gas constant of air
k = 1.4; %specific heat ratio of air
K = (k-1)/k;
cp = R_g/K; %specific heat of air under constant pressure

% Shop air reservoir conditions ---------------------------------------
p0 = 6e5; %Pa
p0 = p0 + 1.01325e5; %Pa
T0 = 293; %Degrees K
rho0 = p0/R_g/T0; %kg/m^3

% Maximum possible steady mass flow of air and properties from shop air
% system --------------------------------------------------------------
% State 1: stagnant conditions (i.e. M1 = 0)
% State 2: critical conditions (i.e. M2 = 1)
dstar = 3e-3; %m, approximate throat diameter of valve
Astar = pi*dstar^2/4; %m^2, critical area at throat
rhostar = rho0*isendens(0,1,k); %kg/m^3
Tstar = T0*isentemp(0,1,k); %Degrees K
astar = sqrt(k*R_g*Tstar); %m/s, speed of sound
mdotstar = rhostar*astar*Astar; %kg/s, choked mass flow rate

% Target pipe flow conditions -----------------------------------------
p1 = 0e5; %Pa
p1 = p1 + 1.01325e5; %Pa
T1_i = T0*(p1/p0)^K; %Degrees K
T1 = T0-1*(T0-T1_i); %Degrees K

% Air motor power -----------------------------------------------------
P_motor = mdotstar*cp*(T0-T1); %W, work done by isentropic expansion
P_motor60 = 0.6*P_motor; %W, work done at 60% of mass flow rate

% Flow speed and air properties in pipe after passing through the
% retrofitted vacuum pump ---------------------------------------------
```

```
76 d1 = 100e-3; %m, outlet piping diameter
77 A1 = pi*d1^2/4; %m^2, outlet pipe area
78 rho1 = p1/R_g/T1; %kg/m^3, outlet air density
79 u1 = mdotstar/rho1/A1; %m/s, maximum possible outlet air speed
80 T1c = T1-273; %Degrees C
81
82 % Air consumption at standard conditions --------------------------------
83 rho_amb = 101.3e3/R_g/293; %kg/m^3
84 Q = mdotstar/rho_amb; %m^3/s
85
86 %% DEPRAG Air Motor Exhaust Temperature and Pressure Drop Predictions
87 eff = 0.6; %efficiency of motor
88 P_act = P*eff; %W, actual work able to be extracted from pressurised air
89
90 % Assuming 60% losses
91 Tair_1 = -(P_act/(mdotstar*cp)-T0);
92 ex_1 = (Tair_1/T0)^(-1/(k-1));
93 pair_1 = p0*ex_1^(-k);
94
95 % Assuming fully efficient
96 Tair = -(P/(mdotstar*cp)-T0);
97 ex = (Tair/T0)^(-1/(k-1));
98 pair = p0*ex^(-k);
99
100 %% Air Motor Band Brake
101 % Actuating and anchoring forces
102 beta = pi/9; %rad, half of pulley's wedge angle, taken as 20 degrees
103 f = 0.5; %coefficient of friction, taken as 0.5
104 F2 = 60*P/(2*pi*n*r*(exp(f*phi/sin(beta))-1));
105 F1 = F2*exp(f*phi/sin(beta));
106 F_fric = F1-F2;
107
108 % Heat generation predictions
109 L = 2*r*pi*(pi/(2*pi)); %m, length of v-belt
110 t = 0.01; %m, thickness of v-belt
111 w = 0.0085; %m, effective rectangular width of v-belt
112 V = L*t*w; %m^3, volume of v-belt
113 rho_band = 1150; %kg/m^3, density of rubber
114 mass_band = rho_band*V; %kg, mass of v-belt
```

```
115 cp_band = 2010; %J/kgK, specific heat of rubber
116 frac = 0.5; %assumed percentage of power converted to heat
117 dTdt = frac*P/(mass_band*cp_band); %K/s, rate of temperature rise per sec
118
119 %% Results
120 display('--------------------')
121 display('SIMULATION RESULTS')
122 display('--------------------')
123 display(['*PARAMETERS*: P1(gauge) = ',num2str((p0-1.01325e5)/10^3),...
124     ' kPa, T1 = ',num2str(T0-273),' degC.'])
125 display(['Minimum exit pressure(gauge) = ',num2str((p1-1.01325e5)/10^3),...
126     ' kPa'])
127 display(['Static flow temperature in pipe = ',num2str(T1c),' degC'])
128 display ' '
129 display(['Max flow speed in pipe = ',num2str(u1),' m/s'])
130 display(['Max mass flow through system = ',num2str(mdotstar*1e3),...
131     ' grams/s'])
132 display(['Max volumetric flow at standard conditions = ',num2str(Q*60),...
133     ' m^3/min'])
134 display ' '
135 display(['Max air motor flow power = ',num2str(P_motor),' W'])
136 display(['Max air motor flow power @ 60% m.f.r = ',num2str(P_motor60),...
137     ' W'])
138 display('-------------------------------------')
139 display('DEPRAG AIR MOTOR SIMULATION RESULTS')
140 display('-------------------------------------')
141 display(['*PARAMETERS*: P1(gauge) = ',num2str((p0-1.01325e5)/10^3),...
142     ' kPa, T1 = ',num2str(T0-273),' degC.'])
143 display '[100% efficient]'
144 display(['Minimum exit pressure(gauge) = ...
        ',num2str((pair-1.01325e5)/10^3),...
145     ' kPa'])
146 display(['Static flow temperature in pipe = ',num2str(Tair-273),' degC'])
147 display(['Expansion ratio = ',num2str(ex),''])
148 display(['Temperature difference = ',num2str(T0-Tair),' degC'])
149 display ' '
150 display '[60% efficient]'
151 display(['Minimum exit pressure(gauge) = ...
        ',num2str((pair_1-1.01325e5)/10^3),...
```

```
152      ' kPa'])
153  display(['Static flow temperature in pipe = ',num2str(Tair_1-273),' degC'])
154  display(['Expansion ratio = ',num2str(ex_1),''])
155  display(['Temperature difference = ',num2str(T0-Tair_1),' degC'])
156  display('------------------------------')
157  display('BAND BRAKE SIMULATION RESULTS')
158  display('------------------------------')
159  display(['*PARAMETERS*: P = ',num2str(P),' W, n = ',num2str(n),' rpm' ...
160       ', r = ',num2str(r),' m'])
161  display(['Anchoring Force = ',num2str(F1),' N'])
162  display(['Actuating Force = ',num2str(F2),' N, or ',num2str(F2/9.81),' ...
        kgf'])
163  display(['Friction Force = ',num2str(F_fric),' N'])
164  display(['Instantaneous Rate of Temp Rise = ',num2str(dTdt), ' K/s'])
165
166  %% INTERNAL SCRIPT FUNCTIONS
167  % --------------------------------------------------------------------
168  % Ratio of Isentropic Flow Equations (Credit: David Buttsworth)
169  function P2P1=isenpress(M1,M2,g)
170  G=g/(g-1);
171  P2P1=isentemp(M1,M2,g).^G;
172
173  function T2T1=isentemp(M1,M2,g)
174  G=(g-1)/2;
175  T2T1=(1+G*M1.^2)./(1+G*M2.^2);
176
177  function r2r1 = isendens(M1,M2,g)
178  r2r1 = isenpress(M1,M2,g)./isentemp(M1,M2,g);
```

B.2 Refined Air Motor Simulation - predict.m

```
%% SIMULATION MODEL
%% Summary
% ENG4111-2 FINAL YR PROJECT (2015)

% This code will simulate the volume and pressure of air in the working
% chamber of a multivane air motor over a single full rotation. This in
% conjunction with thermodynamic priniples will help to determining the
% approximate expected temperature drop and flow power generated by the
% device.


% INPUTS
% Number of vanes in air motor's rotor (z)
% Inlet-port position (in_p) in degrees, refer to thesis for convention
% Exhaust-port position (out_p) in degrees, refer to thesis for convention
% Internal radius of casing (ro) in metres
% Radius of eccentrically offset rotor (ri) in metres
% Shortest distance from rotor edge to casing wall (s) in metres
% Internal depth of casing (L) in metres
% Option of producing plots (plots)

% WRITTEN: Rhyan Wall
% DATE MODIFIED: 03/08/15

function [Pressure,r] = predict(z,in_p,out_p,plots)
%% Measurements
% This section lists the geometric measurements of the three models tested
% in comments. These are removed from comments and inputted into the
% program when running the simulation.

global ro ri s
% DEPRAG AIR MOTOR ------------------------------------------------------
% z = 5; %number of vanes
% in_p = 15; %degrees, position of intake port (relative to rotor)
% out_p = 267; %degrees, position of exhaust port
% endin_p = in_p+78; %i.e. assume intake to be point
```

```
37 % endout_p = out_p+78; %i.e. assume exhaust to be point
38 % ro = 0.01852; %m
39 % ri = 0.01600; %m
40 % s = 1e-5; %m
41 % L = 0.04506; %m
42
43 % DEPRAG AIR MOTOR W/ REDESIGNED CYLINDER --------------------------------
44 % z = 5; %number of vanes
45 % in_p = 15; %degrees, position of intake port (relative to rotor)
46 % out_p = 180; %degrees, position of exhaust port
47 % endin_p = in_p+30; %i.e. assume intake to be point
48 % endout_p = out_p+165; %i.e. assume exhaust to be point
49 % ro = 0.01852; %m
50 % ri = 0.01600; %m
51 % s = 1e-5; %m
52 % L = 0.04506; %m
53
54 % VACUUM PUMP ------------------------------------------------------------
55 % endin_p = in_p; %i.e. assume intake to be point
56 % endout_p = out_p; %i.e. assume exhaust to be point
57 % ro = 0.1269; %m
58 % ri = 0.10334; %m
59 % s = 1.00e-04; %m
60 % L = 0.1997; %m
61
62 % PROPOSED DESIGN --------------------------------------------------------
63 % z = 5; %number of vanes
64 % in_p = 9; %degrees, position of intake port
65 % out_p = 214; %degrees, position of exhaust port, carries onto 300 degrees
66 % endin_p = in_p+36;
67 % endout_p = 360-in_p; %end of exhaust port
68 % ro = 0.0475; %m
69 % ri = 0.038; %m
70 % s = 0.025e-3; %m, min distance between the rotor's and cylinder's surface
71 % L = 0.100; %m
72
73 %% Polar Arm Length
74 % The polar arm represents the variable length of a straight line between
75 % rotor's centre to the internal cylinder's surface over theta.
```

```
76
77 d = 360; %desired number of data points per rev, i.e. 1 per degree
78
79 % Range of angles covered by leading vane over full rotation: i.e. from the
80 % min working chamber to the max working chamber and back to the min
81 theta1 = 0:pi/180:2*pi+(d/z)*pi/180; %rad
82
83 % Polar equation of a circle's path given by:(x-a)^2 + (y-b)^2 = ro^2
84 % Polar arm equation for internal path of casing, with origin at centre of
85 % rotor:
86 % (x+(ro-s-ri))^2 + y^2 = ro^2
87 % R^2 + R(2cos(theta)(ro-s-ri) - (ro-s-ri)^2-ro^2 = 0
88 a1 = 1;
89 b1 = 2*cos(theta1)*(ro-s-ri);
90 c1 = (ro-s-ri)^2-ro^2;
91 % Take only the positive root, given length cannot be negative
92 r = (-b1 + sqrt(b1.^2 - 4*a1*c1))/2;
93
94 % Angle between polar arm and the x-axis ---------------------------------
95 theta2 = acos((ro-s-ri+r.*cos(theta1))/ro);
96 % adapt theta2 to be representative of rotation
97 theta2(1+180:360) = 2*pi-theta2(1+180:360);
98 theta2(1+360:end) = 2*pi+theta2(1+360:end);
99
100 %% Volume Calculation
101 % This part of the script runs a simulation of a changing working chamber's
102 % volume over a full revolution, with values at every degree.
103
104 % Area Calculation ------------------------------------------------------
105 %Setting up area values
106  A_lead = zeros(1,length(theta1));
107  A_lag = A_lead;
108
109
110     % Area covered by leading vane relative to axis of symmetry
111     A_lead(1:360) = area(theta1(1:360),theta2(1:360),r(1:360));
112     A_lead(361:end) = area(2*pi+theta1(1:d/z+1),...
113         2*pi+theta2(1:d/z+1),r(1:d/z+1));
114     % Area covered by lagging vane relative to axis of symmetry
```

```
115     A_lag(1:d/z) = area(theta1(361-d/z:360)-2*pi,...
116         theta2(361-d/z:360)-2*pi, r(361-d/z:360));
117     A_lag(d/z+1:end) = area(theta1(1:361),theta2(1:361),r(1:361));
118     % Total area of working chamber is equal to the difference of these
119     % values
120     A = A_lead - A_lag;
121
122     A_lag(1:d/z) = -A_lag(1:d/z);
123     A_lead(361:end) = A_lead(361);
124
125
126 % Volume of chamber ------------------------------------------------------
127 Volume = A*L; %m^3, thickness * area contained within the working chamber
128
129 %% Expansion/Compression Ratios
130 % This part of the code calculates the maximum possible expansion that can
131 % be expected from the setup of the system.
132
133 % Filling volume, i.e. the volume of the chamber just as the lagging rotor
134 % passes into and beyond the inlet port:
135 V_fill1 = Volume(1+in_p);
136 V_fill2 = Volume(1+endin_p+d/z);
137
138 % Exhaust volume, i.e. the volume of the chamber just as the leading
139 % rotor is about to pass into and beyond the outlet port:
140 V_ex1 = Volume(1+out_p);
141 V_ex2 = Volume(1+endout_p);
142
143 % Expansion/Compression Ratios
144 ex_s = V_ex1/V_fill2;
145 max_ex = max(Volume)/V_fill2;
146 com = V_ex1/max(Volume);
147
148 %% Target Temperature Drop and Power Rating Prediction
149 % This part of the script runs the thermodynamics analysis of the system
150 % and determines the maximum temperature drop, flow power generated,
151 % pressure fluctuation between the intake and exhaust points and exhaust
152 % temperature based on power generation efficiency.
153
```

```
154 % Air properties ------------------------------------------------------
155 R_g = 287; %universal gas constant of air
156 k1 = 1.35; %expansion polytropic coefficient
157 k = 1.4; %ratio of heat coefficients
158 K = (k1-1)/k1;
159 cp = R_g/(k-1)*k; %specific heat of air under constant pressure
160 % Shop air reservoir conditions ---------------------------------------
161 p0 = 6e5; %Pa
162 p0 = p0 + 1.01325e5; %Pa
163 T0 = 288; %Degrees K
164 rho0 = p0/R_g/T0; %kg/m^3
165
166 % Maximum possible steady mass flow of air and properties from shop air
167 % system --------------------------------------------------------------
168 % State 1: stagnant conditions (i.e. M1 = 0)
169 % State 2: critical conditions (i.e. M2 = 1)
170 dstar = 3.0e-3; %m, approximate diameter equivalent of valve
171 Astar = pi*dstar^2/4; %m^2, critical area at throat
172 rhostar = rho0*isendens(0,1,k); %kg/m^3
173 Tstar = T0*isentemp(0,1,k); %Degrees K
174 astar = sqrt(k*R_g*Tstar); %m/s, speed of sound
175 mdotstar = rhostar*astar*Astar; %kg/s, choked mass flow rate
176 m = p0*V_fill2/R_g/T0; %kg, mass of air in working chamber
177
178 % Assume isentropic expansion and polytropic compression processes occur
179 % within the air motor (n = 1.03 for small geometry)
180 n = 1.03; %accounts for undefined work done on the air being recompressed
181 eff = 0.85; %assumed isentropic efficiency during compression
182 N = (n-1)/n;
183
184 if out_p ≤ 180+d/z/2 %i.e. if only expansion is experienced
185     p1 = p0*ex_s^-k1; %Pa, where v2/v1 = ex
186     T1 = T0*(p1/p0)^K; %Degrees K, output temperature (pg 358 thermo book)
187
188     %Pressure variation over the expansion processes
189     Pressure = p0.*(V_fill2./Volume(1+endin_p+d/z:out_p+1)).^k1;
190     %Pressure variation over entire cycle
191     if endout_p+d/z < 360+in_p
192     Pressure = [p0*ones(1,endin_p-in_p+d/z),Pressure,101.325e3*ones(1,...
```

```
193         endout_p+d/z-out_p),101.325e3*(Volume(endout_p+d/z)./...
194         (Volume(1+endout_p+d/z:360+in_p-1))).^n];
195     else
196     Pressure = [p0*ones(1,endin_p-in_p+d/z),Pressure,101.325e3*ones(1,...
197         360+in_p-out_p-1)];
198     end
199
200     %Total work done by the expansion process
201     V_beg = L*A_lead(in_p+1);
202     V_rem = L*(A_lead(end)-A_lead(endout_p+1));
203
204     P_motorexp =  mdotstar*(cp*(T0-T1));
205     P_motorT = mdotstar*(cp*(T0-T1)+p0/m*(V_fill2-V_beg)-0.5*(p1+...
206         101.325e3)/m*(V_ex1-V_rem));% W, predicted flow power
207
208 else %i.e. expansion and compression processes are experienced
209     p0a = p0*max_ex^-k1;
210     T0a = T0*(p0a/p0)^K;
211     p1 = p0a*(com)^-n;
212     T1 = T0a*(p1/p0a)^N;
213
214     %Pressure variation over the expansion processes
215     Pressure = p0.*(V_fill2./Volume(1+endin_p+d/z:181+d/z/2)).^k1;
216     Pressure = [Pressure, p0a.*(Volume(182+d/z/2:1+out_p)...
217 ./max(Volume)).^-n];
218
219     %Pressure variation over entire cycle
220     if endout_p+d/z < 360+in_p
221     Pressure = [p0*ones(1,endin_p-in_p+d/z),Pressure,101.325e3*ones(1,...
222         endout_p+d/z-out_p),101.325e3*(Volume(endout_p+d/z)./...
223         (Volume(1+endout_p+d/z:360+in_p-1))).^n];
224     else
225     Pressure = [p0*ones(1,endin_p-in_p+d/z),Pressure,101.325e3*ones(1,...
226         360+in_p-out_p-1)];
227     end
228     %Total work done by the expansion and compression processes
229     V_beg = L*A_lead(in_p+1);
230     V_rem = L*(A_lead(end)-A_lead(endout_p+1));
231
```

```
232     P_motorexp =  mdotstar*(cp*(T0-T0a)+eff*cp*(T0a-T1));
233     P_motorT = mdotstar*(cp*(T0-T0a)+eff*cp*(T0a-T1)+p0/m*(V_fill2-...
234       V_beg)-0.5*(p1+101.325e3)/m*(V_ex1-V_rem));% W, predicted flow power
235
236 end
237
238 % Flow speed and air properties in pipe after passing through the
239 % air motor device ------------------------------------------------------
240 d1 = 12e-3; %m, outlet piping diameter
241 A1 = pi*d1^2/4; %m^2, outlet pipe area
242 rho1 = p1/R_g/T1; %kg/m^3, outlet air density
243 u1 = mdotstar/rho1/A1; %m/s, maximum possible outlet air speed
244
245 % Assuming the additional expansion during the exhaust process will not
246 % further cool the air:
247 T1c = T1-273; %Degrees C, exhaust air temp
248
249 % Air consumption at standard conditions --------------------------------
250 rho_amb = 101.325e3/R_g/293; %kg/m^3
251 Q = mdotstar/rho_amb; %m^3/s
252
253 % Effective expansion ratio, assuming steady flow isentropic expansion
254 ex = (T1/T0)^(-1/(k-1));
255
256 % Rotational Speed ------------------------------------------------------
257 speed =  mdotstar/(z*((p0*V_fill2/(R_g*T0))-(p1*V_rem/(R_g*T1))))*60;
258
259 %% Blowby Calculation
260 % Blowby is a possibility between the small gap between the rotor and
261 % cylinder. This can be estimated from analysing the fluid flow between
262 % two flat plates; which goes to simulate the gap between the rotor and
263 % cylinder. Assuming a linear pressure distribution:
264
265 mu_air = 1.5e-5; %Ns/m^2, average air viscosity
266 U = speed*2*pi/60*ri; %m/s, average linear speed at rotor tip
267 a = s; %m, air gap
268 f = find((r-ri-s)/ro>0.0015);
269 x = pi*2*ri*(2*f(1)/360); %m, width of gap
270 detP = Pressure(in_p+1)-Pressure(361+in_p-d/z);
```

```
271 % Convention dictates +ve is clockwise, therefore take negative value
272 Qdot = -L*((U*a/2)-((1/12/mu_air)*detP/x*a^3)); %m^3/s, blowby flowrate
273
274 %% Results
275 % This section is purposed with displaying outputs on the MATLAB workspace
276
277 disp 'ENG4111-2'
278 disp ' '
279 disp 'Rhyan Wall'
280 disp ' '
281 disp '0061032900'
282 disp ' '
283
284 display('------------------')
285 display('GEOMETRY RESULTS')
286 display('------------------')
287 display(['Volume of working chamber at entry is ', num2str(V_fill2), ...
288     'm^3.'])
289 display(['Volume of working chamber at exit is ', num2str(V_ex1), ...
290     'm^3.'])
291 display(['Maximum volume of working chamber is ', num2str(max(Volume)), ...
292     'm^3.'])
293 display(['Minimum volume of working chamber is ', num2str(min(Volume)), ...
294     'm^3.'])
295 display ' '
296 display(['Expansion ratio for the given geometry is ', num2str(ex_s),'.'])
297 display(['Theoretical maximum expansion ratio for given geometry is ', ...
298     num2str(max_ex),'.'])
299 display('--------------------')
300 display('SIMULATION RESULTS')
301 display('--------------------')
302 display(['*PARAMETERS*: P1(gauge) = ',num2str((p0-1.01325e5)/10^3), ...
303     ' kPa, T1 = ',num2str(T0-273),' degC.'])
304 display(['Minimum exit pressure(gauge) = ',num2str((p1-1.01325e5)/10^3),...
305     ' kPa.'])
306 display(['Static flow temperature in pipe = ',num2str(T1c),' degC.'])
307 display ' '
308 display(['Max flow speed in pipe = ',num2str(u1),' m/s.'])
309 display(['Max mass flow through system = ',num2str(mdotstar*1e3),...
```

```
310      ' grams/s.'])
311  display(['Max volumetric flow at standard conditions = ',num2str(Q*60),...
312      ' m^3/min.'])
313  display(['Blowby = ',num2str(Qdot),' m^3/s or ', num2str(Qdot/Q*100),'%'...
314      ' of max volumetric flow.'])
315  display ' '
316  display(['Max net air motor expansion/compression power = ',...
317      num2str(P_motorexp),' W.'])
318  display(['Max air motor flow power = ',num2str(P_motorT),' W.'])
319  display(['Motor efficiency = ',num2str(P_motorexp/P_motorT*100),...
320      ' %.'])
321  display ' '
322  display(['Effective expansion ratio = ',num2str(ex),'.'])
323  display(['Max geometric expansion ratio = ',num2str(max_ex),'.'])
324  display(['Temperature difference = ',num2str(T0-T1),' degC.'])
325  display(['Rotational speed of shaft = ',num2str(speed),' rpm.'])
326
327  %% Plots
328  % This section commands the plots to be outputted to interpret the model
329  % results graphically.
330
331  if plots == 1
332  % Plotting volume of working chamber over radians/degrees
333  figure(1)
334  plot(theta1(1:end)*180/pi,Volume)
335  title('Volume of Working Chamber')
336  xlabel('Angle of Leading Rotor Position [^o]')
337  ylabel('Volume of Working Area [m^3]')
338  grid on
339
340  % Plotting pressure and volume of working chamber
341  figure(2)
342  plot(Volume(1+in_p:360+in_p),Pressure/1e3)
343  title('Pressure vs Volume')
344  xlabel('Chamber Volume [m^3]')
345  ylabel('Chamber Pressure [kPa]')
346  grid on
347
348  % Plotting pressure of working chamber over radians/degrees
```

```
349 figure(3)
350 plot(theta1(1+in_p:360+in_p)*180/pi,Pressure(1:360)/1000)
351 title('Pressure of Working Chamber During Expansion')
352 xlabel('Angle of Leading Rotor Position [^o]')
353 ylabel('Pressure [kPa]')
354 grid on
355
356 % Plotting area of working chamber and area covered by leading/lagging vane
357 figure(4)
358 plot(theta1(1:end)*180/pi,A_lead,'r',theta1(1:end)*180/pi,A_lag,'k',...
359    theta1(1:end)*180/pi,A,'b')
360 title('Displaced Area Over Full Rotation')
361 xlabel('Angle of Rotor / Leading Vane Position [^o]')
362 ylabel('Area [m^2]')
363 legend('Leading Vane','Lagging Vane','Working Chamber','Location','Best')
364 grid on
365
366 % Plotting polar arm for path of internal casing over theta, with ...
       origin at
367 % centre of rotor:
368 figure(5)
369 plot(theta1*180/pi,r)
370 title('Length of Polar Arm Over Full Rotation of Rotor')
371 xlabel('Angle of Rotor Rotation [^o]')
372 ylabel('Polar Arm Length [m]')
373 grid on
374
375 % Plotting casing and rotor of air motor device
376 % check plot, should produce a circle of radius ro off centre by (ri-s-ro)
377 % with a smaller on centre circle inside of radius ri.
378 figure(6)
379 polar(theta1,r)
380 hold on
381 polar(theta2,ones(1,length(theta2))*ri,'r')
382 title('Geometric Visualisation of Rotor and Casing ')
383 legend('Casing', 'Rotor', 'Location','Best')
384 end
385
386 %% INTERNAL SCRIPT FUNCTIONS
```

```
387 % This last section defines the internal functions used to run the
388 % analyses.
389
390 % -------------------------------------------------------------------------
391 % Area equation based on geometric and trigonometric relationships
392 function A = area(theta1, theta2, r)
393 % Area is a combination of large circle's sector area over theta and
394 % scalene triangle made between the centre of large circle, small circle
395 % and radius/polar arm.
396 % Angle made from centre of larger circle to point of contact with r
397 global ro ri s
398
399 s_a_ro = ro^2.*theta2/2;
400 s_a_ri = ri^2.*theta1/2;
401 triangle = 1/2.*(ro-s-ri).*r.*sin(theta1);
402 A = s_a_ro - triangle - s_a_ri;
403
404
405 % -------------------------------------------------------------------------
406 % Ratio of Isentropic Flow Equations (Credit: Dr. David Buttsworth)
407 function P2P1=isenpress(M1,M2,k)
408 G=k/(k-1);
409 P2P1=isentemp(M1,M2,k).^G;
410
411
412 function T2T1=isentemp(M1,M2,k)
413 G=(k-1)/2;
414 T2T1=(1+G*M1.^2)./(1+G*M2.^2);
415
416
417 function r2r1 = isendens(M1,M2,k)
418 r2r1 = isenpress(M1,M2,k)./isentemp(M1,M2,k);
```

B.3 Experimental Results - experimental_results.m

```
%% ------------------ ENG4111 - FINAL YR PROJECT (2015) ------------------
% This code calls on an EXCEL document that contains the data collected
% during experimentation to calculate secondary data, and produce graphs
% of power and torque against rotational speed. Torque vs. Speed was
% compared with the 400W DEPRAG air motor model specifications provided
% by the manufacturer.

% WRITTEN: Rhyan Wall
% DATE MODIFIED: 18/06/15

clc;clear all;close all

disp 'ENG4111'
disp ' '
disp 'Rhyan Wall'
disp '0061032900'
disp ' '

%% EXPERIMENTAL DATA
%Set parameters in testing
r = 0.038; %m, radius of v-pulley
cp = 1005; %J/kgK, average specific heat of air under constant pressure
p_in = 6e5; %Pa, inlet pressure from regulator
p_out = 1.01325e5; %Pa, minimum pressure of exhaust air
R = 287; %J/kgK, universal gas constant of dry air
mh = 0.102; %kg, mass of hanger
mb = 0.034; %kg, mass of bolt
m1 = 0.225; %kg, mass of 200 g ring
m2 = 0.406; %kg, mass of 1/2 lb ring

%Spring constant
%Calculated by measuring the extension of the spring when subject to a
%known gravitational force.
xi = 75; %mm, initial length of spring
xf = 92.8; %mm, final length of spring
ms = 0.737; %kg, known mass attached to spring end
```

```
ks = ms*9.81/(xf-xi); %N/mm, spring constant

%Measurements (mass, outlet temp, spring length, rotating speed)
table = xlsread('DATA');
t = table(:,1); %test number
m = table(:,2); %kg
xi = table(:,3); %mm
xf = table(:,4); %mm
Tin = table(:,5); %degC
Tout = table(:,6); %degC
n = table(:,7); %rpm
time = table(:,8); %secs
V = table(:,9); %litres

%Secondary calculations
Vdot = V/1000./time; %m^3/s
mdot = Vdot*p_out./(R*(Tout+273)); %kg/s, as in P*Vdot=mdot*R*T
Tau = r*(ks*(xf-xi)); %Nm, brake torque
P = Tau.*2*pi.*n/60; %W, brake power (friction torque generation)
P2 = mdot.*cp.*(Tin-Tout); %W, flow power (1st law of thermodynamics)

%The predicted exhaust temperature according to the amount of brake power
%extracted, assuming full isentropic efficiency:
T_thermo = Tin - P./(mdot.*cp); %deg C, exhaust temp (1st law)

%% RESULTS
figure(1)
plot(n/max(n)*100,Tau,'o')
title('Torque vs. Speed %')
xlabel('% of Max Speed')
ylabel('Torque(Nm)')
grid on

figure(2)
plot(n,P,'bo',n,P2,'ro')
title('Power vs. Speed')
xlabel('Speed(rpm)')
ylabel('Power(W)')
legend('Brake Power','1st Law Power')
```

```
76 grid on
77
78 figure(3)
79 plot(Tau,Tin-Tout,'bo',Tau,Tin-T_thermo,'ro')
80 title('Temperature Difference vs. Torque')
81 xlabel('Toque(Nm)')
82 ylabel('Temperature Difference(^oC)')
83 legend('Measured','Predicted (1st Law)','location','best')
84 grid on
85
86 figure(4)
87 plot(P,(Tin-Tout)./(Tin-T_thermo),'o')
88 title('Temperature Ratio vs. Power')
89 xlabel('Power(W)')
90 ylabel('\DeltaT_{measured}/\DeltaT_{predicted}')
91 grid on
```

B.4 Force and Stress Analysis - Stress_analysis.m

```
%% STRESS ANALYSIS
%% Summary
% ENG4111-2 FINAL YR PROJECT (2015)

% This code will simulate the average forces acting on the air motor's
% vanes over a single rotation. This in conjunction with some rudementary
% stress analysis priniples will help to approximate the stresses ...
    acting on
% the rotor and it's vanes.

% WRITTEN: Rhyan Wall
% DATE MODIFIED: 03/08/15

function [] = Stress_analysis()
clc; clear all;close all
%% Values
% This section lists the geometric measurements of the design model being
% tested and the material properties of the rotor, cylinder and vanes.

global ro ri s r mu_c mu_r t Fb w rs l E
% DESIGN MEASUREMENTS ---------------------------------------------------
ro = 0.0475; %m
ri = 0.038; %m
s = 0.025e-3; %m, assumed achievable tolerance
l = 0.09995; %m, vane/rotor length
rs = 0.020/2; %m, shaft radius
w = ri-rs+s; %m, vane width
t = 0.003175; %m, vane thickness
rpm = 3600; %rpm, predicted rotational speed
% MATERIAL PROPERTIES ---------------------------------------------------
% Note that due to lacking material data, some properties will have to be
% approximated by similar materialsl (e.g. the dynamic coefficients of
% friction of Al2024-T3 & SS4140 in contact with teflon will be
% approximated by Al6061 and SS1032 respectively).
rho_v = 2000; %kg/m^3, avg density of PTFE variants
mu_c = 0.16; %dynamic coefficient of friction between SS1032 and Teflon
```

```
36 mu_r = 0.18; %dynamic coefficient of friction between Al6061 and Teflon
37 m = rho_v*(w*l*t); %mass of vane
38 Su = 485e6; %Pa, ultimate strength of Al2024-T3
39 Sy = 345e6; %Pa, yield strength of Al6061
40 E = 0.5e9; %Pa, modulus of elasticity of Teflon
41
42 %% Pressures and Volumes
43 % This section defines the forces acting on the vane, assuming uniform
44 % pressure values in a working chamber, and sets up the algorithm to define
45 % the unknown forces detailed in the free body diagram over the critical
46 % points of the air motor operation in a single cycle.
47 in_p = 9;
48 out_p = 214;
49 z = 5;
50 [p,r] = predict(z,in_p,out_p,0); %Values gathered from predict.m
51 p = [p(end-in_p+1:end),p(1:end-in_p)]; %Rearranging pressure values
52 p = [p,p];
53 Pb = p(214); %Pa, base/exhaust pressure of the air motor cycle
54
55 %% Forces and Stresses
56 % This section defines the forces acting on the vane and works out the
57 % unknown forces acting on the rotor, necessary for proper stress analysis.
58
59 % Setting up matrices for preallocation of values
60 F = zeros(3,361+72);
61 sig = zeros(4,361);
62 p1 = zeros(1,361+72);
63 p2 = p1;
64 e1 = p2;
65 c = e1;
66 F1 = c;
67 F2 = F1;
68 Fc = F2;
69 Fm = Fc;
70 L = Fm;
71 R = L;
72 sig2 = zeros(2,361+72);
73 D = R;
74 A = D;
```

```
75 detx = A;
76 detT = detx;
77 shaft = zeros(1,361);
78 F_b = shaft;
79
80 % Forces and stesses acting on vane and rotor ----------------------------
81 Fb = Pb*(t*l); %N, the force acting on the base of the vane
82 % Setting up matrix for first value
83 p1(1) = p(1);
84 p2(1) = p(1+72);
85 e1(1) = w-(r(1)-ri); % length of vane in rotor slot
86 c(1) = w-0.5*(r(1)-ri); % centre of pressure on vane
87 A(1) = abs(r(1)-ri)*l; %m,  exposed area of vane
88 detx(1) = r(1)-r(360); %m, vane's linear motion over section
89 detT(1) = (1/360)*60/rpm; %sec, time increment
90 Fm(1) = m*((r(1)-w/2)*(rpm*2*pi/60)^2);
91 F1(1) = p1(1)*A(1);
92 F2(1) = p2(1)*A(1);
93 Fc(1) = 2*m*detx/detT*rpm*2*pi/60;
94 F(1:3,1) = forces(e1(1),c(1),Fm(1),F1(1),F2(1),Fc(1));
95 L(1) = F(1,1);
96 R(1) = F(2,1);
97 % Stress and displacement values for vane
98 [sig2(1:2,1),D(1)] = stress2(F1(1),F2(1),Fc(1),L(1),R(1),...
99     F(3,1),e1(1),c(1));
100
101 % Setting up iterative cycle to determine remaining values
102 for k = 2:361+72;
103 p1(k) = p(k);
104 p2(k) = p(k+72);
105 e1(k) = w-(r(k)-ri); % length of vane in rotor slot
106 c(k) = w-0.5*(r(k)-ri); % centre of pressure on vane
107 A(k) = abs(r(k)-ri)*l; %m,  exposed area of vane
108 detx(k) = r(k)-r(k-1); %m, vane's linear motion over section
109 detT(k) = (1/360)*60/rpm; %sec, time increment
110 Fm(k) = m*((r(k)-w/2)*(rpm*2*pi/60)^2);
111 F1(k) = p1(k)*A(k);
112 F2(k) = p2(k)*A(k);
113 Fc(k) = 2*m*detx/detT*rpm*2*pi/60;
```

```
114 F(1:3,k) = forces(e1(k),c(k),Fm(k),F1(k),F2(k),Fc(k));
115 L(k) = F(1,k);
116 R(k) = F(2,k);
117 % Stress and displacement values for vane
118 [sig2(1:2,k),D(k)] = stress2(F1(k),F2(k),Fc(k),L(k),R(k),...
119     F(3,k),e1(k),c(k));
120 end
121 for k = 1:360
122     % Stress values for rotor section
123     sig(1:4,k) = stress(L(k),R(k),L(k+72),R(k+72),r(k),r(k+72));
124 end
125
126 % Forces and stresses acting on rotor's shaft component and bearings ------
127 Izz = pi/4*(rs)^4;
128 for k = 1:361
129     A_rot = pi*2*ri/5*l;
130     % x component of pressure based force acing on rotor sections
131     Fx = A_rot*(p(k+72)*cosd(k+35)+p(k+144)*cosd(k+107)+...
132         p(k+216)*cosd(k+179)+p(k+288)*cosd(251)+p(k+0*cosd(-37)));
133     % y component of pressure based force acing on rotor sections
134     Fy = A_rot*(p(k+72)*sind(k+35)+p(k+144)*sind(k+107)+...
135         p(k+216)*sind(k+179)+p(k+288)*sind(251)+p(k+0*sind(-37)));
136     % Max shear stress acting on shaft section of rotor
137     shaft(1,k) = 1.5*(0.5*sqrt(Fx^2+Fy^2))/(pi*rs^2);
138     % bending stress at rotor edge contact (i.e. max stress given smallest
139     % radius at shaft)
140     M = sqrt(Fy^2+Fx^2)*l/2 - sqrt(Fy^2+Fx^2)/2*(l+0.5*(0.1+0.0085-l));
141     shaft(2,k) = M*rs/Izz;
142     % bearing force is equal to half of the force exerted by pressures on
143     % each rotor section:
144     F_b(k)=sqrt(Fy^2 + Fx^2)/2;
145 end
146
147 %% Fatigue Calculations
148 % This section details the fatigue calculations made on the rotor.
149
150 sig_max = max(sig(4,:));
151 sig_min = min(sig(4,:));
152 sig_a = 0.5*(sig_max-sig_min); %Pa, alternating stress
```

```
153 sig_m = 0.5*(sig_max+sig_min); %Pa, mean stress
154
155 Sndash = 0.5*Su;
156 % For bending loads (table 8.1)
157 cL = 1; %bending load factor
158 cG = 1; %gradient factor
159 cS = 0.8; %surface factor
160 cT = 1; %temp factor
161 cR = 0.814; %reliability factor
162
163 Sn = Sndash*cL*cG*cS*cT*cR;
164
165 % 10^6 (infinite) life line:
166 x1 = 0:1:Su/1e6;
167 y1 = -Sn/Su*x1 + Sn/1e6;
168
169 % Yield strength line:
170 x2 = 0:1:Sy/1e6;
171 y2 = -x2 + Sy/1e6;
172
173 % Failure line 1: -Sn/Su*x + Sn = sig_a/sig_m*x
174 x31 = 0:1:Sn/1e6/(sig_a/sig_m+Sn/Su);
175 y31 = sig_a/sig_m*x31;
176
177 % Failure line 2: -x + Sy = sig_a/sig_m*x
178 x32 = 0:1:Sy/1e6/(sig_a/sig_m+1);
179 y32 = sig_a/sig_m*x32;
180
181 % Choose which line is shorter
182 if length(y31)<length(y32)
183     x3 = x31;
184     y3 = y31;
185 else
186     x3 = x32;
187     y3 = y32;
188 end
189
190 % Effective FOS for fatigue stress
191 FOS = x3(end)/(sig_m/1e6);
```

```
192
193 display('---------------------------------')
194 display('STRESS/FATIGUE ANALYSIS RESULTS')
195 display('---------------------------------')
196 display(['Max stress in rotor section = ',num2str(sig_max/1e6),'MPa.']);
197 display(['Bearing min rated capacity = ',num2str(max(F_b)),'N.']);
198 display(['F.O.S. for fatigue strength = ',num2str(FOS),'.']);
199 display(['Max absolute deflection of vane = ',num2str(1e3*max(abs(D)))...
200     ,'mm.'])
201 display(['Max stress in vane section = ',num2str(max(sig2(2,:))...
202     /1e6),'MPa.']);
203
204 %% Plots
205 % This section provides the desired plots.
206
207 figure(1)
208 plot(0:360,F(:,1:361),'linewidth',1.5)
209 xlabel('Vane Position (^o)')
210 title('Force Analysis on Rotor Vane Over Full Rotation')
211 ylabel('Force (N)')
212 legend('F_L','F_R','F_f','location','best')
213 grid on
214
215 figure(2)
216 plot(0:length(sig)-1,sig/1e6,'linewidth',1.5)
217 xlabel('Leading Vane Position (^o)')
218 ylabel('Stress (MPa)')
219 title('Stress Analysis on Rotor Section Over Full Cycle')
220 legend('\sigma_{shear}','\sigma_{normal}','\sigma_{normal bending}',...
221    '\sigma_{total}','location','best')
222 grid on
223
224 figure(3)
225 plot(0:length(D)-1,D*1e3,'linewidth',1.5)
226 xlabel('Leading Vane Position')
227 ylabel('Max Vertical Displacement (mm)')
228 title('Max Displacement of Leading Vane Over Full Cycle')
229 grid on
230
```

```
figure(4)
plot(0:360,sig2(:,1:361)/1e6,'linewidth',1.5)
xlabel('Leading Vane Position')
ylabel('Stress (MPa)')
title('Stress Analysis on Vane over Full Cycle')
legend('Shear Stress','Bending Normal Stress')
grid on

figure(5)
plot(0:719,p/1e3,'linewidth',1.5)
xlabel('Leading Vane Position (^o)')
ylabel('Abs Pressure (kPa)')
title('Working Chamber Pressure Over 2 Full Cycles')
grid on

figure(6)
plot(0:360,shaft/1e6,'linewidth',1.5)
xlabel('Leading Vane Position (^o)')
ylabel('Stress (MPa)')
title('Stress Analysis on Shaft Section Over Full Cycle')
legend('Shear Stress','Bending Normal Stress')
grid on

figure(7)
plot(0:360,e1(1:361),0:360,w-e1(1:361),'linewidth',1.5)
xlabel('Vane Position (^o)')
ylabel('Length (m)')
title('Vane length in and out of rotor slot')
legend('length of vane inside rotor slot',...
    'length of vane outside rotor slot')
grid on

figure(8)
plot(x1,y1,x2,y2,x3,y3,sig_m/1e6,sig_a/1e6,'kx','linewidth',1.5)
xlabel('Mean Bending Stress \sigma_m (MPa)')
ylabel('Alternating Bending Stress \sigma_a (MPa)')
title('Constant-Life Fatigue Diagram')
legend('10^6 \approx \infty life','S_y','Failure Line','Operating Point')
grid on
```

```
270
271 figure(9)
272 plot(0:360,F_b,'linewidth',1.5)
273 xlabel('Vane Position (^o)')
274 ylabel('Force on Bearing (N)')
275 title('Force Acting on Bearing')
276 grid on
277
278 function F = forces(e,c,Fm,F1,F2,Fc)
279 % This section deals with the force calculations as derived from basic
280 % reaction moment and force calcs relative to the base of the vane.
281
282 global mu_c mu_r t Fb w
283 % Simplifying expressions to put into matrix
284 a = 1/(mu_c*mu_r); %alpha
285 b = 2*e/(t*mu_r) - 1; %beta
286 z = 2*w/(t*mu_r); %zeta
287 g1 = Fc+F1-F2; %gamma 1
288 g2 = 1/mu_r*(Fm+Fb); %gamma 2
289 g3 = 2*c/(t*mu_r)*(F1-F2) + w/(t*mu_r)*Fc; %gamma 3
290
291 A = [1,-1,1;1,1,a;b,1,z];
292 B = [g1;g2;g3];
293
294 F = A\B;
295
296 function sig = stress(L1,R1,L2,R2,ra1,ra2)
297 % This code deals with the rotor stress calculations as derived from
298 % basic reaction moment and force calcs relative to the point of highest
299 % stress. In this case, this point is at the centre of a line drawn between
300 % the base of two vane slots. Mass of the rotor section was neglected.
301
302 global rs l t w ri
303
304 % Factoring in for the possibility that not all reaction forces are acting
305 % on a specific sector
306 if R1 > 0
307     R1 = 0;
308 end
```

```
309 if L2 > 0
310     L2 = 0;
311 end
312 if L1 < 0
313     L1 = 0;
314 end
315 if R2 < 0
316     R2 = 0;
317 end
318
319 L1 = abs(L1);
320 R1 = abs(R1);
321 L2 = abs(L2);
322 R2 = abs(R2);
323
324 Fvx = cosd(36)*(R1+L1-R2-L2);
325 Fvy = sind(36)*(R2+L2+R1+L1);
326 Mvz = -(cosd(36)^2+sind(36)^2)*(R1*((ra1-w-rs))-R2*((ra2-w-rs)...
327     )+L1*((ri-rs))-L2*((ri-rs)));
328
329 A = l*(2*(rs*sind(36)-t*cosd(36))); % Area of interest
330 Izz = 1/12*l*(rs*sind(36)*2-t)^3; % 2nd moment of area about acting axis
331
332 sig_shearxmax = 1.5*Fvx/A; %VQ/It, shear stress distribution
333 sig_norm = Fvy/A;
334 sig_Mvmax = -Mvz*rs*sind(36)/Izz; % My/I, bending normal stress
335
336 total_norm = sig_norm + sig_Mvmax;
337
338 %Total normal and shear stresses
339 sig = [sig_shearxmax;sig_norm;sig_Mvmax;total_norm];
340
341 function [sig2,D1] = stress2(F1,F2,Fc,FL,FR,Ff,e1,c)
342 % This code deals with the vane stress calculations as derived from
343 % basic reaction moment and force calcs relative to the point of highest
344 % stress. This is found from the max shear force and moment as per a
345 % conventional shear force and bending moment diagrams. This code also
346 % produces a basic display of predicted vane displacement, as per the beam
347 % stiffness analysis method.
```

```
348
349 global w l t
350
351 detx = 0.0001; %m, incremental values
352 x = 0:detx:w;
353 n = length(x);
354
355 Vy = zeros(n,1);
356 Mz = Vy;
357
358
359 for k = 1:n
360
361     % Section 1: 0 < x < w-c
362     Vy(k) = Ff;
363     Mz(k) = Ff*x(k);
364
365     if x(k) ≥ w-c; % Section 2: w-c < x < w-w/2 AND w-c < x < w-e1
366         Vy(k) = Ff+F2-F1;
367         Mz(k) = Ff*x(k)+(F2-F1)*(x(k)-(w-c));
368     end
369     if w/2 > e1;
370         if x(k) ≥ w-w/2; % Section 3: w-w/2 < x < w-e1
371             Vy(k) = Ff+F2-F1-Fc;
372             Mz(k) = Ff*x(k)+(F2-F1)*(x(k)-(w-c))-Fc*(x(k)-(w-w/2));
373         if x(k) ≥ w-e1; % Section 4: w-e1 < x < w
374             Vy(k) = Ff+F2-F1-Fc+FL;
375             Mz(k) = Ff*x(k)+(F2-F1)*(x(k)-(w-c))-Fc*(x(k)-(w-w/2))+...
376                 FL*(x(k)-(w-e1));
377         end
378         end
379     else
380         if x(k) ≥ w-e1; % Section 3: w-e1 < x < w-e1
381             Vy(k) = Ff+F2-F1+FL;
382             Mz(k) = Ff*x(k)+(F2-F1)*(x(k)-(w-c))+FL*(x(k)-(w-e1));
383             if x(k) ≥ w-w/2; % Section 4: w-w/2 < x < w
384                 Vy(k) = Ff+F2-F1+FL-Fc;
385                 Mz(k) = Ff*x(k)+(F2-F1)*(x(k)-(w-c))+FL*(x(k)-(w-e1))-...
386                     Fc*(x(k)-(w-w/2));
```

```
387             end
388         end
389     end
390 end
391 Vy(k)=Vy(k)-FR;
392
393 A = l*t;
394 Izz = (t)^3*l/12;
395 sig_shearmax = 1.5*max(abs(Vy))/A;
396 sig_Mvmax = max(abs(Mz))*t/2/Izz;
397
398 % Displacement calculations using Stiffness Matrix
399 % Given the known acting forces, can determine the expected displacements,
400 % assuming that the points of contact with the rotor have 0 vertical
401 % displacement.
402
403 L1 = w - e1; %m, length of 1st fixed end element
404 L2 = e1; %m, length of 2nd fixed end element
405
406 k = [12/L1^3,6/L1^2,6/L1^2,0;...
407     6/L1^2,4/L1,2/L1,0;...
408     6/L1^2,4/L1,4/L1+4/L2,2/L2;...
409     0,0,2/L2,4/L2]; %Stiffness matrix
410 if w/2 > e1
411 Q = [Ff+(F2-F1)/2-Fc*(w/2-e1)/(w-e1);...
412     -(F1-F2)/8*(w-e1)-Fc*(w/2)^2*(w/2-e1)/(w-e1)^2;...
413     (F1-F2)/8*(w-e1)+Fc*(w/2)*(w/2-e1)^2/(w-e1)^2;...
414     0]; %Loading matrix
415 else
416 Q = [Ff+(F2-F1)/2;...
417     -(F1-F2)/8*(w-e1);...
418     (F1-F2)/8*(w-e1)-Fc*(e1-w/2)^2*(w/2)/e1^2;...
419     Fc*(e1-w/2)*(w/2)^2/e1^2]; %Loading matrix
420 end
421 D = k\Q;
422 D1 = D(1);
423
424 sig2 = [sig_shearmax;sig_Mvmax];
425
```

```
426
427 % % Shear Force Diagram - pretty wizard output
428 % figure(12)
429 % subplot(3,1,1)
430 % xlabel('x (m)')
431 % ylabel('Shear Force (N)')
432 % title('Shear Force Diagram')
433 % plot(x,Vy, 'b', 'linewidth', 2.0)
434 % grid
435 % axis tight
436 % hold on
437 %
438 % % Bending Moment Diagram
439 % subplot(3,1,2)
440 % plot(x,Mz, 'r', 'linewidth', 2.0)
441 % grid
442 % xlabel('x (m)')
443 % ylabel('Bending Moment (Nm)')
444 % title('Bending Moment Diagram')
445 % axis tight
446 % hold on
447 %
448 % % Vertical Displacement Diagram
449 % subplot(3,1,3)
450 % xlabel('x (m)')
451 % ylabel('y (m)')
452 % title('Vertical Displacement Diagram')
453 % plot([0,L1,w],[D(1),0,0], 'b', 'linewidth', 2.0)
454 % grid
455 % axis tight
```

Appendix C

Risk Management Plan

University of Southern Queensland
Risk Management Plan

Date: 01/06/2015	**Faculty/Department:** Faculty of Health, Engineering and Sciences	**Assessment completed by:** Rhyan Wall	**Contact number:** +61 4 3225 4032
What is the task? Work extraction from expanding pressurised air experimentation		**Location where task is being conducted:** P10	
Why is the task being conducted? To investigate the cooling capacity by work extraction of compressed air.			
What are the nominal conditions?			
Personnel Rhyan Wall / under supervision	**Equipment** Air motor rig (incl. band brake) Thermocouples Mass flow readers Pressure regulator	**Environment** Well ventilated controlled temperature	**Other**
Briefly explain the procedure for this task (including reference to other procedures) Running pressurised air through an air motor rig (consisting of an air motor and a band brake) and extracting work from the air stream			

Risk register and Analysis
[ALARP = As Low As Reasonably Practicable]

Element or Sub Element/ Process Step	The Risk: What can happen and what will be the result	EXISTING CONTROLS	Risk Rating with existing controls? See next page			Is it ALARP? Yes/No	ADDITIONAL CONTROLS REQUIRED	Risk Rating with additional controls?			Is it ALARP? Yes/No	Risk Decision: Accept Transfer Treat
List major steps or tasks in process	– Electric shock – Eye infection – Fire / explosion – Physical injury – Cut / graze Chemical burn	List all current controls that are already in place or that will be used to undertake the task eg – List of Personal Protective Equipment (PPE) – Identify types facility, location – Existing safety measurers Existing emergency procedures	Consequences	Likelihood	Rating		Additional controls may be required to reduce risk rating eg – Greater containment (PC2) – Additional PPE – gloves safety glasses Specific induction / training	Consequences	Likelihood	Rating		
Operating air motor rig	NA	NA	NA	NA	NA	NA	NA	NA	NA	NA	NA	NA
Handling of pressurised air	-External and internal injuries when exposed to highly pressurised air	Wearing of proper Personal Protective Equipment (PPEs), i.e. goggles Two people will be operating the rig at any time during experimentation and will advise third parties to stay clear of exhaust port of air motor. A note will also be attached to the rig to tell people to stay away from the exhaust port during operation.	3	D	M	YES	NA	NA	NA	NA	NA	Accept

Handling of brake air motor rig	-Hot and cold surfaces after operation of air motor has ceased -External spinning components -Reverse operation	Handle air motor rig with care, ensuring that air motor rig is not touched during operation; in particular the band brake. The air motor's surface will likely be around -15°C, which is not considered dangerous. Air motor is set up to operate in one direction, and can only be operated in reverse if the entire setup is changed. Make any third party aware of dangers and ensure that direct contact with spinning components is not possible	2	D	L	**YES**	NA	NA	NA	NA	NA	NA	**Accept**
Band brake fixture releasing spring	-Flung components	If released during operation, flung components can possible hit nearby people. However the dangers associated with the part's weight and momentum is so low that any serious injury is not considered possible.	1	C	L	**YES**	NA	NA	NA	NA	NA	NA	**Accept**

USQ RISK RATING ADAPTED FROM AS4360:2004

Note: In estimating the level of risk, initially estimate the risk with existing controls and then review risk controls if risk level arising from the risks is not minimal

TABLE 1 - CONSEQUENCE

Level	Descriptor	Examples of Description
1	Insignificant	No injuries. Minor delays. Little financial loss. $0 - $4,999*
2	Minor	First aid required. Small spill/gas release easily contained within work area. Nil environmental impact. Financial loss $5,000 - $49,999*
3	Moderate	Medical treatment required. Large spill/gas release contained on campus with help of emergency services. Nil environmental impact. Financial loss $50,000 - $99,999*
4	Major	Extensive or multiple injuries. Hospitalisation required. Permanent severe health effects. Spill/gas release spreads outside campus area. Minimal environmental impact. Financial loss $100,000 - $250,000*
5	Catastrophic	Death of one or more people. Toxic substance or toxic gas release spreads outside campus area. Release of genetically modified organism (s) (GMO). Major environmental impact. Financial loss greater than $250,000*

* Financial loss includes direct costs eg workers compensation and property damage and indirect costs, eg impact of loss of research data and accident investigation time.

TABLE 2 - PROBABILITY

Level	Descriptor	Examples of Description
A	Almost certain	The event is expected to occur in most circumstances. Common or repetitive occurrence at USQ. Constant exposure to hazard. Very high probability of damage.
B	Likely	The event will probably occur in most circumstances. Known history of occurrence at USQ. Frequent exposure to hazard. High probability of damage.
C	Possible	The event could occur at some time. History of single occurrence at USQ. Regular or occasional exposure to hazard. Moderate probability of damage.
D	Unlikely	The event is not likely to occur. Known occurrence in industry. Infrequent exposure to hazard. Low probability of damage.
E	Rare	The event may occur only in exceptional circumstances. No reported occurrence globally. Rare exposure to hazard. Very low probability of damage. Requires multiple system failures.

TABLE 3 – RISK RATING

Probability	Consequence				
	Insignificant 1	Minor 2	Moderate 3	Major 4	Catastrophic 5
A (Almost certain)	M	H	E	E	E
B (Likely)	M	H	H	E	E
C (Possible)	L	M	H	H	H
D (Unlikely)	L	L	M	M	M
E (Rare)	L	L	L	L	L

TABLE 4 - RECOMMENDED ACTION GUIDE

Abbrev	Action Level	Descriptor
E	Extreme	The proposed task or process activity MUST NOT proceed until the supervisor has reviewed the task or process design and risk controls. They must take steps to firstly eliminate the risk and if this is not possible to introduce measures to control the risk by reducing the level of risk to the lowest level achievable. In the case of an existing hazard that is identified, controls must be put in place immediately.
H	High	Urgent action is required to eliminate or reduce the foreseeable risk arising from the task or process. The supervisor must be made aware of the hazard. However, the supervisor may give special permission for staff to undertake some high risk activities provided that system of work is clearly documented, specific training has been given in the required procedure and an adequate review of the task and risk controls has been undertaken. This includes providing risk controls identified in Legislation, Australian Standards, Codes of Practice etc.* A detailed Standard Operating Procedure is required. * and monitoring of its implementation must occur to check the risk level
M	Moderate	Action to eliminate or reduce the risk is required within a specified period. The supervisor should approve all moderate risk task or process activities. A Standard Operating Procedure or Safe Work Method statement is required
L	Low	Manage by routine procedures.

*Note: These regulatory documents identify specific requirements/controls that must be implemented to reduce the risk of an individual undertaking the task to a level that the regulatory body identifies as being acceptable.

The task should not proceed if the risk rating after the controls are implemented is still either HIGH or EXTREME or if any risk is not As Low As Reasonably Practicable (ALARP).

This Risk Assessment score of Low (L) is only on the condition that all existing and additional controls are in place at the time of the task being conducted.

Assessment completed by:	
Name: Rhyan Wall	**Signature:**
Position: Undergraduate Student	**Contact No:** +61 4 3225 4032
Date: 01/06/15	
Supervisor	
David Buttsworth	**Signature:**
Position : **Professor (Thermofluids Engineering)**	**Contact No:** x2614
Date: 18/6/15.	

Guidance Notes for review of Controls and Risk Management Plan.

When monitoring the effectiveness of **control measures**, it may be helpful to ask the following questions:

- **Have the chosen control measures been implemented as planned?**
  - Are the chosen control measures in place?
  - Are the measures being used?
  - Are the measures being used correctly?
- **Are the chosen control measures working?**
  - Have any the changes made to manage exposure to the assessed risks resulted in what was intended?
  - Has exposure to the assessed risks been eliminated or adequately reduced?
- **Are there any new problems?**
  - Have the implemented control measures introduced any new problems?
  - Have the implemented control measures resulted in the worsening of any existing problems?

To answer these questions:

- consult with workers, supervisors and health and safety representatives;
- measure people's exposure (e.g. taking noise measurements in the case of isolation of a noise source);
- consult and monitor incident reports; and
- review safety committee meeting minutes where possible.

Set a date for the review of the **risk management process**. When reviewing, check if:

- the process that is currently in place is still valid;
- things have changed that could make the operating processes or system outdated;
- technological or other changes have affected the current workplace; and
- a different system should be used altogether

Appendix D

Model Drawings

D.1 Air Motor Rig (AMR)

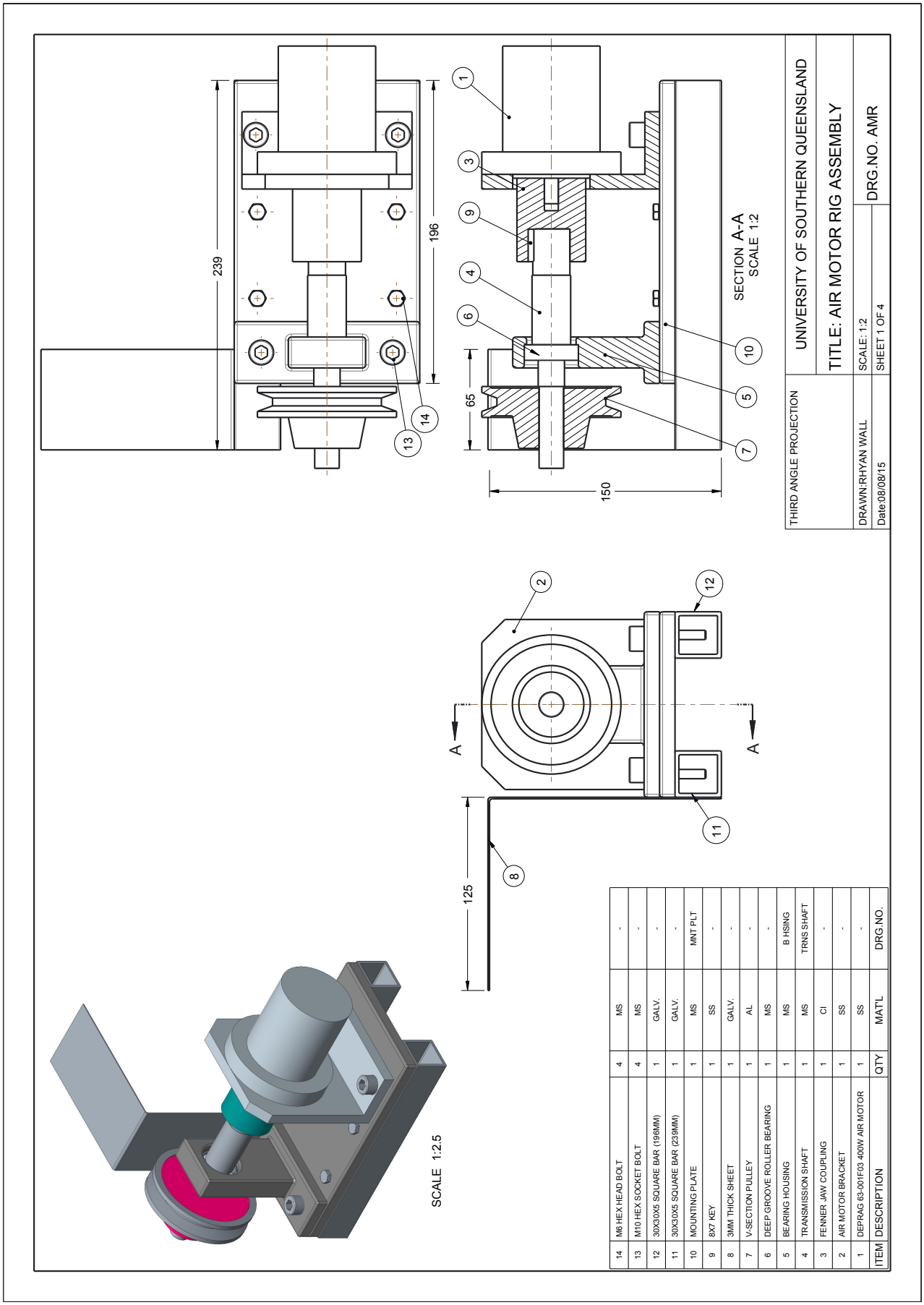

ITEM	DESCRIPTION	QTY	MATL	DRG.NO.
14	M6 HEX HEAD BOLT	4	MS	-
13	M10 HEX SOCKET BOLT	4	MS	-
12	30X30X5 SQUARE BAR (196MM)	1	GALV.	-
11	30X30X5 SQUARE BAR (239MM)	1	GALV.	-
10	MOUNTING PLATE	1	MS	MNT PLT
9	8X7 KEY	1	SS	-
8	3MM THICK SHEET	1	GALV.	-
7	V-SECTION PULLEY	1	AL	-
6	DEEP GROOVE ROLLER BEARING	1	MS	-
5	BEARING HOUSING	1	MS	B HSING
4	TRANSMISSION SHAFT	1	MS	TRNS SHAFT
3	FENNER JAW COUPLING	1	CI	-
2	AIR MOTOR BRACKET	1	SS	-
1	DEPRAG 63-001F03 400W AIR MOTOR	1	SS	-

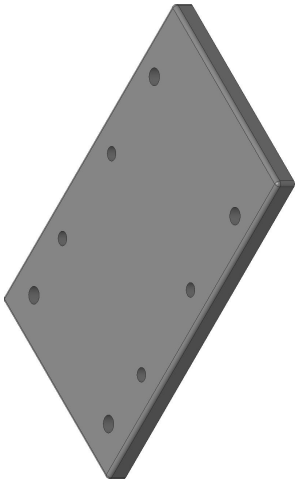

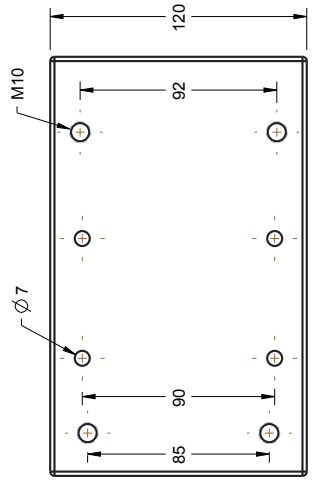

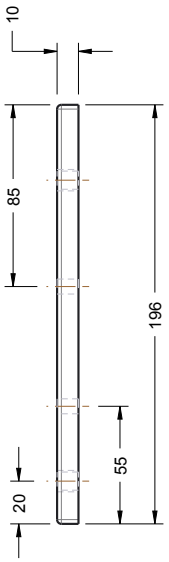

MOUNTING PLATE
MAT'L - MS
1 REQ'D

ALL TOLERANCES ±0.2 UNLESS OTHERWISE STATED ALL RADII R2 THIRD ANGLE PROJECTION 3.2 UNLESS OTHERWISE STATED	UNIVERSITY OF SOUTHERN QUEENSLAND	
	TITLE: MOUNTING PLATE	
DRAWN:RHYAN WALL	SCALE: 1:1	DRG.NO. MNT PLT
Date:01/08/15	SHEET 2 OF 4	

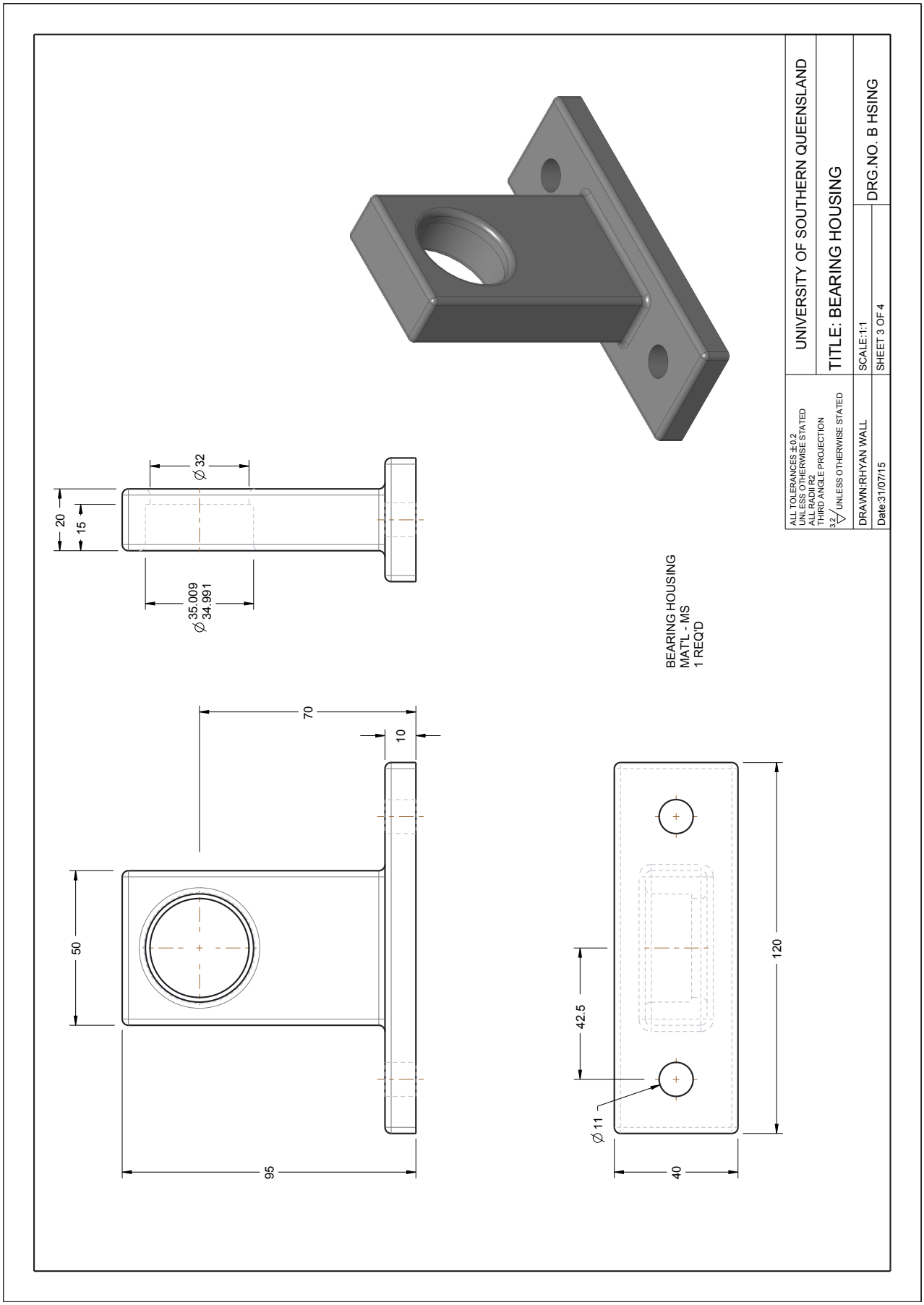
UNIVERSITY OF SOUTHERN QUEENSLAND
TITLE: BEARING HOUSING
SCALE:1:1
DRG.NO. B HSING
SHEET 3 OF 4
DRAWN:RHYAN WALL
Date:31/07/15
ALL TOLERANCES +-0.2
UNLESS OTHERWISE STATED
ALL RADII R2
THIRD ANGLE PROJECTION
UNLESS OTHERWISE STATED
BEARING HOUSING
MATL - MS
1 REQ'D
Ø 32
20
15
Ø 35.009
Ø 34.991
70
10
50
95
42.5
Ø 11
120
40

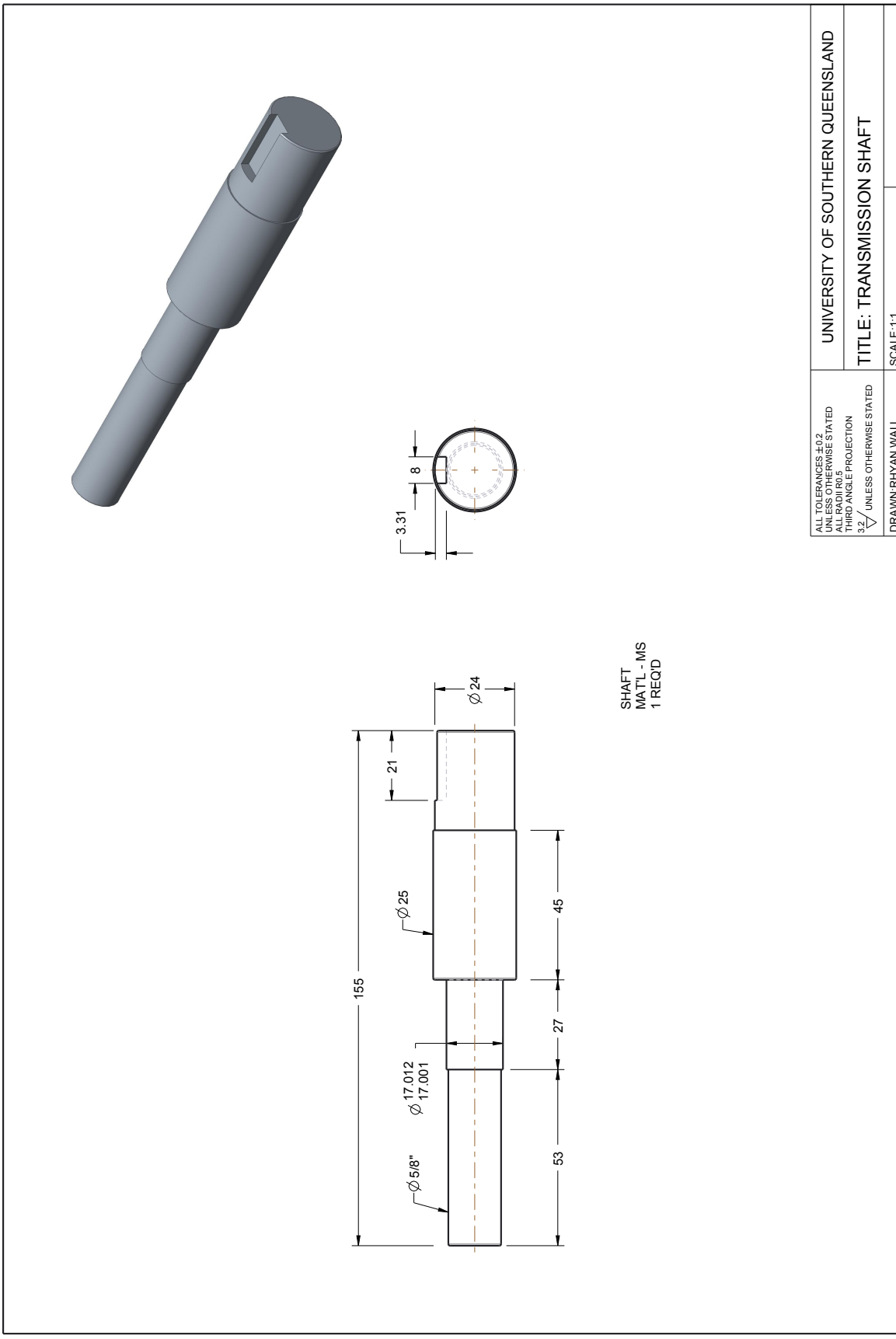
UNIVERSITY OF SOUTHERN QUEENSLAND
TITLE: TRANSMISSION SHAFT
SCALE:1:1
DRG.NO. TRNS SHAFT
SHEET 4 OF 4
DRAWN:RHYAN WALL
Date:01/08/15
ALL TOLERANCES +-0.2
UNLESS OTHERWISE STATED
ALL RADII R0.5
THIRD ANGLE PROJECTION
UNLESS OTHERWISE STATED
SHAFT
MATL - MS
1 REQ'D
8
3.31
Ø24
21
Ø25
155
45
27
53
Ø17.012
17.001
Ø5/8"

D.2 Redesigned DEPRAG Cylinder Rotor Housing

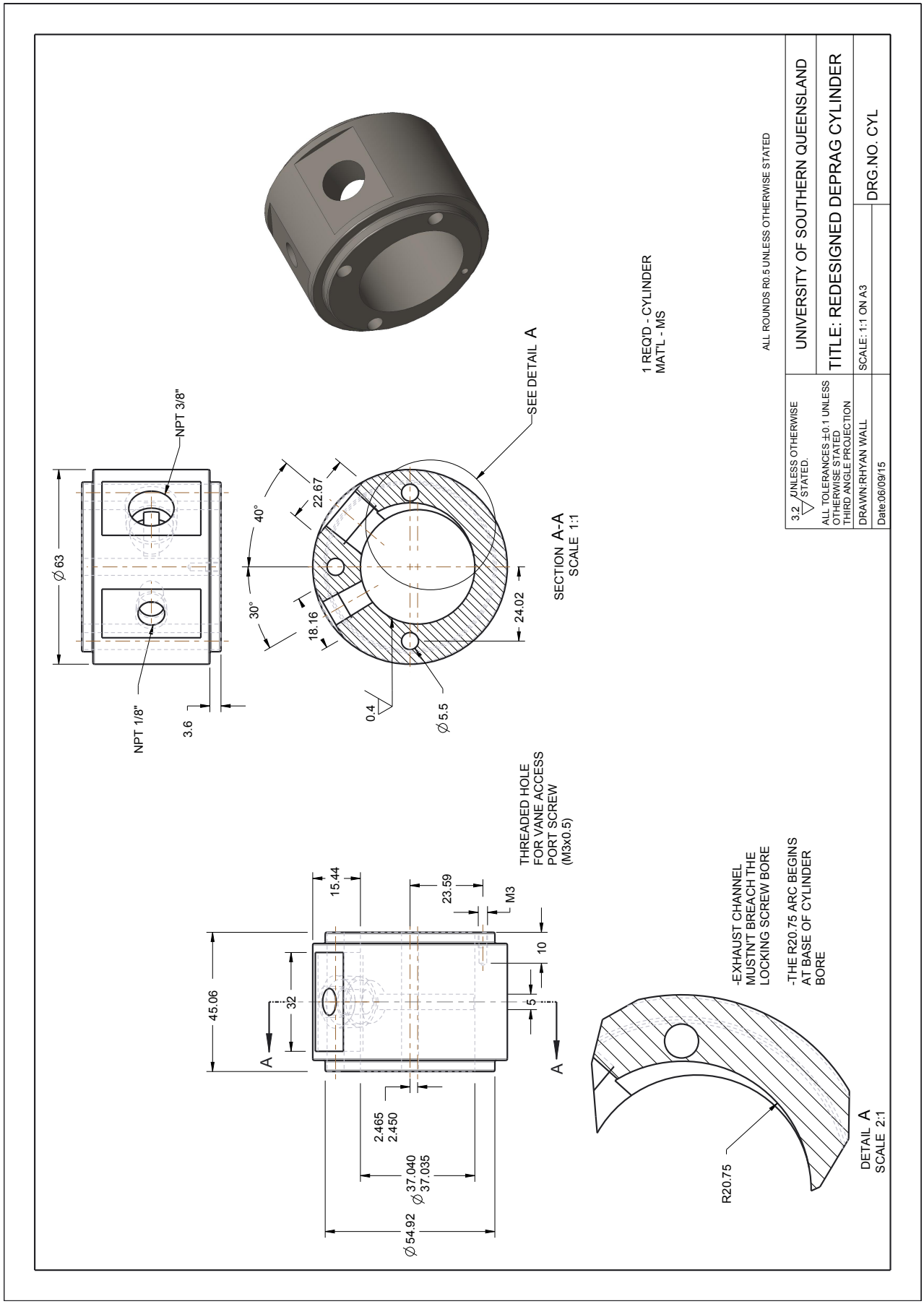
NPT 3/8"
NPT 1/8"
Ø 63
3.6
SEE DETAIL A
40°
30°
22.67
18.16
24.02
0.4
Ø 5.5
SECTION A-A
SCALE 1:1
1 REQ'D - CYLINDER
MAT'L - MS
ALL ROUNDS R0.5 UNLESS OTHERWISE STATED
3.2 UNLESS OTHERWISE STATED.
ALL TOLERANCES ±0.1 UNLESS OTHERWISE STATED
THIRD ANGLE PROJECTION
DRAWN:RHYAN WALL
Date:06/09/15
UNIVERSITY OF SOUTHERN QUEENSLAND
TITLE: REDESIGNED DEPRAG CYLINDER
SCALE: 1:1 ON A3
DRG.NO. CYL
THREADED HOLE FOR VANE ACCESS PORT SCREW (M3x0.5)
15.44
23.59
M3
10
5
45.06
32
A
A
2.465
2.450
Ø 37.040
37.035
Ø 54.92
-EXHAUST CHANNEL MUSTN'T BREACH THE LOCKING SCREW BORE
-THE R20.75 ARC BEGINS AT BASE OF CYLINDER
R20.75
DETAIL A
SCALE 2:1

D.3 Customised Rotary Vane Air Motor (RVAM)

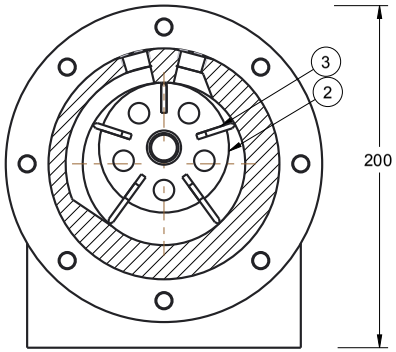

SECTION B-B

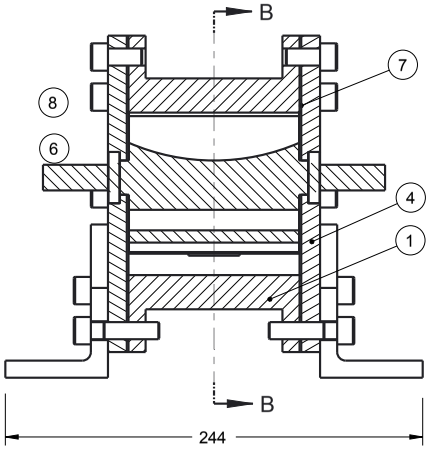

SECTION A-A

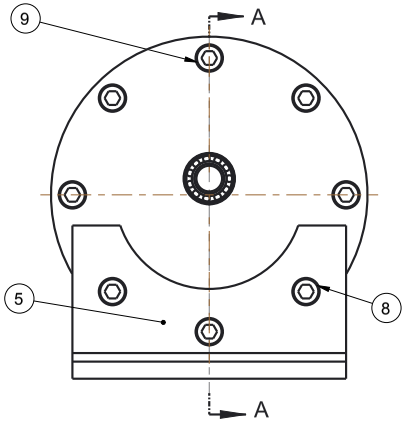

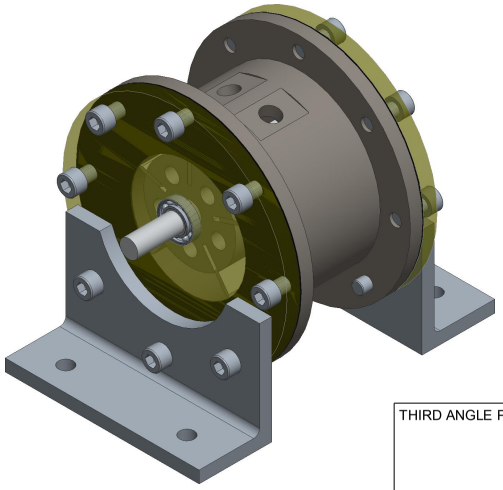

ITEM	DESCRIPTION	QTY	MAT'L	DRG.NO.
9	M10 HEX SOCKET BOLT	6	GALV.	40MM SHAFT
8	M10 HEX SOCKET BOLT	10	MS	20MM SHAFT
7	GASKET	2	CORK	-
6	DEEP GROOVE BALL BEARING	1	-	SKF-61903
5	FOOTING	1	MS	FOOT
4	END PLATE	2	ACRYLIC	EPLATE
3	ROTOR VANE	1	PTFE	RVANE
2	ROTOR	1	AL6106	ROTOR
1	CYLINDER	1	4140	CYL

THIRD ANGLE PROJECTION	UNIVERSITY OF SOUTHERN QUEENSLAND	
	TITLE: AIR MOTOR DESIGN ASSEMBLY	
DRAWN:RHYAN WALL	SCALE: 2:5 ON A3	DRG.NO. ASM DESIGN
Date:02/09/15	SHEET 1 OF 6	

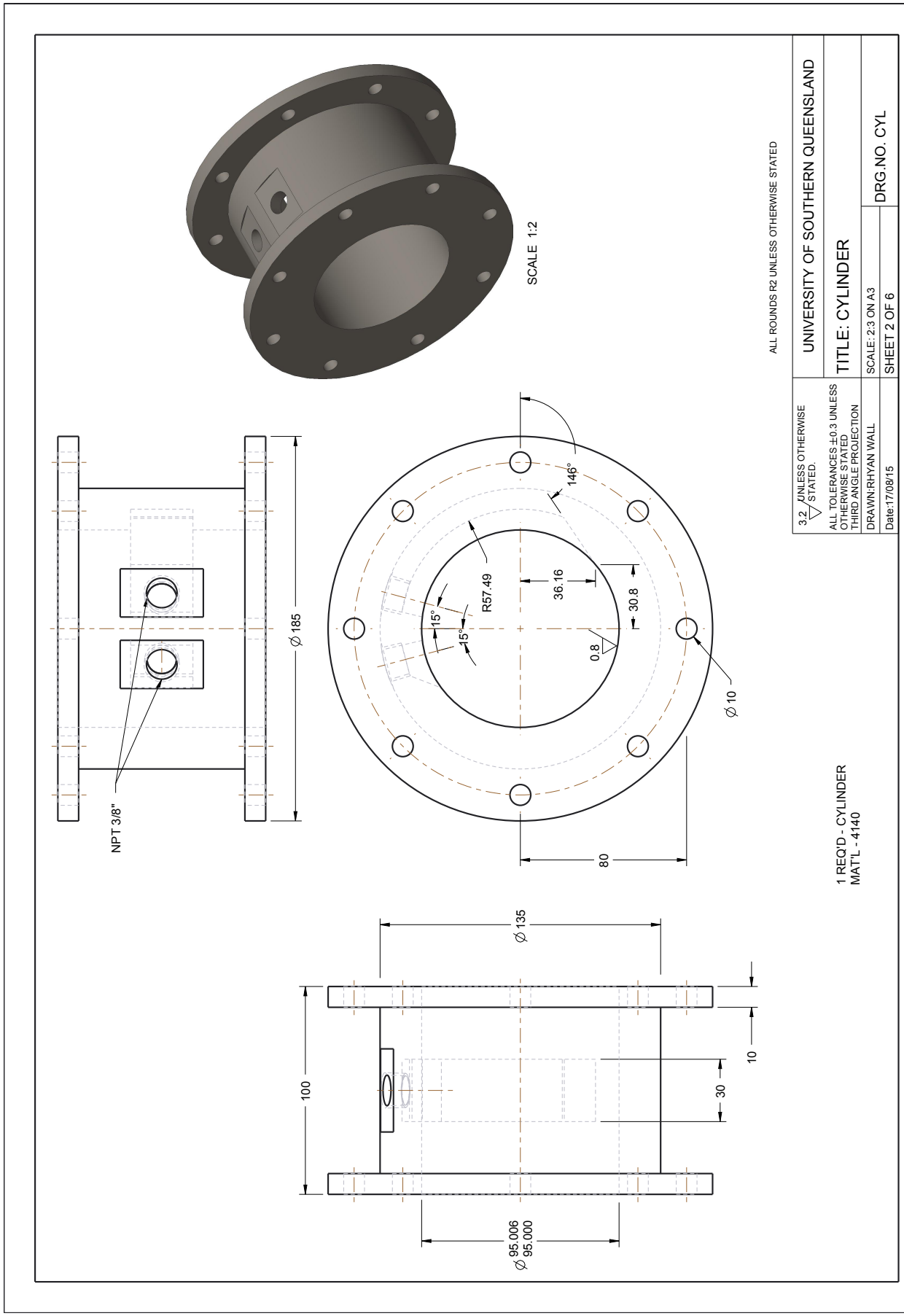
SCALE 1:2
ALL ROUNDS R2 UNLESS OTHERWISE STATED
UNIVERSITY OF SOUTHERN QUEENSLAND
TITLE: CYLINDER
SCALE: 2:3 ON A3
DRG.NO. CYL
SHEET 2 OF 6
3.2 UNLESS OTHERWISE STATED.
ALL TOLERANCES ±0.3 UNLESS OTHERWISE STATED
THIRD ANGLE PROJECTION
DRAWN:RHYAN WALL
Date:17/08/15
1 REQ'D - CYLINDER
MAT'L - 4140
NPT 3/8"
Ø 185
146°
R57.49
36.16
30.8
15°
15°
0.8
Ø 10
80
Ø 135
100
10
30
Ø 95.006
Ø 95.000

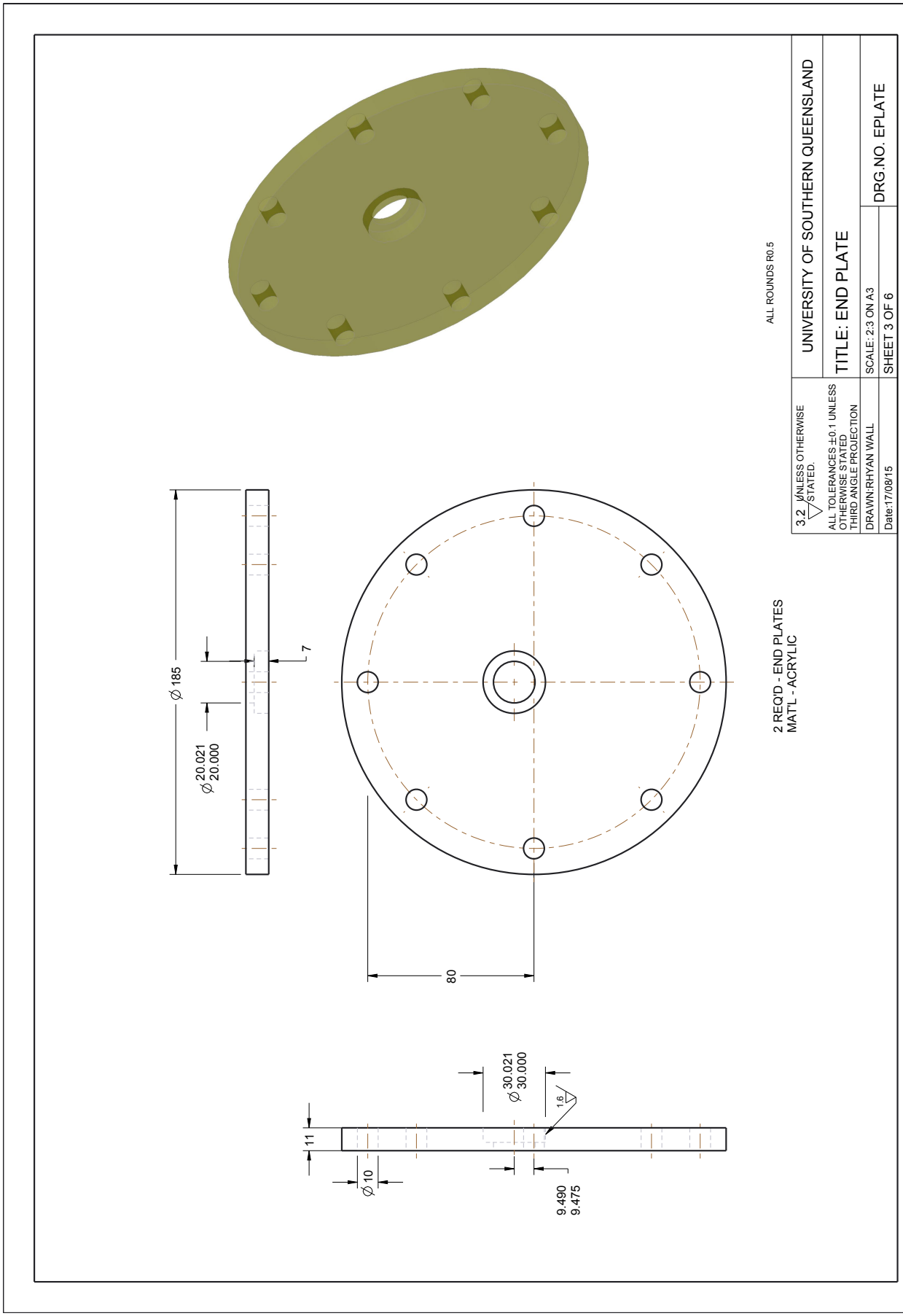
UNIVERSITY OF SOUTHERN QUEENSLAND
TITLE: END PLATE
SCALE: 2:3 ON A3
DRG.NO. EPLATE
SHEET 3 OF 6
DRAWN:RHYAN WALL
Date:17/08/15
ALL TOLERANCES ±0.1 UNLESS OTHERWISE STATED
THIRD ANGLE PROJECTION
3.2 UNLESS OTHERWISE STATED.
ALL ROUNDS R0.5
2 REQ'D - END PLATES
MATL - ACRYLIC
Ø 185
Ø 20.021
20.000
7
80
Ø 30.021
30.000
1.6
11
Ø 10
9.490
9.475

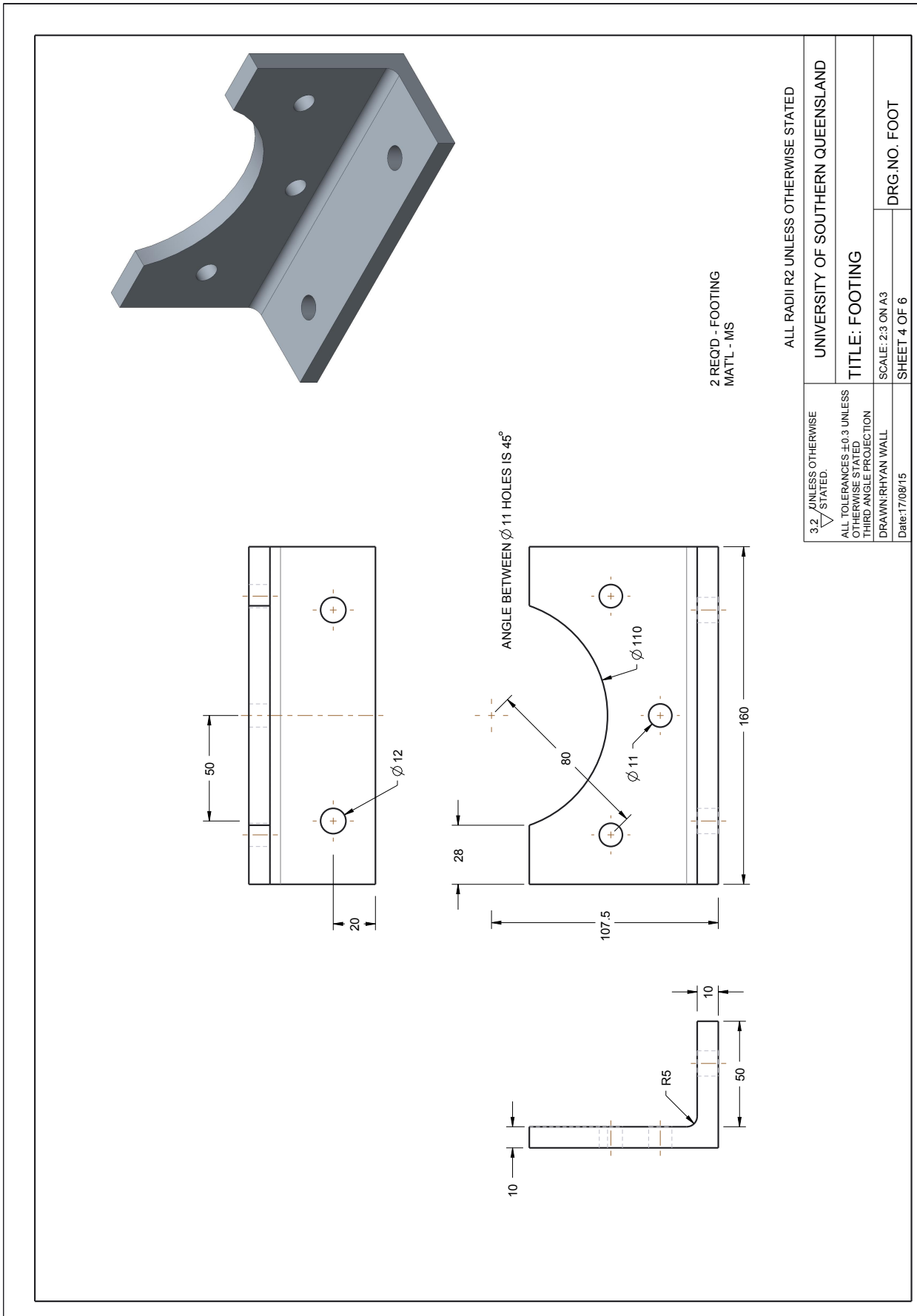
ALL RADII R2 UNLESS OTHERWISE STATED
2 REQ'D - FOOTING
MAT'L - MS
ANGLE BETWEEN ∅ 11 HOLES IS 45°
UNIVERSITY OF SOUTHERN QUEENSLAND
TITLE: FOOTING
3.2 UNLESS OTHERWISE STATED.
ALL TOLERANCES ±0.3 UNLESS OTHERWISE STATED
THIRD ANGLE PROJECTION
DRAWN:RHYAN WALL
Date:17/08/15
SCALE: 2:3 ON A3
SHEET 4 OF 6
DRG.NO. FOOT
50
∅ 12
20
∅ 110
80
∅ 11
160
28
107.5
10
R5
50
10

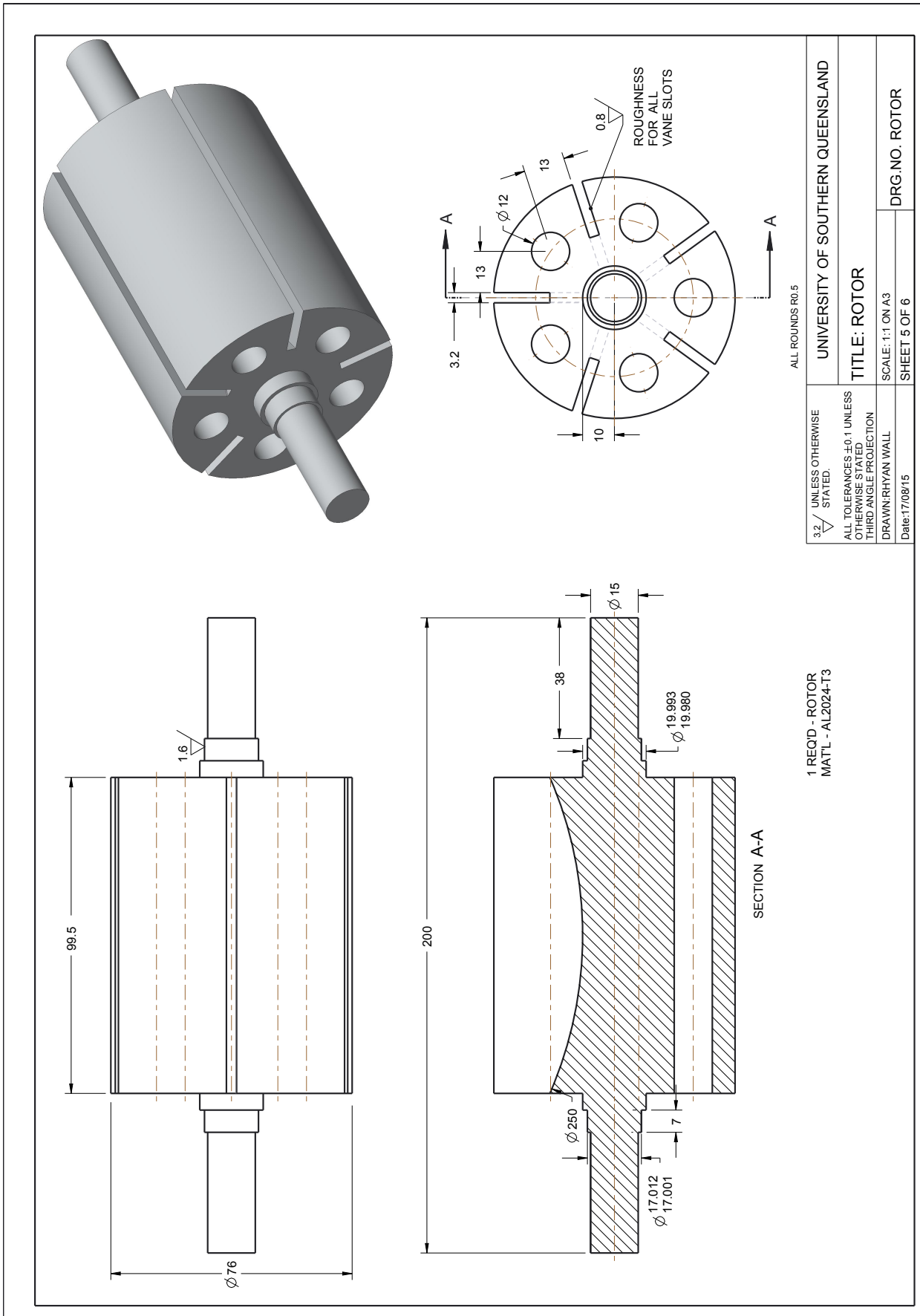
ROUGHNESS FOR ALL VANE SLOTS
0.8
13
Ø12
13
3.2
10
A
A
ALL ROUNDS R0.5
1.6
99.5
Ø76
38
Ø15
19.993
19.980
200
Ø250
7
17.012
17.001
SECTION A-A
1 REQ'D - ROTOR
MAT'L - AL2024-T3
3.2 UNLESS OTHERWISE STATED.
ALL TOLERANCES ±0.1 UNLESS OTHERWISE STATED
THIRD ANGLE PROJECTION
DRAWN:RHYAN WALL
Date:17/08/15
UNIVERSITY OF SOUTHERN QUEENSLAND
TITLE: ROTOR
SCALE: 1:1 ON A3
SHEET 5 OF 6
DRG.NO. ROTOR

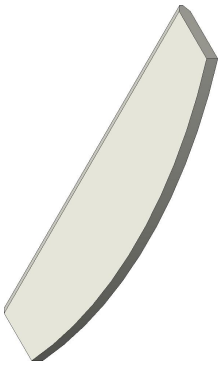

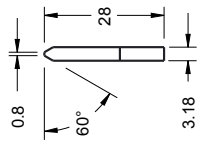

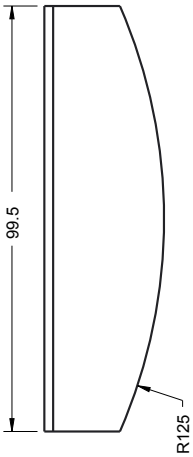

5 REQ'D - ROTOR VANE
MAT'L - PTFE

ALL RADII R2 UNLESS OTHERWISE STATED

3.2 UNLESS OTHERWISE STATED.	UNIVERSITY OF SOUTHERN QUEENSLAND
ALL TOLERANCES ±0.1 UNLESS OTHERWISE STATED THIRD ANGLE PROJECTION	TITLE: ROTOR VANE
DRAWN:RHYAN WALL	SCALE: 1:1 ON A3
Date:17/08/15	SHEET 6 OF 6
	DRG.NO. RVANE